TÉCNICO LISBOA

Biogeochemistry of Permafrost Thermokarst Lakes in the Canadian Subarctic

Leandro Alexandre Mendes Castanheira

Thesis to obtain the Master of Science Degree in

Chemical Engineering

Thesis Supervisors: Dr. João Alfredo Vieira Canário
Professor Warwick F. Vincent

Examination Committee

Chairperson: Professor Benilde de Jesus Vieira Saramago

Committee Member: Professor Maria Matilde Duarte Marques

Supervisor: Dr. João Alfredo Vieira Canário

July 2015

ACKNOWLEDGMENTS

I would like to express my appreciation to my thesis supervisors Dr. João Canário and Professor Warwick F. Vincent. Thank you for giving me the opportunity to be part of the polar research.

Special thanks to Dr. João Canário for his time, patience, and understanding. Special thanks also for Dr. Warwick Vincent and his staff for welcoming me to the CEN (*Centre d'Études Nordiques*) research station in Kuuujjuarapik.

Also, thanks to Ana Padeiro for her help in many steps in this work, and her partnership.

My gratitude also goes to Dr. Maria Fátima Araújo and Susana Gomes from C^2TN for their guidance and help in the ICP-MS results. Thank you for receiving me with kindness and patience.

Special thanks to Dr. Maria Conceição Oliveira and Ana Dias for their efforts to overcome the setbacks and their contributions to the HPLC-MS analyses. I also thank Professor Teresa Duarte and Dr. Vânia André for sharing their knowledge on X-Ray diffraction analysis.

Thanks to Dr. Maria João Ferreira for the many hours spent analyzing the samples in NMR, and for the help to understand the results. Also special thanks to Professors José Ascenso and Teresa Nunes for their valuable contribution on the ssNMR analysis.

The most special thanks go to my best partner and friend, my girlfriend. Susana Carvalho, you gave me your unconditional support and love through all this long process. I love you.

This work was funded by the Fundação para a Ciência e Tecnologia (FCT) through the Portuguese Polar Program (PROPOLAR), by the Canadian project ADAPT (Arctic Development and Adaption to Permafrost in Transition) through the Centre d'etudes nordiques, Laval University and by the FCT project UID/QUI/00100/2013.

ABSTRACT

This research was carried out in the Canadian sub-Arctic in order to better understand the biogeochemical processes occurring in thermokarst lakes. Several soils, sediments and water depths were sampled in lakes localized in different permafrost areas.

To chemically characterize the samples in terms of their composition and trace elements (TEs) content, several analytical techniques were used. In this work, sulphur compounds were measured for the first time.

The reduction of dissolved oxygen and sulfate with depth in the water column of all lakes, suggested their consumption during the mineralization of Natural Organic Matter, such as dissolved organic carbon (DOC) which increased with depth apparently related to molecular diffusion and/or freeze-concentration effects of DOC at the sediment/water interface. More than 14% of analyzed TEs were remobilized in water when the DOC mineralized, which may precipitate by the production of sulphide ions.

High sedimentary organic matter was observed in SAS/KWK lakes samples (max. 94%) while in BGR lake samples lowest levels were determined (<2%). Also, organic-S was less abundant in this lake accounting only 33% whereas for the others more than 50% was observed. A tendency for TEs to increase with higher aluminium content in soils/sediments was verified suggesting an association with inorganic material, with sulphides playing an important role.

This work points to the importance of organic matter composition in the biogeochemical processes occurring in thermokarst lakes, and provides the first evidence of the importance of the sulphur chemistry in these carbon-enriched freshwater systems.

Keywords: Canadian sub-arctic, Permafrost, organic carbon, sulphur, trace elements

RESUMO

De forma a melhor entender os processos biogeoquímicos que ocorrem nos lagos termocarso, amostras de solos, sedimentos e águas foram recolhidos no Subárctico canadiano em diferentes zonas de *permafrost*.

Foram utilizadas diversas técnicas analíticas de forma a caracterizar quimicamente estas amostras, nomeadamente a sua composição química e as respectivas concentrações. Neste trabalho, compostos de enxofre foram pela primeira vez determinados.

Uma diminuição com a profundidade dos teores de oxigénio e sulfato dissolvidos foram observados em todos os lagos, sugerindo o seu consumo na mineralização da matéria orgânica natural, como o carbono orgânico dissolvido (DOC), cujo aumento em profundidade foi observado parecendo estar relacionado com a difusão molecular e/ou "*frozen-effect*" na interface sedimento/água. Este DOC foi identificado como sendo de origem vegetal.

Uma remobilização de elementos traço (ETs) foi observada após mineralização artificial do DOC (>14%). Estes elementos parecem precipitar devido à produção de iões sulfureto na coluna água.

Quantidades elevadas de carbono orgânico sedimentar foram detectadas nos lagos SAS e KWK (máx. 94%), enquanto no BGR níveis mais baixos foram determinados (< 2%), onde a quantidade de enxofre orgânico (ca. 33%) também foi menor. Observou-se uma tendência para o aumento da concentração dos ETs com alumínio nos solos/sedimentos sugerindo que a retenção destes elementos na matriz sólida é feita essencialmente na sua componente inorgânica, possivelmente associada a sulfuretos.

Este trabalho aponta para a importância da composição da matéria orgânica nos processos biogeoquímicos em lagos termocarso, realçando pela primeira vez a importância da química do enxofre nestes sistemas de água doce.

Palavra-Chave: Subárctico Canadiano, *Permafrost*, matéria orgânica, enxofre, elementos traço

ACRONYMS and SYMBOLS

AVS	Acid Volatile Sulphide
CRS	Chromium Reduced Sulphur
DDP	Differential Polarographic Pulse
DGT	Diffusive gradient in thin films
DME	Dropping Mercury Electrode
DO	Dissolved Oxygen
DOC	Dissolved Organic Carbon
ICP-MS	Inductively Coupled Plasma Mass Spectrometry
LD	Limit of Detection
LQ	Limit of Quantification
LOI	Loss-on-Ignition
NOM	Natural Organic Matter
OC	Organic Carbon
OM	Organic Matter
RSD	Relatively Standard Deviation
ssNMR	Solid-state Nuclear Magnetic Resonance
SOM	Sedimentary Organic Matter
SR	Sulfate Reduction
CRM	Certificate Reference Material
TE	Trace Element
XRPD	X-Ray Powder Diffraction

INDEX

FIGURE INDEX

TABLE INDEX

1. Introduction

1.1. Background

1.1.1. Arctic and the Permafrost

The Arctic Ocean is surrounding by land that is characterized by tundra, boreal forests, peat-lands and permafrost (Tuner and Marshall, 2011). The boreal forest consists of coniferous trees and it is located on the edges of the Arctic, north of which is the treeless Arctic tundra, described by persistent winter snow cover and frozen ground which respond rapidly to temperature variation (Boike et al., 2003). For this reason the Arctic suffers strongly with the climate warming (Vincent et al., 2013b), averaging a temperature increase of 3-4ºC over the last century in the Canadian Arctic (Prowse et al., 2009).

With rising temperatures it is predicted a northward shift of the climate zones with a pole ward extension of the boreal forests and the tree line, resulting in a transformation of Arctic landscape, with the northern edge of the boreal forest advancing into tundra (Zhang et al., 2013).

Continued climate change will likely have consequences for many systems throughout the Arctic region, including two significant terrestrial impacts: an increase in river discharge (Smith et al., 2007), and permafrost degradation (Lawrence and Slater, 2005).

Permafrost is defined as the ground that remains at or below 0ºC for more than two consecutive years, and can be differentiated by its spatial extent into continuous (90-100%), discontinuous (50-90%), sporadic (10-50%), and isolated (0-10%) permafrost (Grosse et al. 2013; Marchenko et al. 2013). It is widespread in the Arctic and boreal regions of the Northern Hemisphere (figure 1), and occupying about 22% of Arctic exposed land surface area (Zhang et al. 1999).

The areas of discontinuous permafrost is contained between latitudes 56° and 58°N while the zone of continuous permafrost extends northward where annual temperatures since deglaciation allowed permafrost to reach depths over 150 m and even as deep as 590 m (Allard and Séguin 1987a).

The sporadic permafrost are is mainly confined to peat-lands because of the thermal offset effect related to peat's thermal properties (i.e. peat cools easily when frozen in winter and is a good insulator that prevents warming in summer) (Brown 1970; Burn and Smith 1988).

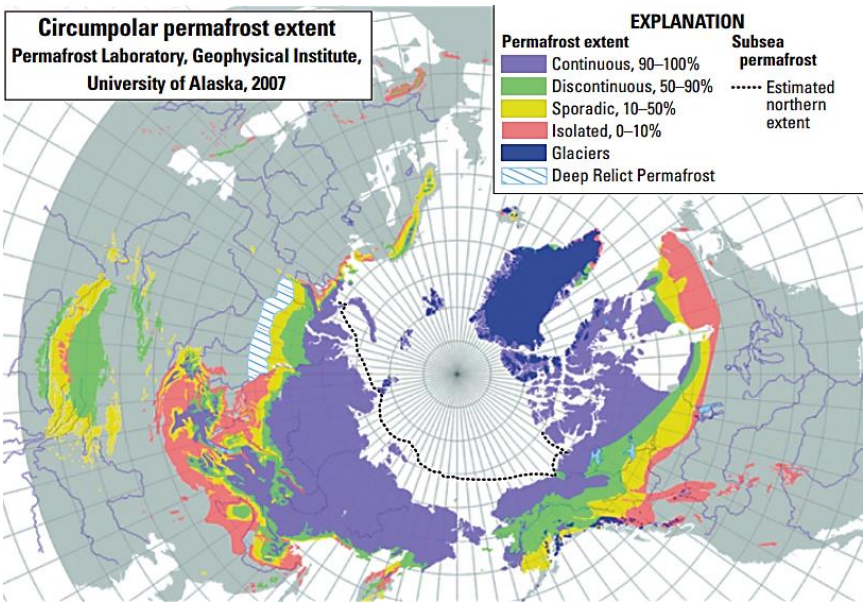

Figure 1: Areal distribution of permafrost on regions of the northern Hemisphere. Source: Frozen Ground Data Centre (http://nsidc.org/fgdc/).

The ground in permafrost regions is characterized by two main layers: the active layer that thaws every summer, refreezing in autumn; and the underlying permafrost layer (unfrozen ground) that remains below 0°C year round (French, 2007). Both the active and transition layers are affected by seasonal temperature variations (figure 2), but only the active layer undergoes seasonal thawing (Williams and Smith, 1989).

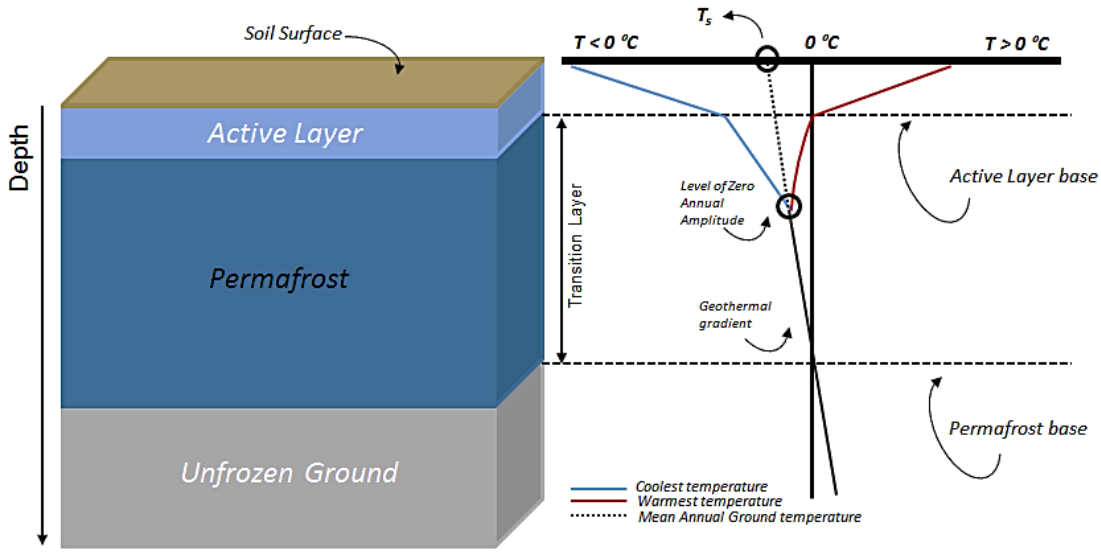

Figure 2: Typical ground-thermal regime found in permafrost soil. T_s is the mean temperature of the ground surface obtained by extrapolating the common linear portion of the profiles upwards. Marchenko et al., 2013.

The level of zero annual amplitude is the maximum depth affected by the annual temperature variations which depends on soil's characteristics and air temperature (French, 2007). Thus, the distribution and thickness of permafrost are controlled by factors that influence its heat balance and heat flow within. Since pore spaces in permafrost are generally blocked by ice, heat flows by conduction (Marchenko and Etzelmuller, 2013).

The active layer ranges from a few tens of centimeters to more than 2 m in the zone of continuous permafrost area (Paulerg et al., 2010), and its thickness increase with atmospheric warming or increased snowfall (Zhang, 2005). The increased thickness of the active layer thaws permafrost from above, while warmer surface temperatures also decrease conductive heat fluxes in the ground, inducing permafrost decay at the base (Matthews, 2012).

Schuur et al. (2015) estimated that terrestrial permafrost contains 1.33–1.58 $x10^{13}$ tons of organic carbon (OC), which with increasing permafrost degradation, becomes more available for microbial activity, and thus more involved in the annual carbon cycle (Ciais and Sabine, 2013).

The organic matter (OM) exposed by permafrost thawing may be oxidized via microbial decomposition to CO_2 in well-aerated environments, increasing the flux of this gas into atmosphere (Walter et al., 2007). However, in a more anoxic environment microbial oxidation of OM produces CH_4, which has a much stronger greenhouse effect than CO_2 (Zimov et al. 1997).

Thus, permafrost thawing increases the flux of greenhouses gases into atmosphere, which enhance the greenhouse effect; this in turn leads to an increase of air temperature that aggravates permafrost degradation, in a vicious cycle where permafrost thawing has a positive feedback to climate warming (Schuur et al. 2008).

In short, rising temperatures due climate change may have the twofold effect on terrestrial permafrost-carbon cycle by: (1) thickening the active layer, and thus increasing the portion of soil carbon stock involved in the seasonal cycle and (2) shifting the balance between the annual carbon sink and source (photosynthetic uptake of CO_2 by Arctic vegetation and release of CO_2 due to soil respiration and/or emission of methane respectively) (Streletskiy et al., 2015). Callaghan et al. (2011) observed that tundra regions currently act as sources of carbon in warm and dry years and as sinks in cold and wet years.

Warming of the permafrost accompanied by thaw and release of ancient organic carbon is one of the most significant environment threats within global climate change scenario (Schuur et al. 2008; DeConto el al., 2012), and is predicted to continue on this trajectory on this century (Romanovsky et al. 2010).

Degradation of permafrost is a complex process involving interactions with climate, hydrology ecosystems, and geology, all with a competing influence on the ground thermal regime and permafrost stability (Jorgenson et al., 2010). Indigenous peoples such as the Inuit who live in the north, are also influenced by permafrost degradation, because it provided a solid structure for their infrastructures, and thus permafrost thawing can lead to damage of buildings, roadways, airports and utilities (Instanes, 2005; Vincent et al., 2013a).

1.1.2. Thermokarst Lakes

A typical form of permafrost degradation involves the formation and growth of “thermokarst lakes” (Wallace, 1978; Hopkins, 1949), defined as lakes that occupy depressions formed by settlement of ground following thawing of ice-rich permafrost (van Everdigen, 2005). Grosse et al. (2011) estimated that in the circumpolar arctic region there exist more than 61 000 lakes with a total area of more than 200 000 km^2 that are likely to be thermokarst lakes.

The formation of these lakes is widespread in the Arctic and sub-Arctic lowlands region with ice-rich permafrost during the Late Pleistocene-Holocene transition (Rampton, 1988; Walter et al., 2007). Today, those regions are abundant in permafrost lakes and remnant basins that resulted from their partial or complete drainage (Grosse et al. 2013). Figure 3 presents a map with the probable distribution of thermokarst lakes in the Arctic.

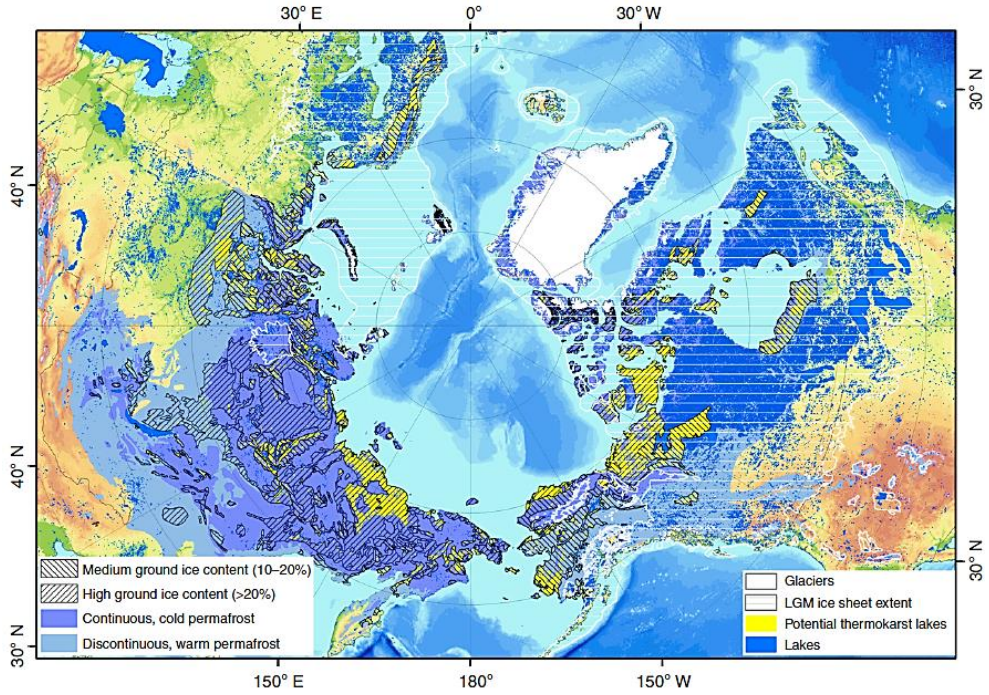

Figure 3: Arctic map showing probable thermokarst lake distribution (Grosse et al. 2013).

The general distribution of thermokarst lakes in Alaska, Russia, and Canada is well known from a number of regional lake studies and maps in various levels of details (e.g. Alaska: Hinkel et al. 2005; Arp and Jones, 2008; Russia: Morgenstern et al., 2011; Canada: Burn, 2002; Coté and Burn, 2002; Turner et al., 2010).

Formation of thermokarst lakes includes coalescence of ice-wedge through ponds above melting ice-wedge networks (figure 4), or through broad but inhomogeneous surface subsidence of ice-rich ground and gradual impoundment of water in coalescing and steadily growing ponds (Czudek and Demek, 1970).

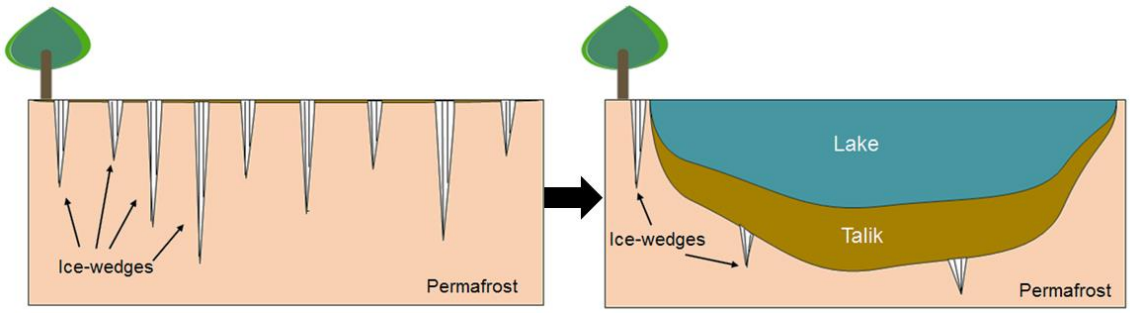

Figure 4: Schematic representation of the formation of a thermokarst lake, from ice-wedges melting.

A fundamental process of thermokarst lake development is the formation of a talik, or thaw bulb, underneath the lake for which the annual lake-bottom temperatures are 0ºC or above (Burn, 2002).

A variety of mechanical and geophysical methods have been used to test the presence of the talik, and its dimensions under thermokarst lakes, including long metal probes that are hammed into the thawed zone until permafrost is encountered, making deep boreholes in which ground temperatures are measured (Lin et al., 2010).

The typical annual heat fluxes of a thermokarst lake show that the lake receives heat energy from atmosphere during summer which is dissipated in the water column and partially transferred to the underlying and surrounding sediments of the talik and forward across the thawing front into the permafrost (Vtyurina, 1960). During autumn and early winter, the lake cools rapidly from surface to bottom while the upper zone of the talik can be warmer than the lake water due to the late summer warmth still present in the talik sediment (Ling and Zang, 2003). In winter, lakes emit heat into the atmosphere (even though being cover by ice) while maintaining heat transfer into the talik that continues to expand by transferring heat into the permafrost (Jeffries et al. 1999).

Thus, the heat fluxes always point from the talik to permafrost, effectively expanding the thawed zone year round, aiding in warming and degradation of adjacent permafrost (Jeffries et al. 1999). The growth of the lake, given sufficient water supply enhances the heat storage capacity of the water body contributing for the heat flux pointed to permafrost (Grosse et al. 2013).

Once initiated, a thermokarst lake also tends to grow laterally by thermal and mechanical erosion into adjacent ice-rich permafrost deposits and soils. Lateral expansion is evidenced by slumping shorelines, much of which is related to thermal degradation of surrounding ground. Expansion rates were observed with remote sensing methods over decadal scales and are largely in the range from 0.3-0.8 m/year (Burn and Smith, 1990; Jones et al., 2011; Jorgenson and Shur, 2007).

This tendency to expand laterally, and the increase thaw of permafrost, can lead eventual to the drainage of the lakes (Mackay 1988). Also various mechanisms could result in an increased of water levels and possible lateral drainage such as long-term positive precipitation-evaporation balance, storms that result in higher waves and strong wave erosion followed by seepage, and high snow accumulation that creates snow dams, causing rising water levels during spring melt (Arp et al., 2010; Hinkel et al., 2007; Hopkins, 1949; Marsh and Neumann, 2001). Figure 5 shows two thermokarst lakes in the North Slope of Alaska: one that drains and other that expand by coalescence.

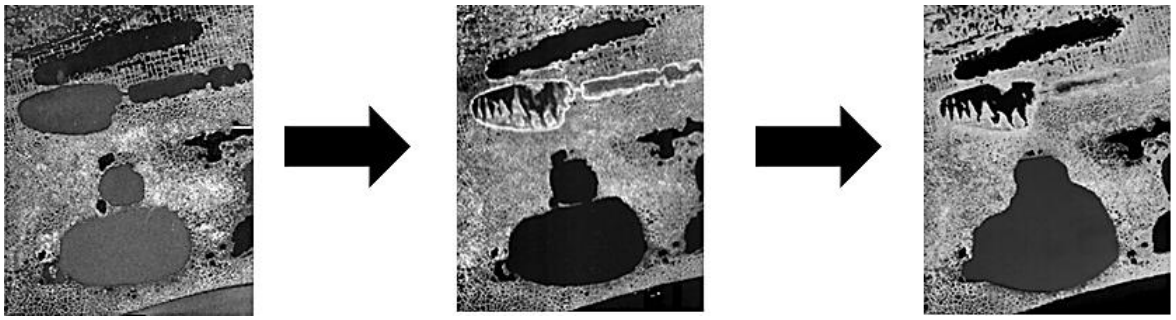

Figure 5: Aerial image time series showing a thermokarst lake expansion and coalescence (up image) and drainage (down image) from the North Slope of Alaska in 1955, 1979 and 2002. Modified from Grosse et al. (2013).

Thermokarst lakes post-drainage processes consist of permafrost aggradation, frost cracking of soils, ice wedges and segregated ground ice formation (Jorgenson and Shur, 2007; Ling and Zhang 2004), slope relaxation (Plug and West, 2009; Ulrich et al. 2010), and peat accumulation (Bockheim et al., 2004; Hinkel et al., 2005).

These lakes have also been identified as an important source for atmospheric greenhouse gases by dissolved organic carbon (DOC) mineralization (Kling et al., 1991; Zimov et al., 1997). Fritz et al. (2015) reported an increase of DOC in these lakes' water, during thaw of ice-wedges. Biological processing of DOC occurs prior to and upon hydrologic delivery into these waterbodie (Michaelson et al., 1998).

Also in these lakes sulfate reduction (SR) in the mineralization of organic matter can be a significant process in anoxic environments when this specie is available (Sinke et al., 1992). The overall OM mineralization reaction during SR can be described by (Bener, 1980):

$$2CH_2O(org.) + SO_4^{2-}(aq) \rightarrow H_2S(aq) + 2HCO_3^-(aq) \qquad \Delta G^o = -77\ kJ.mol^{-1}OM$$

Some authors have reported metals ions association with insoluble sulphide precipitates, which are formed by SR in connection with decomposition of organic matter (Canavan et al. 2007; Di Toro et al. 1996; Huerta-Diaz et al. 1998). Manasypov et al. (2014) showed close relationships between diagenetic processes and the remobilization of contaminants (e.g. trace elements) from the sediments to water.

1.1.3. Soils

A soil is defined as a porous medium mixture of minerals, water, gases, organic matter, and microorganisms, with texture based on sand, silt, and clay fractions amount present (SSSA, 10/05/2015). The identification of these fractions is based on their relative size and for the US are (USDA site, 10/05/2015): Sand: 2.00 – 0.05 mm in Ø; Silt: 0.05 – 0.002 mm in Ø; and Clay < 0.002 mm in Ø.

One of the major components of the soil is the humus (Adriano, 2001), also known as soil organic matter which are divide in two types of compounds: non-humic and humic substances. Non-humic substances include low-molecular-mass organic acids, simple carbohydrates, polysaccharides, amino sugars, amino acids, peptides, proteins, and lignin (Essington, 2005). Humic substances can be classified as humic acids, fulvic acids, and humin, and are generally characterized to have yellow to black color, high-molecular-mass, and refractory nature (Aiken et al., 1985).

Natural organic matter or humic substances that contain carboxyl and amino groups have a tendency to form strong complexes with metal cations, which increase their mobility in aqueous phase (Iskrenova-Tchoukova et al. 2010).

Humic acids influence trace elements retention and mobility in soils and water (Evans et al., 1989; Ginsquiani et al., 1992). The stability constants described in Pandey et al. (2000) for different metal-humic acids complexes suggests the following order of the stabilities: Cu > Fe > Pb > Ni > Co > Ca > Cd > Zn > Mn > Mg.

The accumulation of large carbon stocks in the form of soil organic matter in the Arctic regions is the result of variety of ecosystem limitations such as temperature, and the availability of substrates, soil's water and oxygen (Davison and Janssens, 2006) suggesting that there is a link between carbon stocks, vegetation and climate in the Arctic ecosystem.

1.2. State of the Art

Thermokarst lakes in northern Québec vary greatly in color, shape, number and size (Watanabe et al., 2011), which make their biogeochemical study of the most interest. Figure 6 illustrates the Canadian sub-arctic landscape, showing the variety of lakes.

Figure 6: Landscape photo of thermokarst lakes in northern Québec taking during work field.

Many studies have been published about thermokarst lakes, mainly related to the microbiological formation, fluxes and release of CO_2 and CH_4 or on less extend the chemical composition of thermokarst lakes soils and waters (Negandhi et al., 2013). Walter et al. (2007) suggested important key factors related to the CH_4 production, global budget and climate change impact, while others have dedicated more of their research to the biotic side of this issue and also to the limnological aspects involved (e.g., Crevecoeur et al., 2015; Vincent et al., 2013).

Also great importance has been placed on the role of natural organic matter (NOM) in the thaw lakes processes. Breton et al. (2009) showed the importance of low molecular weight organic compounds in the CO_2 production and this group also identified *Proteobacteria* as the main CH_4 and CO_2 producer's (Crevecoeur et al., 2015).

In northern Québec region, characterized from continuous, discontinuous and sporadic permafrost, thermokarst lakes maximum depths range from 1 to 3.5 m (Breton et al. 2009, Bouchard et al., 2014).

A study on water color and light attenuation in these lake's waters showed that the lake surface color was dependent upon the combined concentration of dissolved organic carbon and suspended non-algae particulate material (Watanabe et al., 2011).

According with Sepulveda-Jáuregui et al. (2015) lakes that are more colored strongly absorb solar radiation, and thus a surface water warming temperature is observed, which combined to cooled bottom waters by the permafrost beneath, leads to a vertical thermal and density gradients in these lakes (Laurion et al., 2010). This stratification is more pronounced in summer, and it can occur in waters less than 2 m deep in northern Québec (Laurion et al., 2010).

The DNA database for bacteria in permafrost soils, which often contain anaerobic groups such as sulfate reducers, Fe (III) reducers and denitrifiers, and many aerobic groups including actinobacteria and methanotrophs is now growing (Jansson and Tas, 2014). RNA sequencing of thermokarst lakes in northern Québec showed that dominant bacterial taxa were beta-proteobacteria, especially the genera *Variovorax* and *Polynucleobacter*, and *Methylbacter* (Crevecoeur et al., 2015)

which are known to occur in environments where both oxygen and CH_4 are available (Kankaala et al., 2006).

Trace element biogeochemical studies are scarce and mostly published by Pokrovsky group (e.g. Pokrovsky et al. 2013) where all the published studies were done in Siberia mainly focused in thaw lakes trace elements colloidal speciation, chemical composition or microbial activity.

In spite of these works, many scientific gaps still persist in order to understand the geochemical processes in thaw lakes and how their chemistry affect the gas release and microbial activity, mainly related to NOM composition and their relation to trace element speciation, partitioning and transport.

This thesis is then a valuable contribution to the thaw permafrost lakes studies because, for the first time, relate the chemical composition of the organic matter in those lakes with their chemistry, and particularly with the biogeochemical processes involving OM and trace element speciation, partitioning and fate.

1.3. Thesis Statement

This work will focus on four primary themes: thaw lake soils/sediments/water, thaw lakes organic matter, thaw lakes trace element partitioning, speciation and fate, and thaw lakes impact. The goals are to obtain a better knowledge of the chemical composition of NOM in thaw lakes, their relation with lake chemistry and the role on trace element biogeochemistry.

The aim was to provide scientific information concerning the nature of NOM and their role on the lability of some trace elements. Therefore thaw lakes sediments, soils and waters samples were collected from subarctic Canada and brought to Lisbon to be analyzed by different analytical techniques.

Thus, the main objectives of this work were to:

1) Improve knowledge of the chemical composition of natural organic matter (NOM) in permafrost thaw lakes;
2) Evaluate the geochemical mechanisms responsible for trace element distribution, partitioning, speciation and fate, in respect with the role of NOM and inorganic matter in those processes;
3) Propose a biogeochemical model that explains the biogeochemical processes.

1.4. Thesis Organization

This thesis is divided into 6 sections. The first presents a general introduction of the theme and a literature review of the concepts used on this work. The second is the experimental work performed, and the third is a description of the analytical methods used. Chapter four is the results and subsequent discussion. Finally chapter five and six present the main conclusions and suggestions for future research respectively. Lastly there is a bibliography with cited references and annexes.

2. Study Area and Sampling

2.1. Study Sites

All samples (waters/sediments/soils) were collected between Jun 26th and July 3th 2014. Four thermokarst lakes on discontinuous and sporadic permafrost region of Canadian sub-arctic (table 1) were sampled: three close to *Whapmagoostui-Kuujjuarapik* (W-K) village at SAS and KWK valleys; and one (BGR 1 Lake) in the Sheldrake River valley near to the village of *Umiujaq*, Québec, Canada.

In figure 7 are presented the sampled sites.

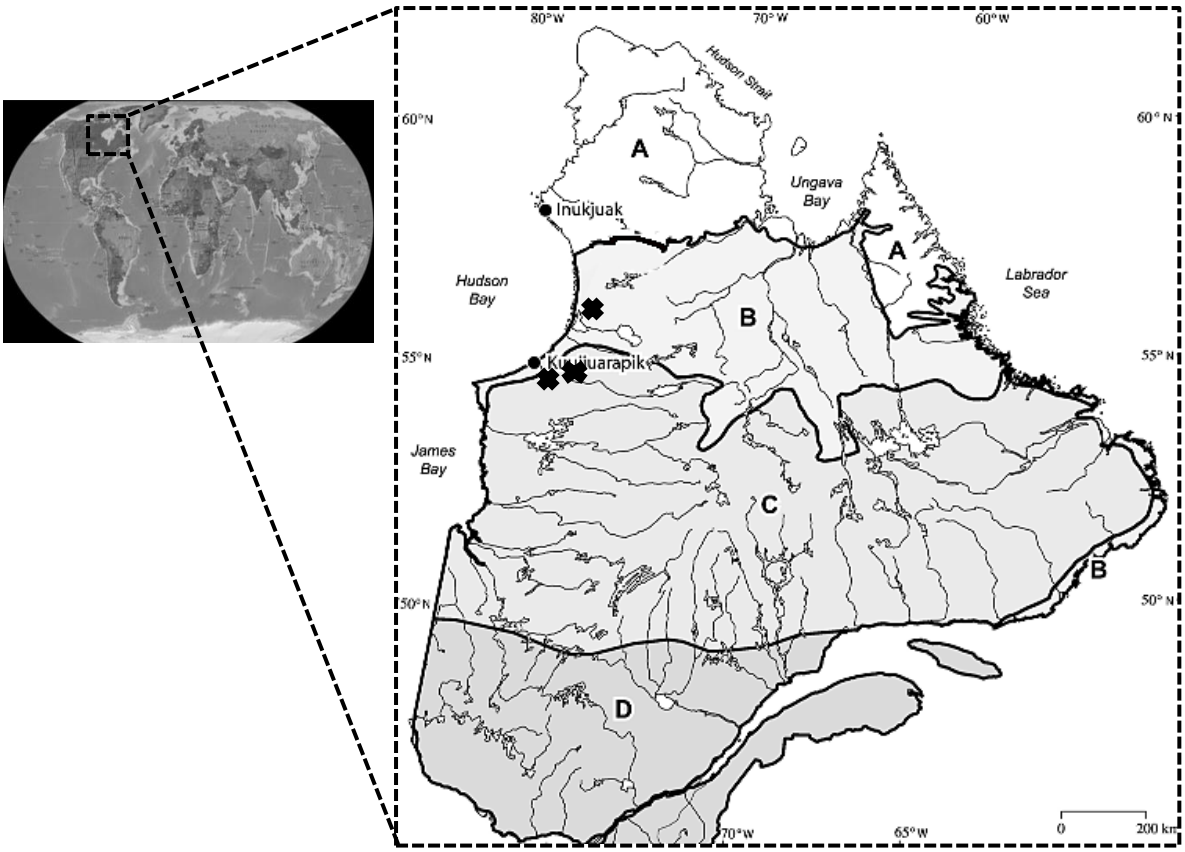

Figure 7: Location of the study sites and permafrost distribution in Québec-Labrador. A: Continuous permafrost; B: Discontinuous permafrost; C: Sporadic permafrost; D: Seasonal frost (Modified from Payette, 2001).

Table 1: Geographic coordinates of the sampled lakes and permafrost characterization of the area.

Lake	Coordinates	Permafrost extent type
SAS 1A	55º13N 77º43W	Sporadic
SAS 2A	55º14N 77º42W	Sporadic
KWK12	55º20N 77º30W	Sporadic
BGR 1	56º37N 76º13W	Discontinuous

The SAS thaw lakes are part of a permafrost peatland, covering approximately 5 km^2 at a mean altitude of 105 m above sea level (Lamarre et al., 2012). The site is located in the sporadic permafrost zone in the *Sasapimakwananisikw* River Valley (SAS Valley) located 7 km to the south to the village of K-W at the edge of Hudson Bay, subarctic Québec, Canada (Przytulska et al., 2014). These thaw lakes are black, highly stratified and lie adjacent to rapidly degrading palsas (Allard and Séguin, 1987b; Bhiry et al., 2011). They originated from palsas (mounds of peat containing a permafrost core of peat or silt) after their collapsing (Arlen-Pouliot and Bhiry, 2005; Gurney, 2001). The SAS valley vegetation is dominated by *Carex* and *Sphagnum* (Arlen-Pouliot and Bhiry, 2005; Bhiry et al., 2011).

The KWK thaw lakes lie in a zone of sporadic permafrost in the *Kwakwatanikapistikw* River valley, 110 m above sea level and 12 km to the east of W-K (Watanabe et al., 2011). These numerous lakes span a wide range of colors and have been derived from fully thawed lithalsas, with extensive tree and shrub development around the lakes (Bhiry et al., 2011; Watanabe et al., 2011). Over 95% of the permafrost mounds in this valley thawed and disappeared between 1959 and 2006, and subarctic forest vegetation (black spruce trees) expanded by 326% during this same period (Bouchard et al., 2014).

The BGR ponds lie in the Sheldrake River valley, in the discontinuous permafrost region. The ponds have formed in thawing permafrost mounds that are primarily organic (peat) or mineral (Crevecoeur et al., 2015). BGR and KWK ponds originated from the thawing of lithalsas and are surrounded by shrubs (*Salix planifolia* and *Betula glandulosa*) and sparse trees (*Picea mariana*, *Picea glauca*, *Larix laricina*) (Calmels et al., 2008; Breton et al., 2009).

Figure 8: Sampled Thermokarst lakes: SAS 1A (a), SAS 2A (b), KWK12 (c), and BGR1 (d).

2.2. Sampling

Before sampling all material was acid decontaminated according to the protocol described by Canário (2004). For this proposed all material were immersed in 20% solution of HCl for 24h and after washed several times with Milli-Q ultra-pure water. After this procedure the material was again immersed for 48h, this time in a 25% solution of HNO_3, raised with Milli-Q water and finally dried in an oven at 105ºC. After dried the field material was stored in sealed plastic bags.

In the field work a total of 33 different lake samples were collected: 21 water samples (at different depths) and 12 solid samples. Replicates samples were also collected. Before water sampling vertical profiles of several physico-chemical parameters were measured.

2.2.1. Physico-Chemical Parameters

Vertical profiles of physico-chemical parameters from the sampled thaw ponds were recorded: pH, DO (dissolved oxygen), conductivity and temperature. These parameters were measured with 600R multi-parametric probe (Yellow Spring Instrument). (Annex A).

.

2.2.2. Water Sample Collection

Water collection was made at different depths previously chosen according to the water profiles obtained (section 2.2.1). The criterion for the depths to be sampled was where a significant reduction of DO was observed (see profiles). Sampled waters were used to determined dissolved trace elements (total and labile), dissolved organic carbon (DOC), dissolved sulphur species (sulfate and sulphide), and for δ^{13}C-DOC analysis.

Figure 9: Water collection on SAS 2A Lake using a pump with a graded hose.

The waters were collected from an inflatable boat held near the center of the ponds using ropes tethered to shore, using a Teflon pump with a graded hose, as indicated in figure 9. The boat was moved by rowing to avoid contamination of the samples by the fuel. Table 2 presents the depths in which each water sample was collected.

Table 2: Sampled water depths for each study lake.

Lake	SAS 1A	SAS 2A	BGR 1	KWK12
Depth (m)	Surf	Surf	Surf	Surf
	0.3	0.2	1.8	0.5
	0.6	0.3	2.3	1.0
	0.9	0.4	2.8	1.5
	Bot. (1.1)	1.8	Bot. (3.2)	Bot. (2.2)
		Bot. (2.3)		

All samples were filtered *in situ* with a 0.45 µm pore size cellulose?acetate filters (Whatman) for sulphur and total trace-element analysis or glass fiber filter (Whatman) for organic carbon determinations. The samples for sulphur and carbon were frozen upon arrival at the laboratory (less than 2h) and the waters for trace elements were acidified with 10µL of double distilled HNO_3 (to reduce any biological process and to avoid the adsorption onto the containers) in 10 mL polyethylene tubes. For sulphur analysis a 1 mL dark sealed glass tube was used to store the samples. The tubes were immediately sealed to prevent sulphide oxidation (Metzler, 2003). The filled water tubes were then transported back to the laboratory and processed within 2h maximum where they were frozen until analysis. For labile trace element concentrations the Diffusive Gradient in Thin Film (DGT) was used and are described in more detail in section 3.1.2.

2.3. Soils and Sediments Sampling

Surface soils and sediments (< 5 cm depth) were collected near the lakes (less than 3 m from the shore), with a plastic spatula. The samples were stored in a plastic bag, and transported to the laboratory within 2h. In the laboratory, the samples were oven dried at 40ºC overnight (to avoid loss of volatile compounds), desegregated (separation of roots), pulverized in an agate mortar and stored frieze-dried in polyethylene tubes for future analysis.

3. Analytical Methods

On this work a variety of analytical methods were used to characterize the thermokarst lakes in study. A schematic representation of used methods is presented in figure 10.

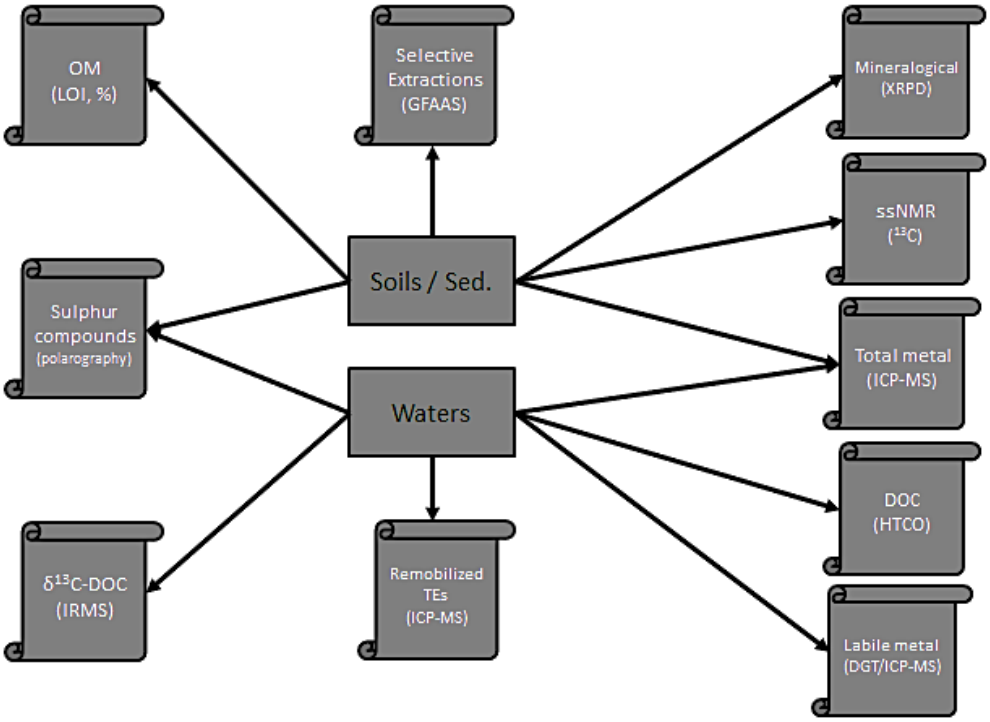

Figure 10: Analytical techniques used on soils/sediments and water samples.

3.1. Water samples

3.1.1. Dissolved Organic Carbon (DOC)

Dissolved organic carbon (DOC) represents the most important organic reservoir in the water, although it is probably also the least known in terms of composition and role in the different biological and geochemical cycles (Cauwet, 1994).

Its determination was made using high temperature catalytic oxidation (HTCO) method proposed by Sugimura and Suzuki (1988) as a rapid and precise method for the determination of non-volatile DOC in seawater. The principle of this method is based on CO_2 detection by spectroscopic methods that result from organic matter oxidation (Spyres et al., 2000).

After acidification and bubbling with air (without CO_2) to remove all inorganic carbon present (e.g. carbonates), an aliquot of 100 µL of water sample was pumped by a glass syringe and injected in a vertical furnace. The combustion tube, made of quartz, is filled with a catalyst of 0.5% Pt on aluminum oxide (Al_2O_3) and its temperature is fixed at 680°C.

The CO_2 formed is measured in a non-dispersive infrared detector, by integration of peak area. Carbon concentration is determined by calibration curve method using potassium hydrogen phthalate solution as standard (0-100 mM). Each value was determined from a minimum of three injections, with a variation coefficient of less than 2%.

According with Benner and Storm (1993) the catalyst is considered to be a major source of carbon contamination in the system, whereby a blank quantification of the system was made before and after the analysis by injected water Milli-Q until low and stable values were reached.

All water samples and blanks were measured in a Shimadzu TOC 5000A as represented in figure 11.

Figure 11: Shimadzu TOC 5000A instrument used for the HTCO analysis.

3.1.2. Stable Carbon Isotope of DOC (δ^{13}C-DOC)

δ^{13}C-DOC measurements were done in a partner laboratory using the method described by Brandes (2009).

The instrumentation used was a Thermo Electron Surveyor Lite autosampler equipped with a 25-µL sample loop, a Surveyor MS HPLC pump, and a LC Isolink interface coupled to a Thermo Scientific Delta V plus stable isotope mass spectrometer. The Isolink is an integrated chemical reactor/gas extraction manifold and standard reference gas injection device. In normal operation, an incoming liquid stream from the HPLC is mixed with both phosphoric acid and persulfate oxidant, and the resulting fluid passed through a heated stainless-steel capillary column reactor to convert organic compounds to CO_2. The mixture is cooled and subsequently passed through a gas–liquid separation manifold, allowing the CO_2 to be extracted into a He stream. This He + CO_2 stream passes through two Nafion driers and an open split before introduction to an Isotope Ratio Mass Spectrometer (IRMS). The system was run in isocratic mode with no separation column. The mobile phase was degassed (90 min under vacuum in a 40°C ultrasonic bath) deionized water with 1 drop of 85% H_3PO_4 added

(Fisher Scientific HPLC grade). The same solution composition was used as the autosampler wash solution. Mobile-phase flow rate was 300 µL/min. A phosphoric acid solution (10% v/v of 85% H_3PO_4 in Milli-Q water, followed by degassing under vacuum as described for the mobile phase) was continuously mixed into the mobile phase within the Isolink at a rate of 50 µL/min. The Isolink reactor was set to 80°C.

Analytical runs were performed with three injections per sample, spaced 225 s apart. The three peaks were typically averaged, although if one peak was found to differ in peak area by more than 5% from the mean of the other two, it was discarded. Three CO_2 gas injections by the Isolink interface were also used to provide internal references for the mass spectrometer's Isodat software. Total run time was 11 min per sample. Overall precision of this method is ±0.04‰ (SD) on replicate samples (n = 10).

An internal standard seawater solution, consisting of a filtered, autoclaved coastal seawater sample allowed to equilibrate with the atmosphere at room temperature for 1 week before encapsulation in vials, was used periodically to provide a reference. This internal standard was calibrated to NBS 19 CaCO3 standard defined as having an isotopic composition of 1.95‰ versus VPDB (Coplen, 1996) using the method of Torres et al. (2005). Results are expressed as δ-values relative to the VPDB (Pee Dee Belemnite), as isotopic ratio between ^{13}C and ^{12}C defined:

$$\delta^{13}C(‰) = \left[\frac{\left(\frac{^{13}C}{^{12}C}\right)_{sample}}{\left(\frac{^{13}C}{^{12}C}\right)_{standard}} - 1 \right] \times 1000 \quad (1)$$

3.1.3. Labile Trace Element Concentrations

The labile trace elements concentration was measured using the Diffusive Gradient in Thin films (DGT) technique described by Larner et al. (2006). This technique was developed for the sampling and measurement of dissolved labile metals and is based on their diffusion through a diffusion layer of known thickness to a binding phase where they are concentrated (Davison and Zhang, 1994; Zhang and Davison, 1995). Thus it has the advantage of pre-concentrating the analyte in the binding phase, and eliminates matrix effects (Davison et al., 2000).

DGT samplers had been used for measuring labile metal concentrations in water (Davison et al., 1994), and also had been deployed in soils and sediments as a mean of determining pore water concentration of metals and their resupply flux from the solid phase (Harper et al., 1998).

The DGT device consists of a 4 cm diameter disk that uses a layer of Chelex resin impregnated in a hydrogel to accumulate the metals (www.dgtresearch.com, 12/01/15). The resin-layer is also covered by a filter membrane (figure 12) which is selective for free and weakly complexed species making this technique a reliable method for measuring the labile fraction of metals in solution (INAP, 2002).

Metals diffuse from solution across the filter and gel layers to the underlying resin where sorption process takes place (Practical guide for dealing with loaded DGT samplers – www.dgtresearch.com, 12/01/2015). It is the establishment of a constant concentration gradient in the diffusive layer that forms the basis for measuring metal concentrations in solution (INAP, 2002). According with manufacture (www.dgtresearch.com, 12/01/15), the optimal deployment time for DGT is 24 – 48h to achieve this equilibrium.

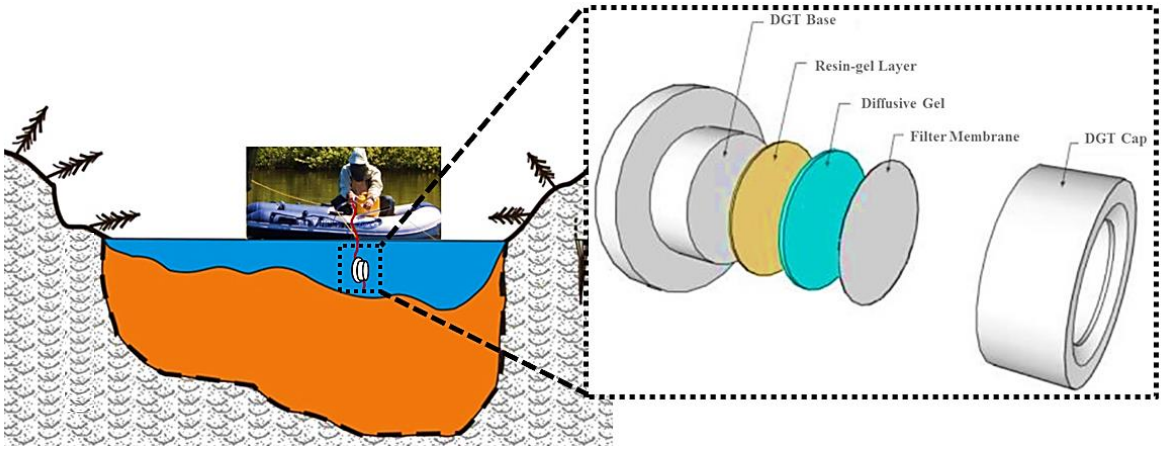

Figure 12: Schematic representations of DGT sampling on water at certain depth (on the left), and the components of a DGT unit (on the right).

The DGT samplers (purchased from DGT Research Ltd, UK) were used to quantify the labile metal fraction on water at different depths in all thermokarst lakes (table 2) with a minimum deployment time of 48h (table 3). Elution of metals from the Chelex binding phase (3.14 cm^2) was carried out by immersion in 5.0 ml of 1% (v/v) bi-distilled HNO_3. The elution extracts were then diluted with Milli-Q water (18 MΩ, Millipore) prior to ICP-MS analysis.

Table 3: Deployment time of DGT samplers on each lake.

Lake	SAS 1A	SAS 2A	BGR 1	KWK12
Deployment Time	2d 5h 46 min	2d 6h 20 min	2d 0h 0 min	3d 2h 30 min

The concentrations of Cu, Cr, Ni, Pb and Zn in the DGT's elution solution were measured by Inductively Coupled Plasma Mass Spectrometry (ICP-MS - Perkin Elmer ELAN DRC-e) using the follow isotopes: ^{63}Cu, ^{52}Cr, ^{60}Ni, ^{208}Pb, and ^{66}Zn.

ICP-MS is a type of mass spectrometry technique which is capable of detecting metals at concentrations as low as ppb (part per billion) on interfered low-background isotopes. This was achieved by ionizing the sample (ICP) and after using a mass spectrometer to separate and quantify those ions (Barshick, 2000). It is a technique with high precision and sensitivity, and with a low detection limit (Dean, 2005).

Typical ICP-MS equipment consists of a sample introduction system (a nebulizer and spray chamber), an inductively coupled plasma source, differentially pumped interface, ion optics, a mass spectrometer, and a detector as illustrated in figure 13 (Settle, 1997).

The ICP is a flowing, partially ionized gas (typically argon because of its simple background spectrum; Dean, 2005) which ionizes elements. Ionization efficiencies in the plasma are nearly 100% for elements with ionization potentials less than about 9 eV (Barshick, 2000).

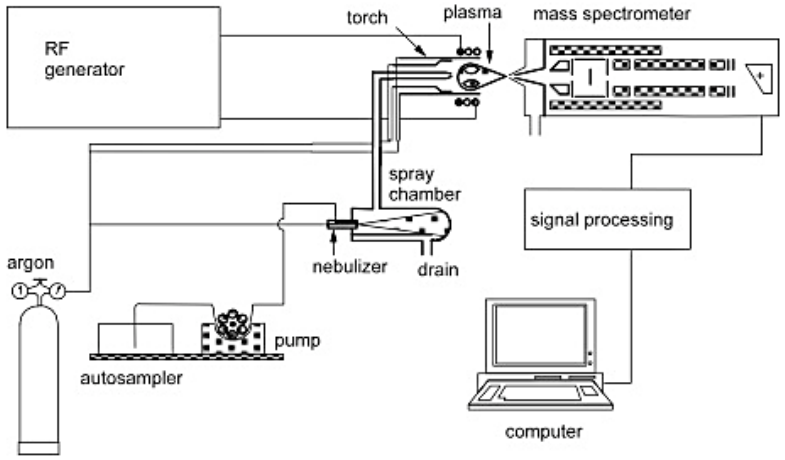

Figure 13: Schematic representation of an ICP-MS system. Extracted from http://www.chromedia.org/dchro/gfx/ZkanitsIK.jpeg (09/07/2015)

Mass spectra produced by ICP-MS are the mass-to-charge ratio intensity for elemental ions, polyatomic ions produced from plasma and solvent, and polyatomic ions produced from sample and solvent (Barshick, 2000). These can generate mainly isobaric and polyatomic interferences (Dean, 2005). Isobaric interferences result from the fact that elements have more than one isotope and can be avoided by selecting an alternative isotope (Kenneth, 2010). Polyatomic interferences are derived from the combination of two or more isotopes from different elements, which occur in the plasma (Dean, 2005; Kenneth, 2010).

Table 4 represented the isobaric and polyatomic interferences noted in the literature for the elements in this work. No isobaric interferences were predicted for the isotopes targeted in the present study. Polyatomic interference can and does occur in ICP-MS. However the use of cold plasma or reaction cells techniques can reduce or minimize this kind of interference (Dean, 2005).

Table 4: Interferences in ICP-MS. Isobaric interference reproduced from Dean (2005), and polyatomic extracted from May and Wiedmeyer (1998).

Element	Abundance (%)	Isobaric Interference	Polyatomic interference
^{27}**Al**	100	-	$^{12}C^{15}N^+$, $^{13}C^{14}N^+$, $^{14}N_2$ spread, $^{1}H^{12}C^{14}N^+$
^{52}**Cr**	83.8	N/D	$^{35}Cl^{16}O^{1}H^+$, $^{40}Ar^{12}C^+$, $^{36}Ar^{16}O^+$, $^{37}Cl^{15}N^+$, $^{34}S^{18}O^+$, $^{36}S^{16}O^+$, $^{38}Ar^{14}N^+$, $^{36}Ar^{15}N^{1}H^+$, $^{35}Cl^{17}O^+$
^{60}**Ni**	26.1	N/D	$^{44}Ca^{16}O^+$, $^{23}Na^{37}Cl^+$, $^{43}Ca^{16}O^{1}H^+$
^{63}**Cu**	69.1	N/D	$^{31}P^{16}O_2^+$, $^{40}Ar^{23}Na^+$, $^{47}Ti^{16}O^+$, $^{23}Na^{40}Ca^+$, $^{46}Ca^{16}O^{1}H^+$, $^{36}Ar^{12}C^{14}N^{1}H^+$, $^{14}N^{12}C^{37}Cl^+$, $^{16}O^{12}C^{35}Cl^+$
^{66}**Zn**	27.8	N/D	$^{192}Pt^{16}O^+$
^{208}**Pb**	52.3	N/D	$^{50}Ti^{16}O^+$, $^{34}S^{16}O_2^+$, $^{33}S^{16}O_2{}^{1}H^+$, $^{32}S^{16}O^{18}O+$, $^{32}S^{17}O_2^+$, $^{33}S^{16}O^{17}O^+$, $^{32}S^{34}S^+$, $^{33}S_2^+$

For this work, a dynamic reaction cell (DRC) was filled with a reactive gas (e.g. NH_3), and positioned between the ion optics and the mass spectrometer quadrupole. Interfering and analyte ions interact differently with the gas, and only the analyte ions pass through the cell to the mass spectrometer (Kenneth, 2010; Tannera and Baranova, 1999).

The quantification was made by an internal calibration method using Rhodium (^{103}Rh) as the internal standard, as follows: to an aliquot of 5 mL of each water sample was added Rh 10 ppb, prepared from a stock solution 1000 ± 10 ppb, to correct any instrument drifts.

Multi-element stock standard 3 solution (Perkin Elmer), ultrapure water (18 MΩ, Millipore), and bi-distillate 1% HNO_3 were used for prepared standard solutions of elements between 50 ng/L and 200 µg/L. Also blanks were prepared for quality control. Rh 10 ppb was added to all standard solutions and blanks.

Samples, standard solutions and blanks were analyzed five times by the ICP-MS. Table 5 indicates the operating conditions used.

Table 5: Operate conditions for ICP–MS during DGT samples analysis.

Parameter	Operating condition
ICP RF Power	1100.00 W
Nebulizer gas flow	0.78 L/min
Auxiliary gas flow	1.20 L/min
Plasma gas flow	15.00 L/min
Replicates	5
Monitored isotopes	^{63}Cu, ^{52}Cr, ^{60}Ni, ^{208}Pb, and ^{66}Zn
Acquisition Time	~12 min/element

Calibration curves obtained by standards are represented in table 6, where slope, intercept, and correlation coefficient values for each curve are represented with 95% confidence. In annex B the calculation of these errors (for solid samples) are provided.

Table 6: Calibration curves parameters with 95% confidence for each element.

Element	Slope (x10^{-2})	Intercept (x10^{-3})	R^2
Cr	4.7 ± 0.5	-1± 3	0.9998
Ni	1.17 ± 0.02	(1 ± 4)x10^{-1}	0.9999
Cu	2.5 ± 3.6	-1 ± 2	0.9999
Zn	(6.7 ± 0.1)x10^{-1}	1 ± 6	0.9998
Pb	7.9 ± 0.2	1 ± 2	0.9997

The dissolved metals concentration on samples ($\boldsymbol{C_{DGT}}$) were calculated using the follow equation (Larner et al., 2006):

$$\boldsymbol{C_{DGT}} = \boldsymbol{C_{ICP}} \times \frac{\boldsymbol{V_{HNO_3}} + \boldsymbol{V_{gel}}}{\boldsymbol{f_e}} \times \frac{\Delta \boldsymbol{g}}{\boldsymbol{D.t.A}} \qquad (\mathbf{2})$$

Where:
$\boldsymbol{C_{ICP}}(\mu g/L) - concentration\ of\ metal\ in\ the\ elution\ solution, measured\ directly\ by\ ICP-MS$
$\boldsymbol{V_{HNO_3}} - volume\ of\ acid\ added\ to\ the\ resin\ gel$
$\boldsymbol{V_{gel}} - resin\ gel\ volume\ (0.15\ mL)$
$\boldsymbol{f_e} - elution\ factor\ representing\ the\ eluted\ to\ bound\ metal\ ratio\ (0.8)$
$\Delta \boldsymbol{g} - thickness\ of\ the\ diffusive\ gel\ plus\ the\ thickness\ of\ the\ filter\ membrane\ (0.78\ mm)$
$\boldsymbol{D}(cm^2.s^{-1}) - the\ difusion\ coefficient\ of\ metal\ in\ the\ gel$
$\boldsymbol{t} - the\ deployment\ time$
$\boldsymbol{A} - exposure\ area\ (3.14\ cm^2)$

Diffusion coefficients were corrected for the field temperature (in ºC) using the equation (Zang and Davidson, 1995):

$$\log(D_T) = \frac{1.37023 \times (T-25) + 8.36 \times 10^{-4} \times (T-25)^2}{109 + T} + \log\left(\frac{D_{T=25°C} \times (273+T)}{298}\right) \qquad (3)$$

Values of $D(T = 25ºC)$ were extracted from the practical guide of DGT search (www.dgtsearch.com, 12/01/15), and the calculated D are indicated in annex E.

3.1.4. Total Element Concentrations

For the determination of the total concentrations of trace elements the ICP-MS technique described in the previous section was used by analyzing directly the filtered and acidified water samples. Again, internal standard method was used to quantify these elements using Rhodium (^{103}Rh) as internal standard.

Multi-element stock standard 3 solution (Perkin Elmer), ultrapure water (18 MΩ, Millipore), and bi-distillate 1% HNO_3 were used for prepared standard solutions of elements between 100 ng/L and 200 µg/L. Also blanks were prepared for quality control. Rh 10 ppb was added to all standard solutions and blanks.

Table 7 indicates the operating conditions used.

Table 7: Operating conditions for ICP–MS during water samples analysis.

Parameter	Operating condition
ICP RF Power	1100.00 W
Nebulizer gas flow	0.78 L/min
Auxiliary gas flow	1.20 L/min
Plasma gas flow	15.00 L/min
Replicates	5
Monitored isotopes	^{27}Al, ^{63}Cu, ^{52}Cr, ^{60}Ni, ^{208}Pb, and ^{66}Zn
Acquisition Time	~12 min/element

Calibration curves obtained by standards are represented in table 8, where slope, intercept, and correlation coefficient values for each curve are represented with 95% confidence.

Table 8: Calibration curve parameters with 95% confidence limits for each element.

Element	Slope (x10^{-2})	Intercept (x10^{-3})	R^2
Al	4.5 ± 0.3	(0.5 ± 1.0)x10^{2}	0.9969
Cr	(5.6 ± 0.6)x10^{-1}	-0.2± 1.4	0.9989
Ni	1.48 ± 0.7	-1.7 ± 3.7	0.9994
Cu	3.1 ± 0.2	-2 ± 6	0.9994
Zn	(9.6 ± 1.2)x10^{-1}	-1 ± 6	0.9954
Pb	7.3 ± 2.3	(-0.1 ± 2.5)x10^{2}	0.9954

The total metal concentration on water samples ($\boldsymbol{C_{water}}$) were determined directly by the calibration curves:

$$\boldsymbol{C_{water}[\mu g/L] = C_{ICP}} \qquad (\mathbf{4})$$

3.1.5. Total Dissolved Inorganic Sulphide

Total dissolved inorganic sulphide, $[\mathrm{HS^-}]_t$ ($\sum[\mathrm{H_2S}] + [\mathrm{HS^-}] + [\mathrm{S^{2-}}] + [\mathrm{S_X^{2-}}]$), was measured by differential pulse cathodic stripping voltammetry (DPCSV) (Luther et al., 1985; Luther and Tsamakis, 1989).

Voltammetry conducted with a dropping-mercury electrode (DME) is called polarography (Harris, 2010). Polarography is an analytical technique that was used to quantify sulphur in sediments for the first time in 1991 (Henneke et al., 1991). It is an electrochemical method of analyzing solutions described by Jaroslav Heyrovský, in 1922 (Bond, 1980).

In stripping analysis, dissolved sulphide from a solution is concentrated into a thin film of Hg by electro-reduction described by the equation (Luther et al., 1985):

$$HS^{-}(aq) + Hg^{0}(l) + OH^{-}(aq) \rightarrow HgS\ (ads) + 2e^{-} + H_2O(l) \qquad (5)$$

Reversing the direction of the voltage sweep sulphide re-dissolves, regenerating the mercury electrode (Luther et al., 1985):

$$HgS\ (ads) + H_2O(l) + 2e^{-} \rightarrow Hg^{0}(l) + HS^{-}(aq) + OH^{-}(aq) \qquad E_{1/2} = -680\ mV \qquad (6)$$

Peak current measured during oxidation is proportional to the quantity of sulphide that was deposited (Harris, 2010).

For our samples an aliquot of 100-1000 µL of water was added to a polarographic cell containing 10 mL NaCl 36 $g.dm^{-3}$ solution at pH 10-12 (measured in 1M NaOH solution) and following by degassed with nitrogen.

Total dissolved sulphide in these samples was measured in a Metrohm apparatus equipped with a 693 VA processor and a 694 VA station (figure 14). This model has a DME incorporated (work electrode) and both an Ag/AgCl/NaCl (36‰) standard electrode and a platinum electrode as an auxiliary.

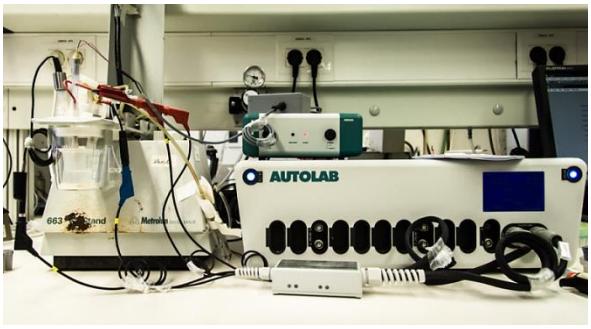

Figure 14: Metrohm apparatus used to determine the sulphide concentration.

A standard curve was constructed using 500 mg/L of $Na_2S.H_2O$ (anhydrous, Alfa product) as standard solution, dissolved in Milli-Q water also degassed with nitrogen. The quantification of the analyte was made using the standard addition method. For that, 100 and 200 µL of the standard sulphide solution was added to the samples during measurements

The deposition of HgS was made during 60s at constant potential of -400 mV, and the cathodic sweep was made using 5 mV/s potential scan rate from -400 to -900 mV. The quantification of standards and samples was made by the height of the peak at -680 mV by DPCSV method using the standard addition method.

3.1.6. Dissolved Sulfate

The determination of sulfate in water was made by turbidimetric methods where precipitation of sulfate with barium ions is followed by photometric monitoring of the resulting suspension (Elenkova et al., 1979; Kolmert et al., 2000).

The turbidimetric method was described by Rossum and Villarruz (1961). To an aliquot of 100-200 µL of water sample diluted in 21 mL of Milli-Q water, was added 5 mL of the conditioning reagent. This reagent contained 75 g of NaCl, 50 mL of glycerol, 30 mL of concentrated HCl, and 100 mL of ethanol (90% (v/v)), made up to 500 mL with Milli-Q water.

To the mixture, crushed barium chloride dihydrate crystals ($BaCl_2.2H_2O$ from Merck, Germany) were added until the saturation point was reached. The solution was mixed in a magnetic stirrer for 60 s at a constant speed.

The absorbance of the suspension was determined at 400 nm using a Hitachi U-2000 spectrophotometer providing a light path of 5 cm (figure 24). A mixture made up to 500 mL with Milli-Q water, with 5 mL of the conditioning reagent and crushed $BaCl_2.2H_2O$ crystals (without sulfate) served as blank.

Figure 15: Hitachi-2000 spectrophotometer used for the sulfate analysis.

Concentrations of sulfate were determined by the calibration curve method using anhydrous Na_2SO_4 solution as standard (0-10 mM). The standard solutions were submitted to the procedure described above so the turbidity between them and the samples was similar.

3.1.7. Trace Elements Remobilization Tests

Metal-organic complexes may be formed between metallic cations and dissolved organic carbon (DOC). These complexes include those with simple aliphatic or aromatic substances or more structurally complex humic substances (Hooda, 2010).

Several studies on surface waters show that UV induces degradation of organic matter (Corin et al., 1996; Dahlén et al., 1996) which in turn can release and enhance trace elements on water column (Shiller et al., 2006; Winch et al., 2002).

In order to evaluate amount of trace-elements complexed with DOC, sampled water samples were submitted to analytical treatment described by Mann et al. (2015).

Thus, to a 10 mL of surface water sample (acidified) from each lake, 200 µL of $K_2S_2O_8$ was added. After the water was placed in an incubation camera in the presence of ultraviolet light (UV-A + UV-B) for 45 min, to oxidize all DOC to CO_2. The samples were analyzed by ICP-MS as described above. In order to access the remobilization percentage, the ratio between the amount of remobilized element and the initial labile content was used, described by:

$$Remobilization\ (\%) = \frac{Total\ Concentration\ (3.1.7) - Labile\ Concentration\ (3.1.3)}{Labile\ Concentration\ (3.1.3)} \times 100 \qquad (7)$$

3.2. Soil and Sediment Samples

3.2.1. Sedimentary Organic Matter

Loss on ignition (LOI) analysis is a method used to determine the organic matter content (% OM) of a solid sample (Robertson, 2011).

This method involves the removal of organic matter by combustion of a sample at high temperature (375ºC to 800ºC) in a temperature-regulated muffle furnace, but not so high as to decompose carbonates (Schulte and Hopkins, 1996).

The principal errors in this method arise through incomplete combustion when the temperature or time allowed for combustion is insufficient, and through losses resulting from the use of too high a temperature (Carter and Gregorich, 2008; Schulte and Hopkins, 1996).

Also any material that losses moisture below 360°C is a potential source of error, and thus the samples must be dried (105ºC–110ºC) before using LOI method (Carter and Gregorich, 2008). The substance remaining after ignition is the ash (mineral impurities such as sand) and the lost weight on ignition is considered as an approximate measure of the sedimentary organic matter content (Combs and Nathan, 1998). Vessels suggested for ashing are porcelain, quartz, or platinum dishes (Carter and Gregorich, 2008).

In this work an aliquot of each solid sample ($\mathbf{M_{initial}}$) was dried into a high-form porcelain crucible at 105ºC overnight in an oven before ashing, until constant weight ($\mathbf{M_{105}}$). After dried the vessels was allow to cool down in a desiccator and the total humidity (% H) present may be calculated using (Carter and Gregorich, 2008):

$$\%\ H = \frac{M_{initial} - M_{105}}{M_{initial}} \times 100 \qquad (8)$$

The sedimentary organic matter (LOI) content can be estimated by bringing the oven to 450° C for 2h until constant weight (**M_{450}**). According with Williams (1985), at this temperature there is no carbonate decomposition. LOI was calculated by (Carter and Gregorich, 2008):

$$\% \, LOI = \frac{M_{105} - M_{450}}{M_{105}} \times 100 \qquad (9)$$

The measurements for this method were performed in an analytical scale with an error of ±0.0001 g. The errors associated to **$M_{initial}$**, **M_{105}**, **M_{450}** and LOI (%) were calculated according to the propagation of random errors theory (Harris, 2010) where a function $\mathcal{R} = \mathcal{R}(a_1, a_2, \dots, a_n)$ has a total error determined by:

$$\sigma_{\mathcal{R}} = \sqrt{\left(\frac{\partial \mathcal{R}}{\partial a_1}\right)^2 {\sigma_{a_1}}^2 + \left(\frac{\partial \mathcal{R}}{\partial a_2}\right)^2 {\sigma_{a_2}}^2 + \cdots + \left(\frac{\partial \mathcal{R}}{\partial a_n}\right)^2 {\sigma_{a_n}}^2} \qquad (10)$$

With $\sigma_{a_1}, \sigma_{a_2}, \dots, \sigma_{a_n}$ been the errors associated to parameters $a_1, a_2, \dots, a_n$ respectively.

3.2.2. Natural Organic Matter Characterization

The natural organic matter characterization was performed by solid-state nuclear magnetic resonance, ssNMR, which is an absorption spectrometry technique, where a solid sample absorbs electromagnetic radiation in the radio frequency region at their characteristics frequencies, when submitted to a strong magnetic field. This absorption is a function of ^{1}H or ^{13}C nuclei present in the molecule (Fifield and Kealey, 2000). ^{13}C nucleus has a spin number of ½ making it magnetically "active". However, since the natural abundance of ^{13}C is only 1.1% that of ^{12}C, the overall sensitivity compared with ^{1}H is about 1/5700 (Silverstein et al., 1991).

A NMR spectrum represents the intensity of that absorption as a function of the chemical shift (δ, ppm), which normally range from 0 to 200 ppm (ChemWiki Site, 09/07/2015), and are related to the carbon hybridization (sp^3, sp^2, and sp, for ^{13}C spectrum) which absorbs at different strength (Fifield and Kealey, 2000). Typical chemical shift regions of a ^{13}C NMR spectrum are presented in figure 16.

Organic matter analysis of soils by ^{13}C ssNMR provide information regarding the relative quantities of substituted aliphatic, aromatic, phenolic, carboxylic and carbonyl C compounds, with a small amount of sample (200–500 mg of sample depending on the type of NMR probe, Dai et al., 2002).

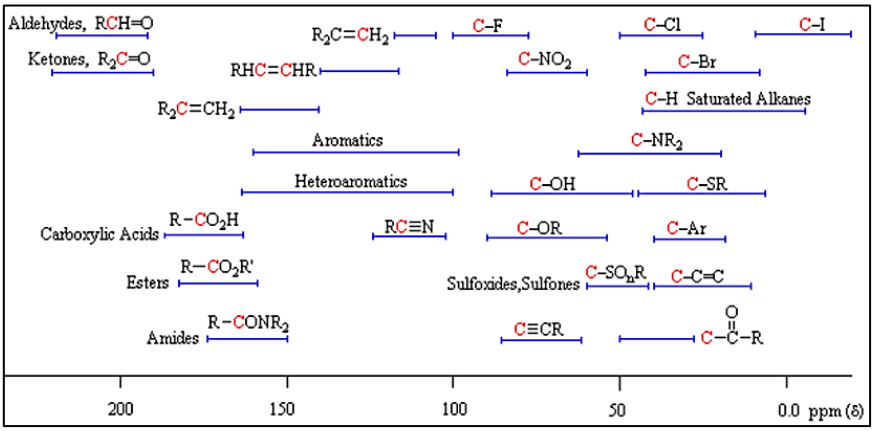

Figure 16: Typical chemical shifts regions on a ^{13}C NMR spectrum. Extracted from http://www.cem.msu.edu/~reusch/OrgPage/nmr.htm (09/06/2015)

Lake samples (200–400 mg) were packed into 7 mm zirconium rotors closed with Kel-F caps. High-resolution ^{13}C ssNMR spectra were measured using Magic Angle Spinning (MAS) and Cross Polarization (CP) recorded on a Bruker Avance 300 MHz spectrometer (figure 17) equipped with a 7 mm Wide Bore MAS probe operating at ^{13}C resonating frequency of 75.5 MHz (Piccolo et al., 2008).

The qualitative and semi-quantitative compositions were obtained by cross polarization (CP) and total sideband suppression (TOSS) at a spinning speed of 5 kHz and a CP time of 1 ms with a ^{1}H 90º pulse-length of 4 µs and a recycle delay of 5 s (Cao et al., 2011).

Figure 17: ^{13}C NMR spectrometer Bruker Avance 300 MHz used in IST-UL NMR lab.

Glycine was used as a reference for the carbonyl signal set at 176.03 ppm (Pines et al., 1973). In order to interpret the ^{13}C ssNMR results each spectrum was divided into eight shift regions, and assigned according to published studies as indicated in table 9 (Cao et al., 2011; Mao et al., 2011).

Table 9: Region assignments of chemical shift (ppm) in ^{13}C ssNMR spectra to types of carbon representing structural units or molecular components of soil organic matter.

Chemical shift region (ppm)	General assignment	Carbon type in relation to structural units
0 – 45	Alkyl C	CH_x; most commonly in lipids and aliphatic chains of amino acids
45 – 63	Methoxyl or N-alkyl C	OCH_3 feature in lignin components; NCH occurs in peptides
63 – 90	O-alkyl C	OCH or OC commonly in polysaccharides
90 – 110	Anomeric C	Double oxygen substituted alkyl-C, present in polysaccharides sugar ring
110 – 143	Aromatic C	Non-substituted, alkyl-substituted, or fused-ring carbons in aromatic rings
143 – 161	Aromatic C – O	Oxygen-substituted carbons on aryl rings, common in lignin
161 – 190	Carbonyl C (type II)	C=O in COO (carboxyl group) or N-C=O (peptides)
190 – 220	Carbonyl C (type I)	C=O in ketones and aldehydes

Analyses were performed without any sample treatment, except for BGR 1 lake samples. Due to the low organic matter content on them, it was necessary to eliminate any non-material (such as silicates), and thus increasing the OM content.

The procedure used on these samples is described in Schmidt et al. (1997), and it's based on hydrofluoric acid treatment. According to Rumpel et al. (2004) treatment with HF has been proven to increase the ^{13}C spectra resolution. Thus, for the BGR samples, to a 3 g of sample of soil 25 mL of 10% (v/v) HF was added in a Falcon tube, with 1 min of vigorous agitation. The resulting suspension was let to settle for 24h, after which Milli-Q water was added for washing. The mixture was then decanted, and the solid fraction dried at 40ºC on an oven. The supernatant was discharged. The dried solid was pulverized in an agate mortar for ^{13}C ssNMR analysis.

3.2.3. Mineralogical Composition

X-Ray diffraction analysis is the premier tool for a direct identification of crystalline compounds soil minerals (Essington, 2005).

X-radiation is produced by bombarding a metal foil (commonly Cu foil) with electron beam. The bombarding electrons collide with electrons that reside in the electronic orbitals of the foil metal, displacing the orbital electrons and leaving vacancies in the orbitals. The resulting unstable electronic configuration is immediately stabilized by outer shell electrons that drop down (in energy and location) to fill the vacancies (Essington, 2005; Pansu and Gautheyrou, 2003). The energy lost in this process is released in the form of x-radiation. The X-Rays produced by this process are termed characteristic X-Rays, meaning that the wavelength of the X-Rays is characteristic of the element being bombarded (Essington, 2005).

The X-Ray produced consists of several components characteristic of the target material (Cu, Fe, Mo, and Cr), and thus a filter foil or monochromatic crystal, is required to produce monochromatic X-Rays needed for diffraction, as illustrated in figure 18 (Pansu and Gautheyrou, 2003).

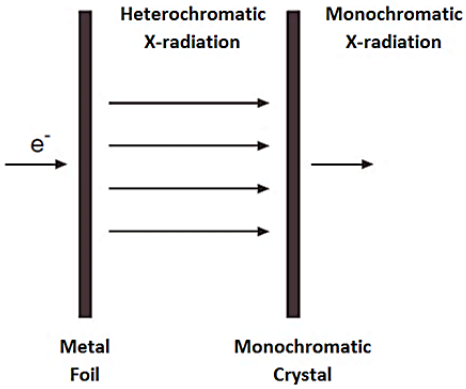

Figure 18: Production of heterochromatic radiation by a metal foil (Cu, Cr, Fe or Mo). Because a monochromic radiation is need to X-Ray diffraction, the use of a monochrometer is necessary. Modified from Essington (2005) pp 92.

Once produced, the monochromatic X-Rays are focused on the sample. Some of the X-Rays pass through the sample, while some are diffracted or scattered by the atoms in the various minerals (Barnett et al., 1999). As the sample and detector are rotated, the intensity of the reflected X-Rays is recorded. When the geometry of the incident X-Rays impinging the sample satisfies the Bragg Equation, constructive interference occurs and a peak in intensity occurs (Jenkins, 1986).

The geometry of an X-Ray diffractometer is such that the sample rotates in the path of the collimated X-Ray beam at an angle θ while the X-Ray detector is mounted on an arm to collect the diffracted X-Rays and rotates at an angle of 2θ (Essington, 2005). For typical powder patterns data is collected typically at 2θ from 5° to 70° angles present in an X-Ray scan such as represented in figure 19.

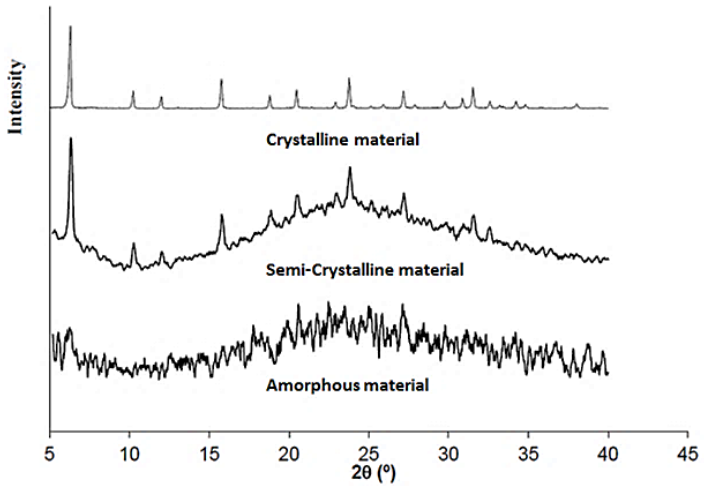

Figure 19: Typical diffractogram of three different materials: (a) crystalline material; (b) semi-crystalline material; (c) amorphous material.

In this work, 200-300 mg of solid samples was submitted to X-Ray Power Diffraction (XRPD) analysis, and data was collected by specialized technicians in a D8 Advance Bruker AXS θ-2θ diffractometer (figure 20), with Ni-filtered Cu Kα radiation (λ = 1.5406 Å) operated at 40 kV and 40 mA. The diffractometer is equipped with an Anton Paar HTK 16N high-temperature chamber, and an Anton Paar TCU 200N temperature control unit (André and Duarte, 2014).

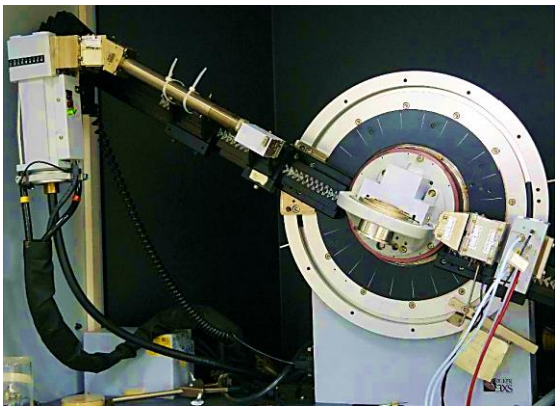

Figure 20: X-Ray diffractometer of Bruker D8 Advance used on this work.

Bragg's law, defined by $\mathbf{n\lambda = 2d.sin\theta}$ that relates the wavelength of the electromagnetic radiation and the number of diffraction planes (n) to the diffraction angle (θ), and the lattice spacing in a crystalline sample (d), was used to compute the crystallographic spacing (Caglar et al., 2009). A 2θ ranging from 5 to 80º was used for experiments pattern acquisition using a scanning rate of $60^{o}.h^{-1}$ (Martinez et al., 2008).

In the resultant diffractogram, the space between planes of atoms (d) determines the peak positions, and their intensity depends on the atoms present in the plane (Hillier, 1999).

A pattern fitting of sample diffractograms was carried out, with an ICDD (International Centre for Diffraction Data) software database (PDF-2). This software proposes a list of patterns supposed to fit with the experimental data. The comparison of standard patterns to experimental patterns was made by specialized technician.

3.2.4. Total Element Concentrations

Total elemental concentrations in samples were determined by ICP-MS. Samples analyzed by this technique are usually liquid (or a solution), and therefore dissolution of solid samples is required (Voellkopf et al., 1992). In the case of organic matrices, an oxidizing mixture is used to destroy the entire matrix and solubilize the analytes (Winefordner, 2003). Accordingly hydrogen peroxide may be added to increase the oxidizing power of the digestion solution.

In our work approximately 200 mg of each sample were digested in closed Teflon bombs with 1 mL of *aqua regia* (double-distilled 35% (v/v) HCl; bi-distilled 65% (v/v) HNO_3) and 6 ml of 40% (v/v) HF on an oven at 100°C for 1h. *Aqua regia* mixture is used to digested metals, alloys, sulfides and other ores, and HF digests inorganic material, e.g. silicates (Winefordner, 2003).

Evaporation to dryness was performed after acid digestion in a sand bath at 90°C in order to evaporate the HF acid. To the residue obtained was added 6 mL of a 1:2 mixture of H_2O_2 (30% w/v; Panreac, Spain) and bi-distilled HNO_3 1% (v/v).

The mixture was heated at 80ºC for 1h in open Teflon bombs. After cooling to room temperature the samples digests were carefully transferred to sample vials and diluted to 50 mL using ultrapure Milli-Q water, and refrigerated at 4ºC until analysis.

The certificate reference materials (CRM) used for recovery and quality control studies were from NIST (National Institute of Standards and Technology, Gaithersburg, MD, USA): CRM 1646 (estuarine sediment), CRM 2704 (river sediment) and CRM IAEA-SOIL-7 (superficial soil). For correcting any instrument drifts Rhodium (^{103}Rh) 10 pbb (prepared from a stock solution 1000 ± 10 ppb) was added as internal standard to all samples and CRMs. In addition, a blank digestion was performed in order to correct the obtained analytical results.

Multi-element stock standard 3 solution (Perkin Elmer), ultrapure water (18 MΩ, Millipore), and bi-distillate 1% HNO_3 were used for prepared standard solutions of elements between 100 ng/L and 200 µg/L.

Digested samples, standard solutions and blanks were analyzed five times by ICP-MS (Perkin Elmer ELAN DRC-e) as illustrated in figure 21. Table 10 indicates the operating conditions used.

Table 10: Operate conditions for ICP–MS during digested samples analysis.

Parameter	Operating condition
ICP RF Power	1100.00 W
Nebulizer gas flow	0.80 L/min
Auxiliary gas flow	1.20 L/min
Plasma gas flow	15.00 L/min
Replicates	5
Monitored isotopes	^{27}Al, ^{63}Cu, ^{52}Cr, ^{60}Ni, ^{208}Pb, and ^{66}Zn
Acquisition Time	~12 min/element

Figure 21: ICP-MS filter quadrupole mass of ELAN DRC-e Perkin Elmer used on this work (C^2TN).

Calibration curves obtained with the standards are presented in table 11, where slope, intercept, and correlation coefficient values for each curve are represented with 95% confidence.

Table 11: Calibration curves parameters with 95% confidence for each element. The errors are calculated in annex B.

Element	Slope (x10^{-2})	Intercept (x10^{-1})	R^2
Al	4.5 ± 0.3	1 ± 1	0.9984
Cr	5.6 ± 0.2	1 ± 1	0.9997
Ni	1.40 ± 0.04	0.2 ± 0.3	0.9997
Cu	3.2 ± 0.2	0.3 ± 1.0	0.9988
Zn	0.83 ± 0.03	0.1 ± 0.3	0.9998
Pb	6.3 ± 1.0	1 ± 2	0.9965

The elements concentration in the samples was calculated using the follow equation:

$$\boldsymbol{C_{soil/sed}[\mu g/g_{soil/sed}] = C_{ICP}[\mu g/L] \times 50\ mL \times \frac{1}{M_{soil/sed}[mg]}} \qquad (11)$$

Where C_{ICP} is the element concentration determined directly by the calibration curve, and $M_{soil/sed}$ is the mass of solid samples used for digestion. The uncertain of $C_{soil/sed}$ was calculated by expression indicated in annex B.

3.2.5. Solid Sulphur Compounds

Before the analysis of the sulphur compounds, total sulphur concentrations were determined in sediment samples by elemental analysis on a partner laboratory. This analysis was performed in a CHNS Fissons NA1500 Analyser following the method described in Canário (2004).

The usually reduced sulphur species found in sediments are pyrite, acid volatile sulfides (AVS = ΣH_2S + FeS), and elemental sulfur (S^0) and their sum are defined as the total inorganic sulphur (Zopfi et al., 2008):

$$S_{inorganic} = AVS + Pyrite + S^0 \qquad (12)$$

In this work the concentration of pyrite and S^0 in sediments were determined by the chromium reduced sulphur (CRS = S^0 + FeS_2) method described by Canfield et al. (1986). The AVS concentration is obtained by acid attack (HCl 1M) to produced H_2S that is then trapped on NaOH 1M solution (Henneke et al., 1991; Zopfi et al., 2008). The base of these methods is the reduction of sulphur compounds to H_2S, which is collected in alkaline solution following the equation:

$$H_2S(g) + OH^-(aq) \rightarrow HS^-(aq) + H_2O(l) \qquad (13)$$

CRS has proven to be specific for inorganic sulphur with an accuracy that is not affected by the presence of organic sulphur (Canário et al., 2003). Before analysis, S^0 was extracted from 100 mg of dried sediment by 16h stirring with 20 mL of acetone followed by centrifugation (3000 rpm/10 min) and filtration through 0.45 µm membranes. The residue was then placed in the reaction vessel with 10 mL HCl 1M and purged with N_2 for 20 min to release AVS (reaction time of 15 min). After, 50 mL of $CrCl_3$ in 1 *N* HCl was added and let to react over 1h, during which the solution was stirred and flushed with N_2.

The H_2S produced was collected in 20 mL of 1M NaOH. Method recoveries were evaluated by using the same methodology with standard pyrite sample (Alfa Aesar products). Recoveries were more than 97% using this procedure.

Elemental sulphur was determined using the same CRS method but in the acetone extracts. The measurements of the released H_2S were made by Differential Pulse Polarography (DPP) using a Metrohm apparatus equipped with a 693 VA processor and a 694 VA station (described above). This model has a DME incorporated (work electrode) and both an Ag/AgCl/NaCl (36‰) standard electrode and a platinum electrode as an auxiliary.

Acid volatile sulphides, mainly amorphous iron sulfides and poorly crystallized Fe-oxides were extracted with 1M HCl during 30 min (Luther et al., 1991; Henneke et al., 1991). Sulphide was trapped in 20 mL de-aerated NaOH solution and analyzed by DPP as described above. Figure 22 represents the AVS extraction procedure used.

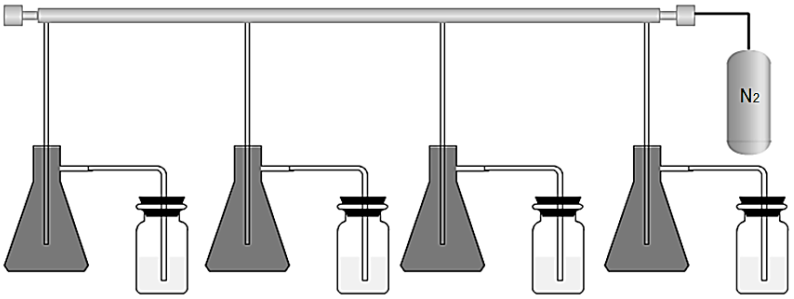

Figure 22: AVS extraction scheme. Erlenmeyer contain HCl solution, and in the flask contain NaOH solution.

A calibration curve was constructed using 500 mg/L $Na_2S.H_2O$ (anhydrous, Alfa product) as standard solution, dissolved in Milli-Q water degassed with nitrogen. 100 and 200 µL of it was added to the samples.

The quantification of standards and samples was made by the peak height at -680 mV using the standard addition method.

3.2.6. Sequential extractions

The basis of sequential extractions is that the most labile metals are removed in the first fraction and continue in order of decreasing of mobility (Zimmerman and Weindorf, 2010). In this work the sequential extraction method used is the one described by Tessier et al. (1979).

Each sediment sample (~ 1g) was stirred for 6h with 20 mL of $NH_2OH.HCl$ 0.04 M solution in CH_3COOH (25%) according to the method described by Chester and Hughes (1967). The supernatant solution was removed by centrifugation at 3000 rpm for 10 minutes and filtered through 0.45 mm membranes.

The solid residue is then submitted to HCl 1M extraction, which extract the sulphide present, and also the metal associated to it (Simultaneously Extracted Metals, SEM), according with (Madureira, 1997):

$$MeS(aq) + 2HCl(aq) \rightarrow H_2S(\uparrow) + MeCl_2(aq) \qquad (14)$$

Where Me represents a generic metal associated to sulphide. The supernatant was then removed by centrifugation at 3000 rpm for 10 minutes and filtered through 0.45 mm membranes.

The last extraction consisted on addition of H_2O_2 followed by UV irradiance, which extracts the metals bounded to organic matter, which under oxidizing conditions can be degraded, leading to a release of soluble trace metals (Tessier et al., 1979). Again supernatant was then removed by centrifugation at 3000 rpm for 10 minutes and filtered through 0.45 mm membranes.

Trace elements were determined in all extracted solutions by Graphite Furnace Atomic Absorption Spectrometry (GFAAS, Perkin Elmer AAnalyst 600).

3.3. Quality Assurance and Quality Control

Quality control of results was a major concern in all analytical methods applied. Thus, replicates were used to validate the accuracy and precision of the obtained results. The Limit of Detection (LD) and Limit of Quantification (LQ) were calculated from the calibration curves obtained using the following expressions (Harris, 2010):

$$LD = 3\frac{S_y}{m} \qquad (15)$$

$$LQ = 10\frac{S_y}{m} \qquad (16)$$

Where m is the slope of each curve and S_y is the standard deviation determined by:

$$S_y = \sqrt{\frac{\sum(y_i - y)^2}{N - 2}} \qquad (17)$$

Also the variation coefficient (CV_m) of each method was determined using

$$CV_m(\%) = \frac{S_m}{\bar{x}} \times 100 \qquad (18)$$

Where $\bar{x}$ is the average of the standard solutions used and S_m is the standard deviation of the method calculated by:

$$S_m = \frac{S_y}{m} \qquad (19)$$

Blanks, certificate reference materials (CRM) and five random replicates were used to validate the accuracy of the obtained results, and their precision on digestion procedure. Also two blanks of DGT were prepared to check any water and nitric acid contaminations. During ICP-MS analysis of samples, calibration check was performed using a 20 ppb standard solution, and blanks prepared daily. Table 12 presents the concentration for elements (µg/L) in the blanks used.

Table 12: Concentration of elements (µg/L) in the blacks obtained for each element.

µg/L	Cr	Ni	Cu	Zn	Pb	Al
***Blank I**	132.8	156.5	0.7	1.3	0.2	40.2
Blank II	0.2	0.1	0.5	5.0	0.7	90.5
Blank III	0.6	0.2	0.3	19.5	8.9	12.2
DGT Blank I	0.1	0.2	0.4	1.0	0.1	-
DGT Blank II	0.2	0.2	0.3	1	0.6	-

An abnormal contamination of elements was found in blank I used on the first day of soils and sediments digestion. Because *aqua regia* used were freshly made every day, we can attribute these values probable to a random event of contamination such the falling of a piece of dust into the sample, the inadvertent touch of a dirty glove, or even by the presence of high analyte in the adjacent sample.

In order to evaluate the accuracy of the procedure, three certificate reference materials (CRM) were used in acid digestion from NIST (National Institute of Standards and Technology, Gaithersburg, MD, USA): CRM 1646 (estuarine sediment), CRM 2704 (river sediment) and CRM IAEA-SOIL-7 (superficial soil). Table 12 compares the certificates values obtained, to the experimental values. The recovery of trace elements is also represented, which were determined by:

$$Recovery(\%) = \frac{Observed\ Value}{Certificated\ Value} \times 100 \qquad (20)$$

Table 13 represents the mean values obtained, and the standard deviation of Al (%), and Cr, Ni, Cu, Zn and Pb in µg/g for CRMs 1646, 2704 and IAEA-SOIL-7.

Table 13: Mean values obtained and standard deviation of Al (%), and Cr, Ni, Cu, Zn and Pb in µg/g. The recovery (%) is also presented.

CRM		Cr (µg/g)	Ni (µg/g)	Cu (µg/g)	Zn (µg/g)	Pb (µg/g)	Al (%)
SRM 1646	Certificated	76 ± 3	32 ± 3	18 ± 3	138 ± 6	28.2 ± 1.8	6.25 ± 0.20
	Obtained	60 ± 2	31 ± 1.3	18 ± 2	115 ± 4	23 ± 3.4	4.94 ± 0.08
	Recovery (%)	80 ± 4	96 ± 10	99 ± 19	84 ± 4.6	82 ± 13	79 ± 3
SRM 2704	Certificated	135 ± 5	44.1 ± 3.0	98.6 ± 5.0	438 ± 12	161 ± 17	6.11 ± 0.16
	Obtained	111 ± 3	42±1.5	70 ± 4.4	353 ± 13	121 ± 80	4.69 ± 0.08
	Recovery (%)	83 ± 3.8	95 ± 7.3	71 ± 5.8	81 ± 3.7	75 ± 9.4	77 ± 2.4
IAEA-Soil-7	Certificated	60 ± 13	26 ± 8	11 ± 2	104 ± 6	60 ± 15	4.7 ± 0.4
	Obtained	39 ± 1	25 ± 1	8.2 ± 1.5	91 ± 3	15 ± 2	0.86 ± 0.03
	Recovery (%)	66 ± 14	95 ± 30	75 ± 19	87 ± 6	25 ± 7.4	18 ± 1.7

High recovery of metals was obtained ranging from 71 to 99% with exception of lead and aluminum in IAEA-Soil-7 that was 25 and 18% respectively. Also chromium appears to have a lower recovery percentage in this soil, compared with the other two. This wasn't possible to explain although a possible deficiency in acid attack may justify it.

In order to evaluate the precision of ICP-MS on digested sample analysis, replicates of five random samples were used. In table 14 the relatively standard deviation (RSD, %) for each element are represented. The associated results are indicated in annex C.

Table 14: Resume of RSD (%) obtained for replicates used for total element concentrations on soils by ICP-MS. n > 10% represent the number of samples that presented a RSD > 10%.

RSD (%)	Cr	Ni	Cu	Zn	Pb	Al
Minimum	4.3	12.4	1.9	1.7	5.2	1.0
Maximum	30.0	12.4	45.2	40.7	73.1	34.0
Mean	18.4	-	13.1	14.7	29.3	10.7
n > 10%	4	1	1	2	3	1

High values of RSD (%) were obtained, demonstrating the high heterogeneity presented in our samples. Also isobaric and polyatomic interferences may contribute for these discrepancies (Dean, 2005).

Table 15 show the values of LD, CV_m, and precision (measured as standard deviation) for dissolved sulfate (µM) and sulphide (pM) measured in the water samples.

Table 15: Limit of detection, and precision of dissolved sulfate (µM), and sulphide (pM).

Parameter	LD	CV_m (%)	Precision (%)
Sulfate (µM) (n = 10)	2.1 ± 0.4	7.9 ± 1.8	10 ± 1.2
Sulphide (pM) (n = 16)	23.7 ± 5.4	1.5 ± 0.5	5.2 ± 1.1

Table 16 presents the LD, CV_m, precision, and accuracy of the extractions performed on sediment for AVS in µmol/g and for pyrite and S^0 in nmol/g.

Table 16: Detection limit, precision, and accuracy (*p<0.05*) of the extractions procedure performed on sediment for AVS µmol/g, pyrite (nmol/g) and S^0 (nmol/g).

Extraction	Parameter	LD	CV_m (%)	Precision (%)	Accuracy	
					Certificated	Obtained
HCl (1M) (n = 12)	AVS (µmol/g)	0.104 ± 0.002	2.1 ± 0.5	5.2 ± 0.8	-	-
CRS Method (n = 6)	Pyrite (nmol/g)	12 ± 1.3	4.8 ± 0.9	2.8 ± 0.7	2.2 ± 0.3	2.18 ± 0.08
	S^0 (nmol/g)	26 ± 2.6	5.1 ± 1.1	4.3 ± 1.0		

The nonexistence of certificated materials turned impossible the determination of the accuracy in some cases. For pyrite, a natural pyrite standard (Alfa Aesar) was used.

4. Results and Discussion

4.1. Water Samples

4.1.1. Physico-Chemical Parameters

Figures 23, 24, 25 and 26 present the temperature (ºC), dissolved oxygen (DO, mg/L), conductivity (µS/cm), and pH vertical profiles observed for the sampled lakes.

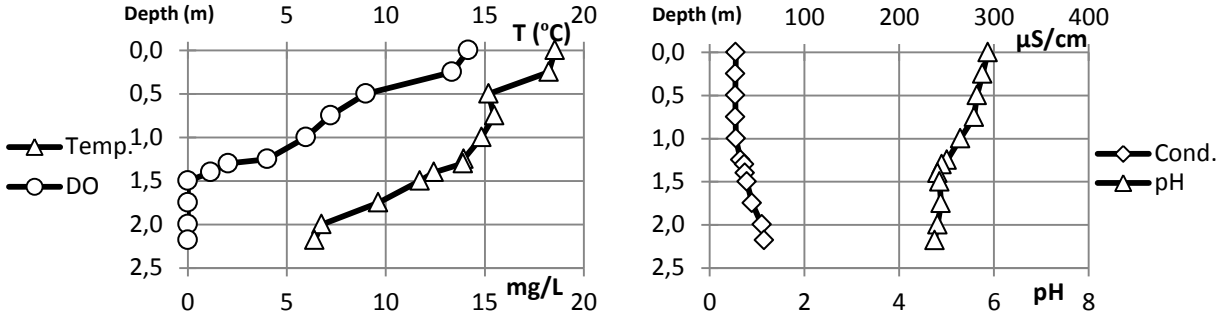

Figure 23: KWK12 vertical profiles for temperature (ºC), DO (mg/L), conductivity (µS/cm) and pH.

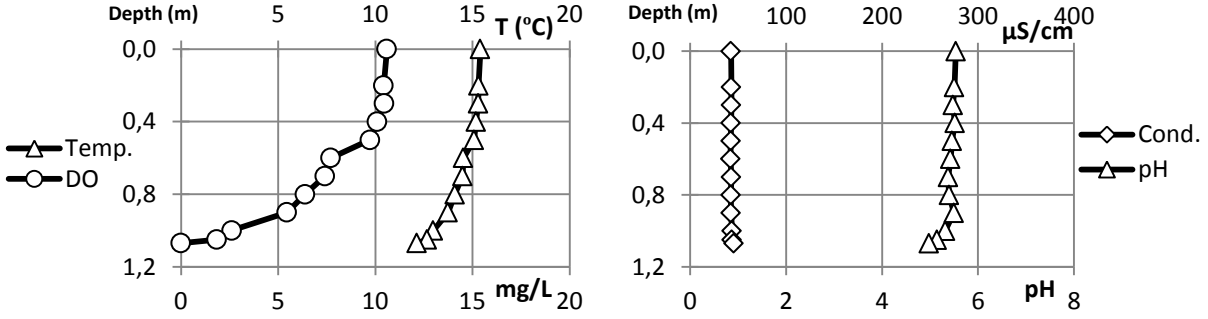

Figure 24: SAS 1A vertical profiles for temperature (ºC), DO (mg/L), conductivity (µS/cm) and pH.

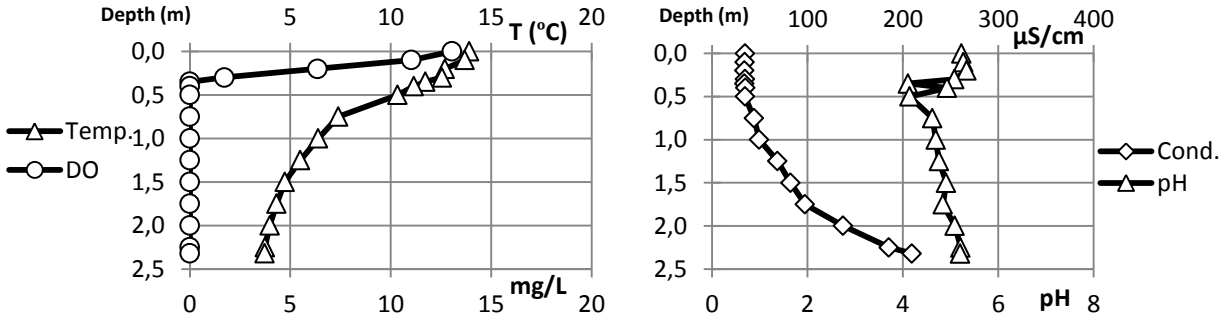

Figure 25: SAS 2A vertical profiles of temperature (ºC), DO (mg/L), conductivity (µS/cm) and pH.

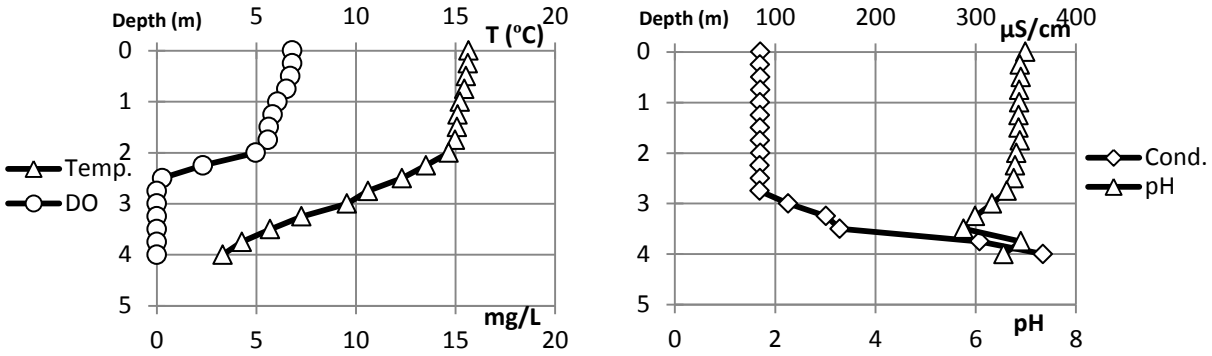

Figure 26: BGR1 vertical profiles of temperature (°C), DO (mg/L), conductivity (µS/cm) and pH.

The vertical profiles were used to characterize the redox status of the lakes, and also for choosing the depths for water collection. In all the lakes, a clear stratification was observed for DO and temperature, and a slight for conductivity and pH, suggesting that these lake waters are poorly mixed.

The decrease of DO with depth observed in all lakes, suggests progressive oxygen consumption, probably due to organic matter degradation according to (Paul, 2014):

$$\boldsymbol{CH_2O(org.) + O_2(g) \rightarrow CO_2(\uparrow) + H_2O(l)} \qquad \boldsymbol{\Delta G^o = -475\ kJ.mol^{-1}OM}$$

In the pH vertical profiles a general decrease was also observed in all lakes. This decrease may be attributed to the dissolution of CO_2 in water (Wang et al., 2015):

$$CO_2(g) \rightleftharpoons CO_2(aq)$$
$$CO_2(aq) + H_2O(l) \rightleftharpoons H_2CO_3(aq)$$
$$H_2CO_3(aq) \rightleftharpoons HCO_3^-(aq) + H^+(aq)$$

and also to the degradation of dissolved organic matter, a process that is known to decrease pH due to the release of H^+ ions in early diagenetic reactions (Berner, 1980).

These reactions, in spite of being more important in the sediment environment, can also occur in aquatic systems during the mineralization or dissolved organic matter (DOM) my microorganisms (Stumm and Morgan, 1981). In the oxic topmost water of the lakes dissolved oxygen is use as terminal electron accepter (lowest ΔG^o) in the oxidation of DOM. As dissolved oxygen is consumed becomes less available for organic matter mineralization by microorganisms. The diagenetic process then continues by using other electron accepters with $\Delta G^o<0$: nitrate (NO_3^-), iron and manganese oxides, sulfate and methane formation, increasing ΔG^o and therefore spending more energy (Berner, 1980): The reactions for these diagenetic reactions are as follows:

$$5CH_2O(org.) + \boldsymbol{4NO_3^-(aq)} \rightarrow 2N_2(\uparrow) + 4HCO_3^-(aq) + CO_2\ (\uparrow) + 3H_2O(l) \qquad \Delta G^o = -448\ kJ.mol^{-1}OM$$
$$CH_2O(org.) + 3CO_2(g) + H_2O(l) + \boldsymbol{2MnO_2(aq)} \rightarrow 2Mn^{2+}(aq) + 4HCO_3^-(aq) \qquad \Delta G^o = -349\ kJ.mol^{-1}OM$$
$$CH_2O(org.) + 7CO_2(g) + \boldsymbol{Fe(OH)_3(aq)} \rightarrow 2Fe^{2+}(aq) + 8HCO_3^-(aq) + 3H_2O(l) \qquad \Delta G^o = -114\ kJ.mol^{-1}OM$$
$$2CH_2O(org.) + \boldsymbol{SO_4^{2-}(aq)} \rightarrow H_2S(aq) + 2HCO_3^-(aq) \qquad \Delta G^o = -77\ kJ.mol^{-1}OM$$
$$\boldsymbol{2CH_2O(org.)} \rightarrow CH_4(\uparrow) + CO_2(\uparrow) \qquad \Delta G^o = -58\ kJ.mol^{-1}OM$$

These reactions generally occur in the sequence listed above, which is explained by the metabolic free energy yield for each reaction (Berner, 1980). It is assumed that the greater the energy yields of a microbial process, the greater the likelihood that it will dominate over other thermodynamically possible competing reactions (Froelich et al., 1979).

In this work only sulfate were studied (see the following sections), and a decrease from surface to bottom was observed on its vertical profiles, which appears to be in agreement with this assumption. However, the decrease of DO form the surface to the bottom water of these lakes may be explained by this diagenetic mechanism.

Because conductivity is related to ions present in solution (Essington, 2005), it can be assumed that they were increasing. This result may be related also to OM oxidation that produces ions (e.g. H+), or CO_2 which as we saw dissolves in water. A positive significant Spearman correlation ($r_s = 0.426$; *p<0.05*) was found between pH and specific conductivity, which is in agreement to this assumption suggesting the H^+ ion may also play an important contribution for lake conductivity. Apart of this, OM degradation may release trace elements through this process, such Cu, previously in organometallic complexes (Xue and Sigg 1993; Wu and Tanoue 2001), and thus increasing the conductivity of the water.

4.1.2. Dissolved Organic Carbon, Sulfate and Sulphide

Several studies report that dissolved organic carbon (DOC), conductivity, and metal concentrations increase from large lakes to thaw ponds in Western Siberian (Audry et al., 2011a; Pokrovsky et al., 2013).

Table 17 presents the vertical variations of DOC concentrations (mg/L), and levels of dissolved sulphur species (sulfate (mM) and sulphide (µM)), with depth for the sampled lakes.

A systematic increase of DOC from the surface to the bottom waters was observed suggesting a diffusion of DOC from the lake sediments, which had higher content of OM (see section 4.2.1). Additionally, downward ice cover season can be related for this accumulation of DOC in the bottom, as ice form and the remains tends to accumulate at bottom – frozen effect - (Schmidt et al., 1991; Wharton et al., 1993). Thus DOC is strongly excluded from lake ice during winter, and then diffuses upwards in water column in the melting season.

SAS 1A/2A and KWK12 had the higher values of DOC with maximums of 93.1, 79.4 mg/L and 70.2 mg/L respectively, while BGR had the lowest concentration with max. of 26.2 mg/L. This tendency for an enrichment of OM in SAS and KWK sampled compared to BGR is in agreement with the sedimentary organic matter content (see the following sections).

Table 17: Concentration of DOC (mg/L) and total dissolved sulphur species (sulfate (mM) and sulphide (µM)) in water samples.

Sample	Depth (m)	DOC (mg/L)	HS^- (µM)	SO_4^{2-} (mM)
SAS 1A	Surf	6.3	< LD	1.2
	0.3	10.4	0.5	0.6
	0.6	44.2	0.2	< LD
	0.9	55.9	3.7	< LD
	1.1	79.4	8.1	< LD
SAS 2A	Surf	7.0	0.1	0.1
	0.2	15.4	0.2	< LD
	0.3	39.5	0.4	< LD
	0.4	57.6	6.6	< LD
	1.8	81.1	12.3	< LD
	2.3	93.1	21.1	< LD
KWK12	Surf	7.6	0.3	0.6
	0.5	9.3	3.6	0.2
	1	12.4	4.0	< LD
	1.5	54.2	12.6	< LD
	2.2	70.2	13.6	< LD
BGR1	Surf	6.2	0.4	0.3
	1.8	20.4	2.4	0.4
	2.3	17.9	6.5	0.1
	2.8	26.2	5.3	0.2
	3.2	8.7	4.4	< LD

Reuter and Perdue (1977) confirmed that for DOC concentrations higher than 20 mg/L, humic substances become visible to the naked eye by imparting a yellow color to natural waters. Thus, a higher DOC concentration is expected in a darker water color lake. In, fact this was observed in our sampled water lakes (see figure 8).

A negative Spearman correlation ($r_s = -0.647$; *p<0.01*) was found between DOC (mg/L) and DO (mg/L) concentrations (figure 27), which may indicate that OM mineralization by oxygen occurred in the water column.

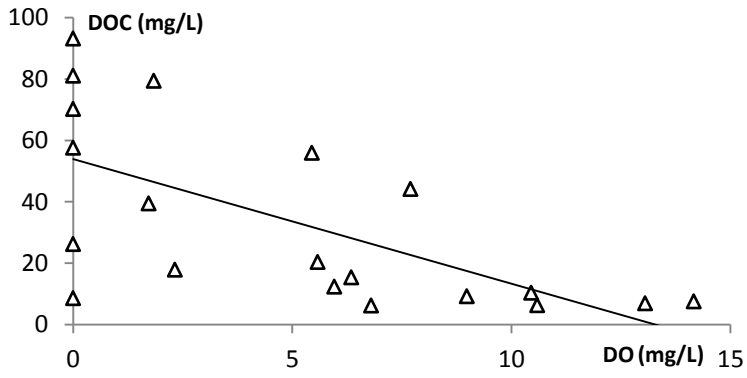

Figure 27: DOC (mg/L) and DO (mg/L) correlation present in water samples. All lakes are included.

As mentioned before, oxygen may act as an electron acceptor in the OM degradation process (Berner, 1980), thus the negative correlation may confirm the OM mineralization in the studied lakes.

Additionally, the decrease of DOC at the surface can also be explained by OM photo-degradation. In fact, Cory et al. (2014) and Shirokova et al. (2013) observed photo-degradation of DOC by UV-radiation in arctic surface waters.

In order to access the DOC origin, δ^{13}C-DOC analysis was performed at SAS 1A waters. Figure 28 presents the obtained relationship between δ^{13}C (‰) and C/N ratio.

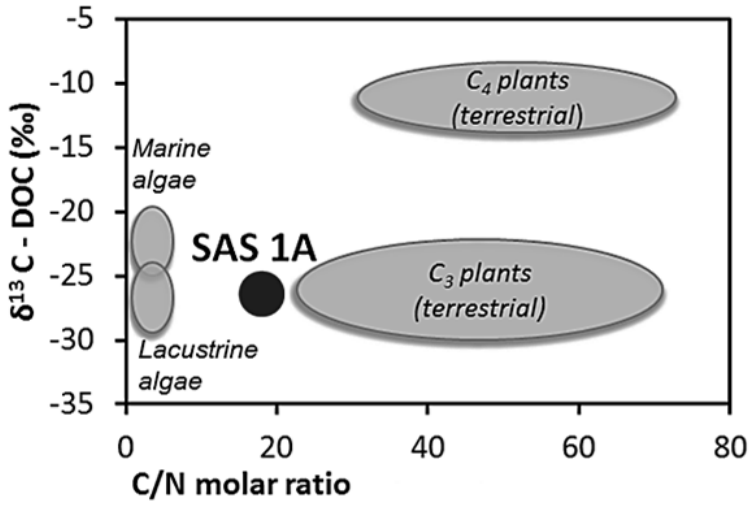

Figure 28: Stable carbon isotopic composition (δ^{13}C, ‰) for dissolved organic matter from Lake SAS 1A.

The results showed that for SAS 1A lake, the dissolved organic carbon was mainly originated from C_3 plants (-27‰) which is consisting of $\delta^{13}C_{DOC}$ results from other studies in the Arctic Regions (e.g. northern Sweden, Karlsson et al., 2010). The similar δ^{13}C values of DOC and terrestrial organic carbon suggest that the lake-water organic carbon pool predominately originated from the terrestrial ecosystems, mainly vegetation, surrounding the lake (e.g. cellulose).

In all lakes sulfate concentrations varied in range from 0.1 to 1.2 mM (1.9 – 118 mg/L) with maxima at the surface of each lake, and decreasing towards the bottom. These values are in the same order of magnitude as values reported previously for different lakes of Canadian Arctic (table 18).

Table 18: Range of sulfate concentrations (mg/L) found in Arctic Canada lakes from different locations.

Location	SO_4^{2-} (mg/L)	References
Nunavik:		
SAS 1A	56-118	This study
SAS 2A	13.4	
KWK12	7.7-60.5	
BGR1	1.9-30.7	
Nunavut	29.9	Hamilton et al., 2001
Axel Heiberg Island	54.2	Michelutti et al., 2002
Bathurst Island	6.3	Lim et al., 2001
Ellef Ringes Island	303.2	Antoniades et al., 2003
Northwest Territories	0.9	Pienitz et al., 1997
Southampton Island	9.3	Mallory et al., 2006

Figure 29, presents the vertical profiles of sulfate (mM) and sulphide (µM) levels obtained from the samples collected in the sampled lakes. To the best of my knowledge this was the first time that sulphide was measured in thermokarst permafrost lakes.

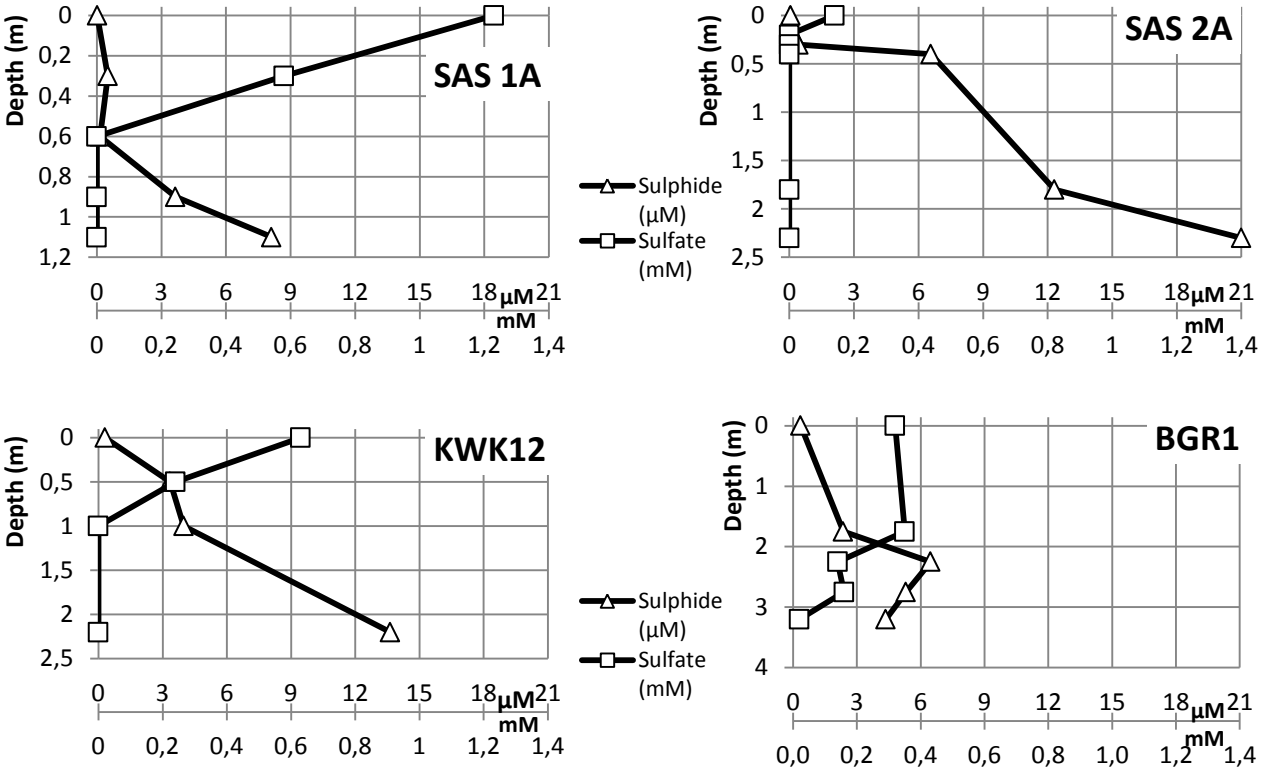

Figure 29: Sulfate (mM) and sulphide (µM) vertical profiles found in sampled lakes water.

Interestingly as sulfate levels decrease with depth, an increase of dissolved sulphide concentration was observed. These results suggests that the OM was also mineralized by using SO_4^{2-} as a terminal electron accepter, which is in agreement with the previously hypothesis, discussed in the DO section. These results are also confirmed by the significant negative correlation obtained (r_s = -0.941; *p<0.05*) between the two sulphur species (figure 30).

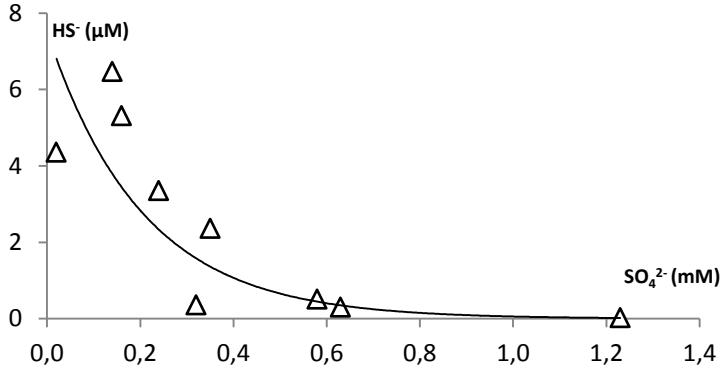

Figure 30: Negative trend observed between sulfate (µM) and sulphide (mM) (Data from all the sampled lakes).

This exponential correlation (instead of a linear one) may be explained by other competitive processes occurring in water column that decrease the amount of dissolved sulphide, like metal-sulphide precipitation (Lewis and van Hille, 2006). As an example, in BGR sulphide vertical profile, a decreasing of sulphide specie is observed at the bottom, probably due to sulphide precipitation.

According with Sinke et al. (1992) sulfate reduction (SR) in the decomposition of organic matter in lakes depends on the amount of OM present and the availability of sulfate. A higher rate of SR is probably driven by a combination of high sulfate concentration and a supply of organic matter from the vegetated zone (Sinke et al., 1992). Blodau et al. (1998) found that in acidic lakes the rate of sulfate reduction was limited by the OM supply rather than sulfate.

4.1.3. Labile and Total Element Concentrations

Figures 31, 32, 33, and 34 present the vertical profiles of dissolved trace elements concentrations (labile and total in µg/L) for each lake.

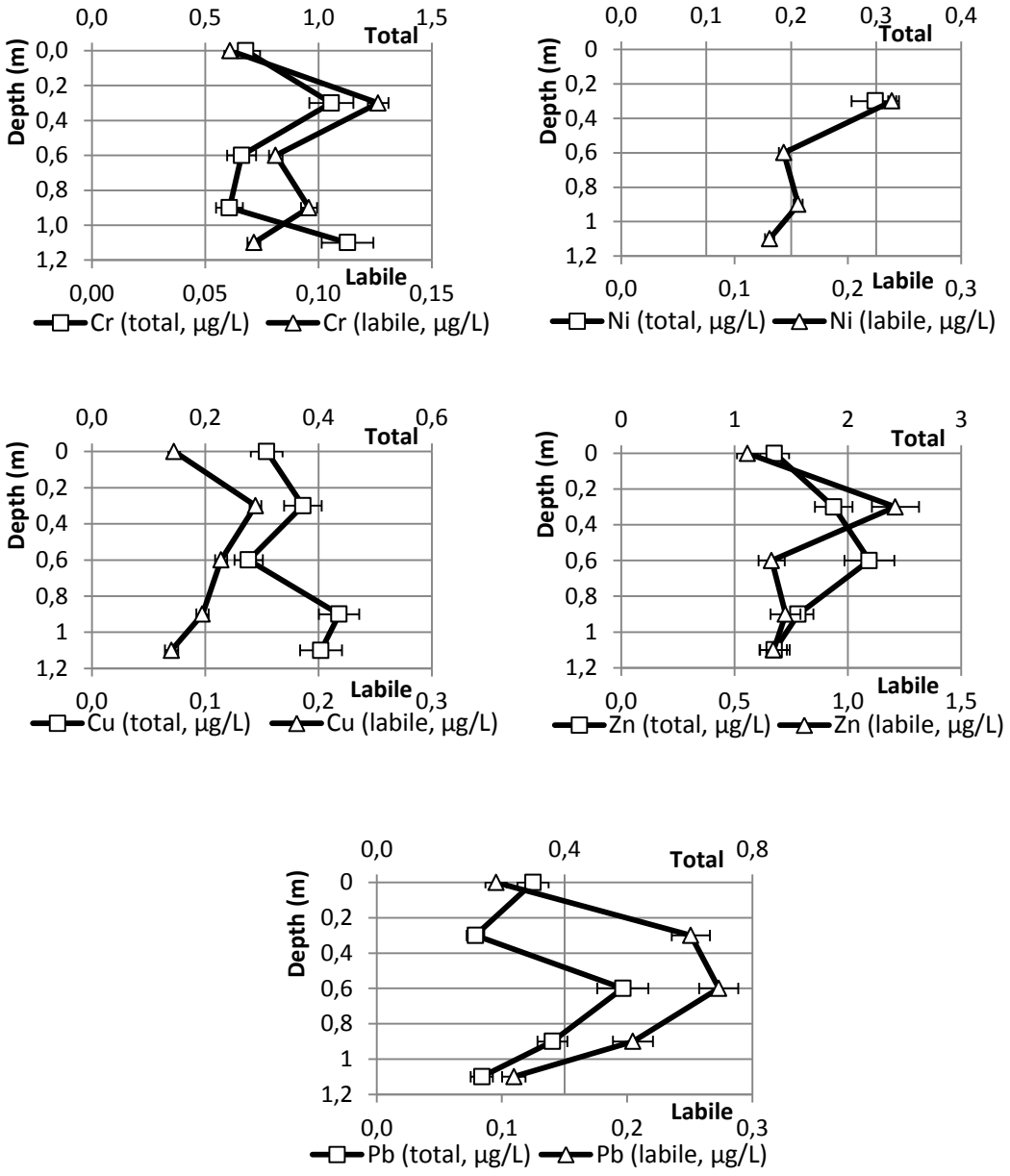

Figure 31: Labile and total concentration profiles in µg/L of elements in water column for SAS 1A with 1 SD.

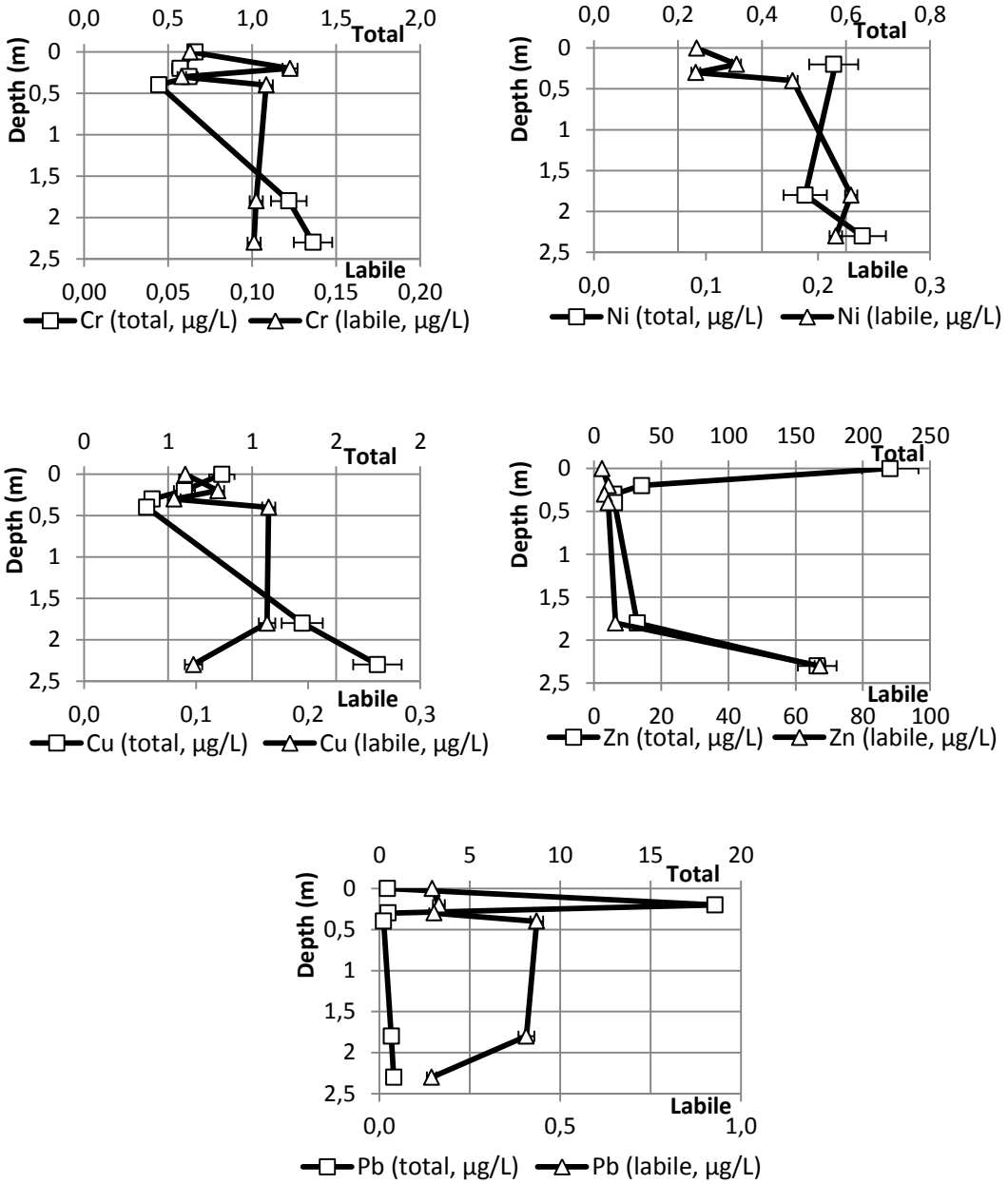

Figure 32: Labile and total concentration profiles in µg/L of elements in water column for <u>SAS 2A</u> with 1 SD.

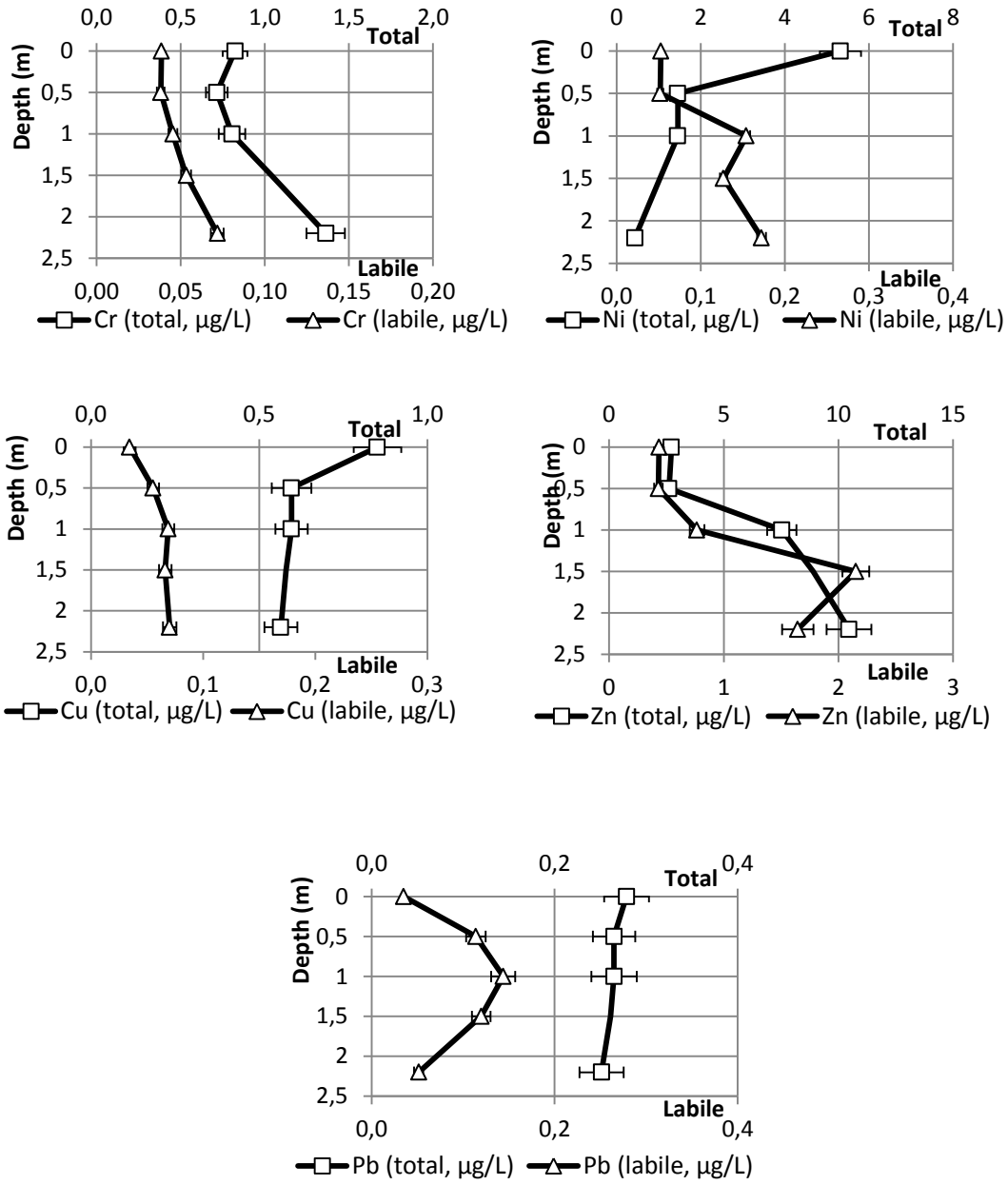

Figure 33: Labile and total concentration profiles in µg/L of elements in water column for <u>KWK12</u> with 1 SD.

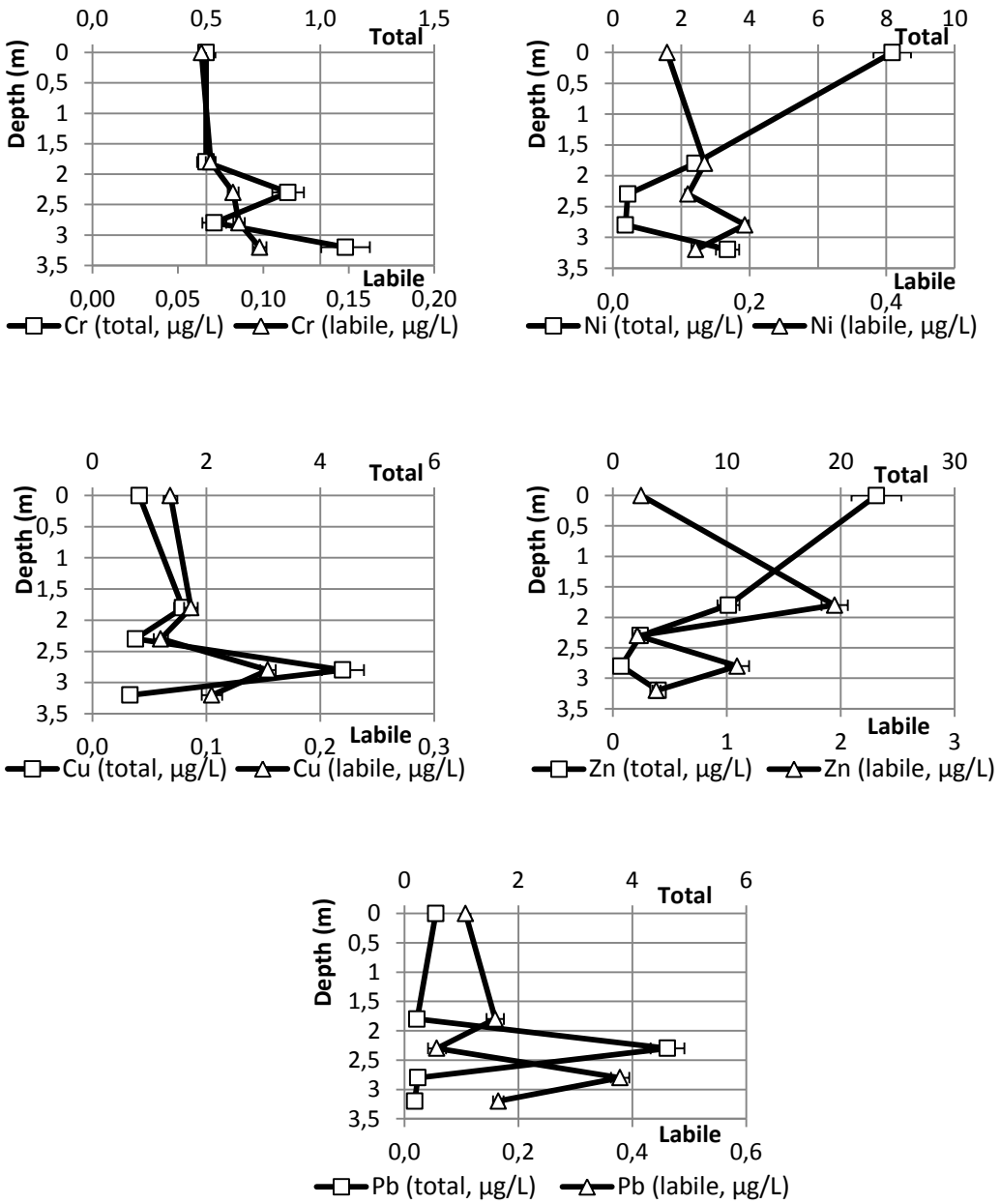

Figure 34: Labile and total concentration profiles in µg/L of elements in water column for <u>BGR1</u> with 1 SD.

To the best of our knowledge there is no published labile and total data on trace element concentration in this type of freshwater lakes. As such, available data for other boreal, but not thermokarst, subarctic and arctic lakes were used to compare our results (Table 19).

Table 19: Range of total trace element concentrations (μg/L) observed in this study and in other arctic lakes.

Location	Element Concentration (μg/L)	References
On This Work	Cr: 0.4 – 1.4 Cu: 0.3 – 4.4 Ni: 0.1 – 11.6 Zn: 0.7 – 220 Pb: 0.2 – 4.6	-
Ellef Ringes Island (High Canadian Arctic)	Cr: 0.1 Cu: 2 Ni: 7 Zn: 6 Pb: 126	Antoniades et al., 2003
Novyl Urengoy (Siberian Arctic)	Cr: 4.3 Cu: 0.3 Ni: 3.4 Zn: 22.6 Pb: 0.28	Manasypov et al., 2013

The comparison shows that, and with the exception of Zn, the concentrations obtained in our lakes are lower than the ones reported in the other two studies, suggesting lower "contamination" or other biogeochemical processes that avoid the presence of these trace elements (TEs) in solution.

With the exception of Cr (max. 24% at SAS 2A) the labile fraction of the studied TEs were elevated. Nickel and Cu presented maximums of 74% and 44% respectively in SAS 2A, and for Zn and Pb the proportion was 43% and 90%, respectively in BGR1. Overall KWK12 was the lake with the lowest labile fraction for all TE in study.

TEs vertical profiles showed that there was pronounced stratification in all lakes, with a more evidence on BGR1, and less stratification on SAS 1A. This can be explained by the depth of water of these lakes, which BGR having a maximum depth of 4.3 m, and SAS 1A having 1.1 m maximum depth and probably with some water column mixing

Interestingly, a positive Spearman correlation ($p<0.01$) between labile fractions of Cu, Ni, and Pb in μg/L was observed suggesting that these elements may have similar origins (table 20).

Table 20: Person's coefficient between labile fraction of Ni, Cu and Pb (μg/L)

TE	Ni	Cu	Pb
Ni	1	-	-
Cu	0.692	1	-
Pb	0.593	0.934	1

Since these TEs have a high affinity for organic matter (Xue and Sigg, 1993; Wu and Tanoue, 2001) we may hypothesize their release during OM degradation.

In order to test this hypothesis a water UV irradiation experiment was performed (see materials and methods) and the amount of the released TEs were quantified. The UV radiation (A and B) is well known for degradation dissolved organic matter releasing the associated TEs (Shiller et al., 2006).

Figure 35 presents the amount (%) of TEs remobilized from observed to water after UV treatment. The percentage indicates the enhancement of the release TE levels compared to the natural labile ones.

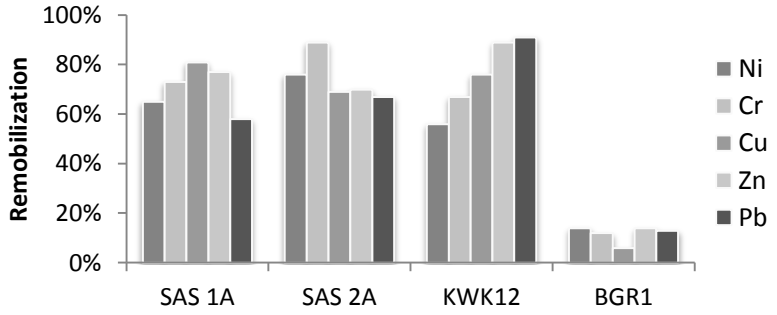

Figure 35: Trace elements remobilization to water column after UV treatment.

The results showed that remobilization was observed for all analyzed elements suggesting that the dissolved organic matter was probably the main source of the labile TEs in the lakes. In fact the high carbon lakes presented the high remobilization proportion (table 21).

Table 21: Remobilization of elements (%), and range of DOC (mg/L) observed in lake's water.

Lake	DOC (mg/L)	Remobilization (%)
SAS 1A	6.3 - 79	58 – 81
SAS 2A	7.0 - 93	67 – 89
KWK1	7.6 – 70	56 – 91
BGR1	6.2 - 26	6 – 14

In other way, photo-oxidation of DOC (that is supposed to occur in surface waters) produces less aromatic compound in one hand, and influence the trace elements speciation by the other (Shiller et al., 2006). Our results then imply a decrease in the organically-complexed form of metals on water with OM degradation, increasing the labile fraction of these elements.

From surface to bottom, processes such as new OM-TE complexation (Benedetti et al., 1996; Stolpe et al., 2010) or precipitation can occur and compete with each other, and thus influence the TE partitioning. In SAS 1A copper and lead, apparently showed OM degradation followed by TE release in labile form and by new OM complexation and possibly precipitation as sulphides (at the bottom).

The elements partitioning can also be influence by other species, such Fe. Urban et al. (1990) determined that high concentrations of Fe are typical found in organic-rich (high DOC), acidic (pH<5), and temperate lakes. Elements may dissolve or desorb from Fe-oxyhydroxides (Viollier et al., 1995) which may influence their reactivity in water. Measurements of Fe and its concentration in these lakes must yet be done to confirm this hypothesis.

4.2. Soil and Sediment samples

4.2.1. Sedimentary Organic Matter

Table 22 presents the sedimentary organic matter determined by the LOI (%) method.

Table 22: Weigh of samples in each LOI step procedure for the determination of organic matter (%), and the standard deviation associated in the solid samples.

Sample	(W) Initial weight sample (g)	(1) Weight after dry at 105ºC (g)	(2) Weight after combustion at 450ºC (g)	(1) – (2) (mg)	LOI (%) = [(1) – (2)]/W] *100
BGR1 Soil#1	0.3286 ± 0.0001	0.3264 ± 0.0001	0.3225 ± 0.0001	3.9 ± 0.2	**1.19 ± 0.06**
BGR1 Soil#2	0.9361 ± 0.0001	0.9317 ± 0.0001	0.9132 ± 0.0001	18.5 ± 0.20	**1.98 ± 0.02**
BGR1 Sed#1	0.3887 ± 0.0001	0.3887 ± 0.0001	0.3872 ± 0.0001	5.6 ± 0.2	**1.44 ± 0.05**
BGR1 Sed#2	0.5268 ± 0.0001	0.5268 ± 0.0001	0.5234 ± 0.0001	9.4 ± 0.2	**1.78 ± 0.04**
KWK12 Soil# 1	0.0351 ± 0.0001	0.0279 ± 0.0001	0.0044 ± 0.0001	23.5 ± 0.20	**67 ± 0.6**
KWK12 Soil# 2	0.0653 ± 0.0001	0.0597 ± 0.0001	0.0188 ± 0.0001	40.9 ± 0.20	**63 ± 0.3**
SAS 1A Soil#1	0.0205 ± 0.0001	0.0207 ± 0.0001	0.0037 ± 0.0001	17 ± 0.2	**83 ± 1.1**
SAS 1A Soil#2	0.0527 ± 0.0001	0.0469 ± 0.0001	0.0056 ± 0.0001	41.3 ± 0.20	**78 ± 0.4**
SAS 1A Sed	0.1779 ± 0.0001	0.1445 ± 0.0001	0.0192 ± 0.0001	125 ± 0.20	**70 ± 0.1**
SAS 2A Soil#1	0.0175 ± 0.0001	0.0164 ± 0.0001	-0.0001 ± 0.0001	16.5 ± 0.20	**94 ± 1.4**
SAS 2A Soil#2	0.0652 ± 0.0001	0.0519 ± 0.0001	0.0004 ± 0.0001	51.5 ± 0.20	**79 ± 0.4**
SAS 2A Sed	0.0381 ± 0.0001	0.0366 ± 0.0001	0.0013 ± 0.0001	35.3 ± 0.20	**93 ± 0.6**

With exception for BGR1 (less than 2%), high content in sedimentary organic matter (> 63%) was determined for all sampled soils and sediments. In BGR1 the obtained results are in agreement with Calmels and Allard (2004) who reported that this region contains mineral soils with clays and silts and a low organic matter content (< 1.5%). This tendency for lower OM content was also observed in the DOC from the same BGR lake.

The high OM founded in SAS valley is assumed to be related to palsas (mounds of peat containing a permafrost core of peat or silt), whereas on KWK and BGR valleys lower OM is related to organic or mineral lithalsas (thawed permafrost mounds) respectively (Crevecoeur et al., 2015).

Rising temperature caused by climate change is projected to cause vegetation shifts favoring taller, denser vegetation, and thus promoted the expansion of forests into the arctic tundra, and tundra into the polar desert (Zhang et al., 2013). For this reason is reasonable to assume that vegetation around the lakes will change, special for BGR located above the tundra line, playing a more important role for supplying organic matter for degradation.

4.2.2. Natural Organic Matter Characterization

Solid-state nuclear magnetic resonance (ssNMR) spectroscopy based on ^{13}C cross polarization (CP) and total suppression of spinning sidebands (TOSS) methods is not fully quantitative (Kögel-Knabner, 1997), however, it can be assumed that the samples analyzed share common types of functional groups and the CP efficiency for the same functional groups is usually similar. Semi-quantitative comparisons between these samples can provide useful comparisons among them (Kögel-Knabner, 1997).

Figures 36, 37, 38, and 39 present the ^{13}C ssNMR spectra obtained for soils and sediments from the sampled lakes.

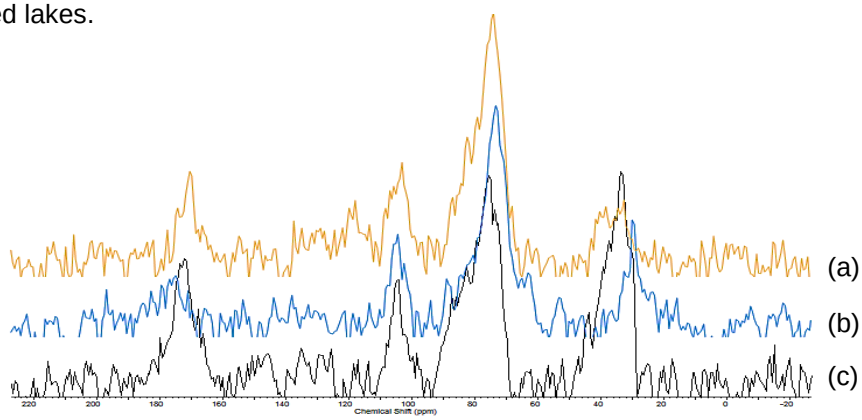

Figure 36: ^{13}C ssNMR spectra of BGR1 samples of soil #1 (a), sed #1 (b) and sed #2 (c).

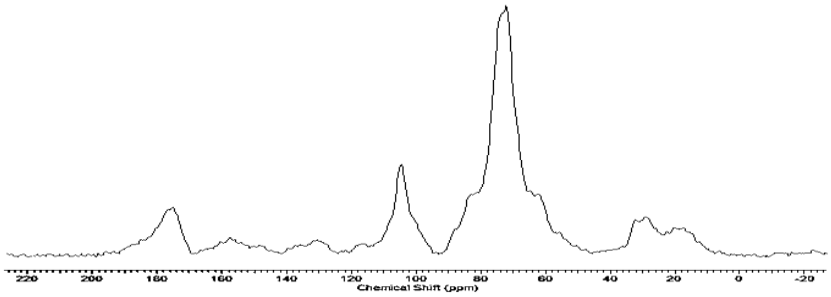

Figure 37: ^{13}C ssNMR spectrum of KWK12 soil#1 sample.

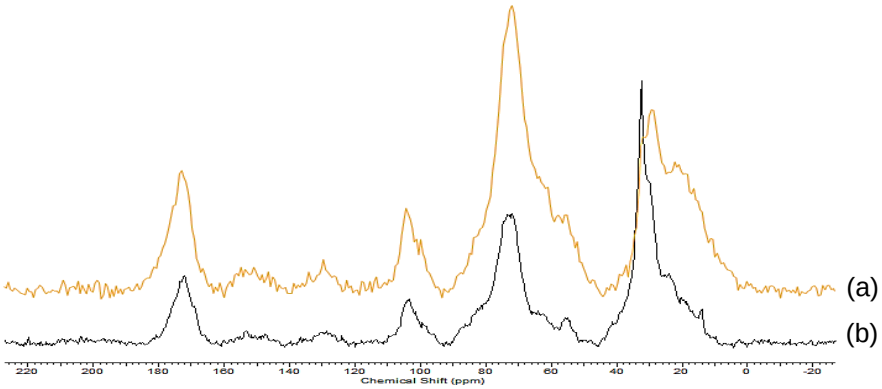

Figure 38: ^{13}C ssNMR spectra of SAS 1A samples of soil #1 (a) and sed (b).

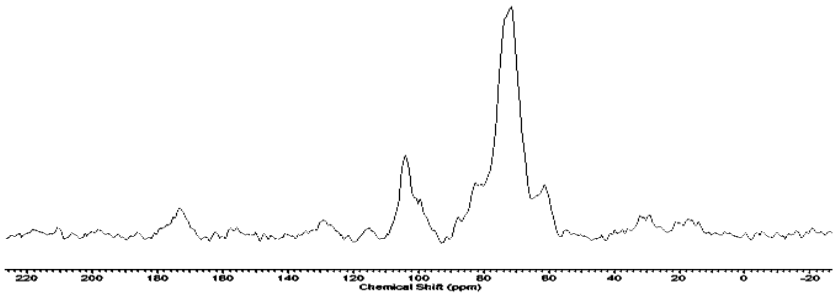

Figure 39: ^{13}C ssNMR spectrum of SAS 2A soil#1 sample.

The ss^{13}CNMR spectra showed that there was no significant difference between soils and sediments from each lake, which is in agreement of similar functional groups assumption.

In order to better interpret the results each spectra was divided into eight chemical shift regions, which were assigned to carbons in different functional groups (Cao et al., 2011; Mao et al., 2011) as indicated in table 9. The spectral areas of the eight regions in each spectrum were integrated to determine the area proportions of individual regions to the total spectral area as indicated in table 23.

Table 23: ^{13}C ssNMR integration results (%) for the analyzed sampled.

ppm / Sample	220-190	190-161	161-143	143-110	110-90	90-63	63-45	45-0	Alkyl-C/O-alkyl ratio
BGR1 Soil #1	0%	11%	0%	11%	13%	51%	0%	14%	0.2
BGR1 Sed #1	5%	15%	3%	0%	10%	49%	3%	17%	0.3
BGR1 Sed #2	2%	16%	2%	2%	9%	37%	0%	32%	0.7
SAS 1A Soil #1	0%	11%	2%	2%	6%	40%	7%	33%	0.7
SAS 1A Sed	1%	10%	2%	2%	6%	32%	3%	44	1.2
SAS 2A Soil #1	2%	5%	1%	3%	13%	67%	0%	9%	0.1
KWK12 Soil #1	0%	9%	3%	4%	12%	60%	2%	11%	0.2
Average	**1%**	**11%**	**2%**	**3%**	**10%**	**48%**	**2%**	**23%**	**-**

In all analyzed samples, the higher ^{13}C signals intensity was observed for O-alkyl-C (averaged 48%) and alkyl-C (averaged 23%) structures with smaller contributions from anomeric-C (averaged 10%) and carboxylic/carbonyl-C groups (averaged 11%). The proportions for aromatic-C, methoxyl, aromatic C-O and carbonyl C in ketones/aldehydes averaged about 3%, 2%, 2%, and 1%, respectively.

These results are in line with previous studies from other sampled soils in Polar Regions where alkyl-C and O-alkyl-C structures dominated solid-state ^{13}C NMR spectra (Beyer et al., 2001; Dai et al., 2002).

The alkyl-C/O-alkyl-C ratio has been used to establish degradation trends from ^{13}C NMR data; this ratio increases with degree of degradation (Baldock and Preston, 1995). Thus, we can assume that our sediments were in a more degraded state than the corresponding soil.

In general, our results suggest that OM on the sampled soils and sediments was mainly composed of polysaccharides and peptides as the main components, with small amounts of lignin (Cao et al., 2011; Nelson and Baldock, 2005; Zhou et al., 2014). These compounds represent the main constituents of plants residues, which are the most important input to the soil organic matter (Cresser, 1993).

Polysaccharides derived from plant tissue consist of cellulose and hemicellulose, which are readily available by microorganism and are converted in CO_2 (Essington, 2005). Like polysaccharides, microbes can also metabolize peptides compounds, consisting of two or more amino acids units. In addition, amino acids may also occur in complex polymeric structures that are thought to be of microbial origin (Essington, 2005).

Lignin is the most refractory substance in soil, described as a group of high-molecular-mass polymer, which is very resistant to the processes of microbial decomposition in anaerobic environments due to its aromatic nature and the diversity of its cross-linkages (Cresser, 1993; Essington, 2005). In aerobic environments lignin degradation may occur, contributing for the formation of the chemically protected organic matter in soil often referred to as the humic acids components (Cresser, 1993).

The ^{13}C ssNMR results suggest therefore that soil organic matter was essentially of plant origin which is in agreement of $\delta^{13}C$-DOC results. Additionally, the presence of organic compounds resulting from cellulose degradation indicated, such as in water column, that the natural organic matter was also in a process of mineralization.

4.2.3. Mineralogical Composition

The crystalline structures were determined in the sampled soils/sediments by comparing different patterns from a database with the experimental data. These patterns were retrieved from PDF2® database (from International Centre for Diffraction Data product), and the comparisons between them require time and experience.

In figures 40, 41 and 42 show the X-Ray powder diffraction (XRPD) obtained for BGR, KWK12 and SAS1A/2A samples.

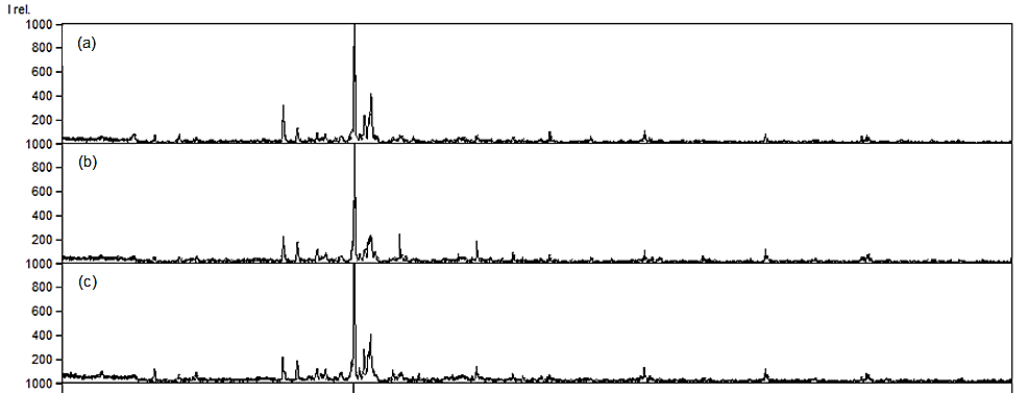

Figure 40: Diffractograms of BGR lakes: (a) BGR1 Soil# 1; (b) BGR1 Soil# 2; (c) BGR1 Sed# 1.

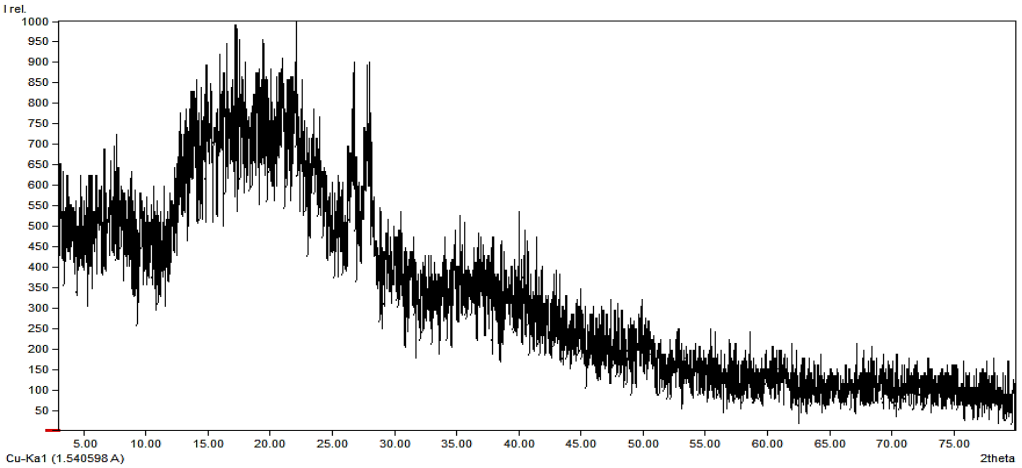

Figure 41: Diffractogram of KWK12 Soil# 1.

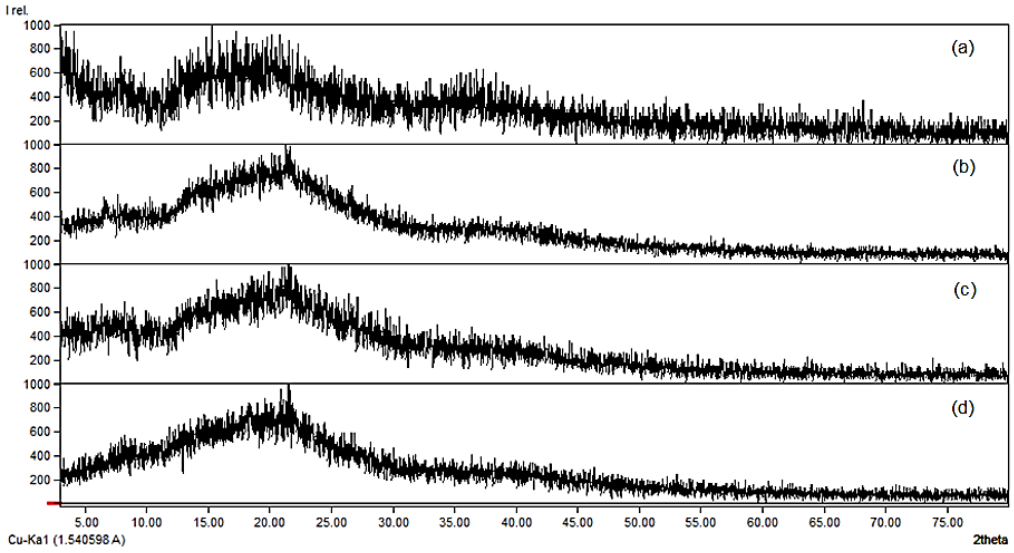

Figure 42: Diffractograms of SAS lakes: (a) SAS 1A Soil# 1; (b) SAS 1A Soil# 2; (c) SAS 1A Sed; (d) SAS 2A Sed.

The diffractograms for KWK and SAS samples showed that these samples were amorphous or mainly amorphous, making their identification impossible. In opposite, BGR analyzed samples were identified as crystalline, and silica was the main inorganic structure identified. Table 24 presents the XRPD crystalline structures identification in the analyzed samples.

Table 24: XRPD analysis results of each lake, and the corresponding structure identified.

Soil/Sediment	Type of sample	Type of crystalline structure
BGR samples	**Crystalline**	Mixture of SiO_2: hexagonal, orthorhombic, monoclinic
KWK samples	Mainly amorphous	-
SAS samples	Amorphous	-

BGR sample diffractograms (figure 40) showed the soils and sediments from this lake were essential constituted by different types of minerals, with no difference in the mineral composition between them. The signals identified were, according to the database, hexagonal, orthorhombic, and monoclinic silica (NIOSH, 2003).

KWK and SAS samples diffractograms (figure 41 and 42) showed that all samples were amorphous which is in agreement with the high organic matter content of these lakes.

The use of another database, Match!® database (www.crystalimpact.com/match/), allowed also the identification of albite ($NaAlSi_3O_8$) in BGR Soil #1 and #2. This primary silicate mineral is usually found in the silt-sized fraction of soils (Essington, 2005).

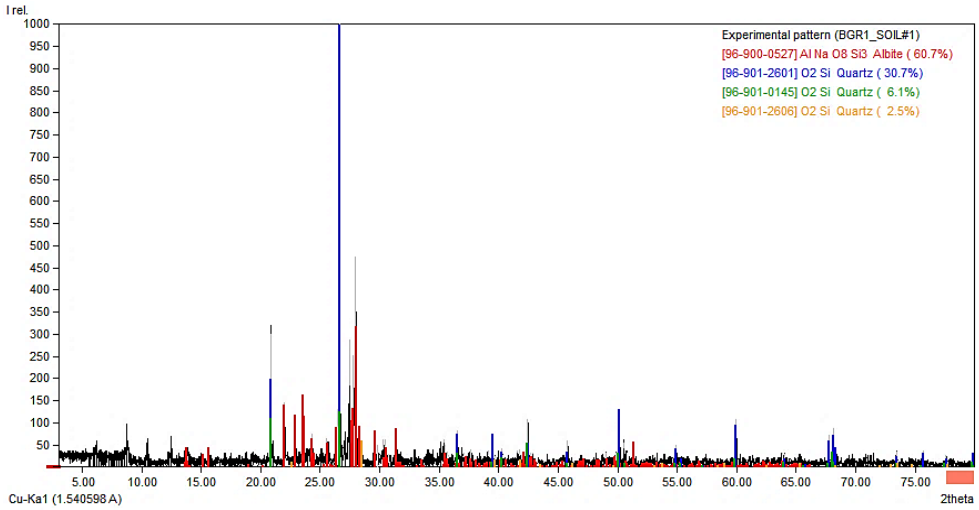

Figure 43: Experimental pattern for BGR1 soil obtained (black) with the possible crystalline structure. Albite is represented in red.

4.2.4. Total Element Concentrations

Table 25 presents the range of concentrations (µg/g) for each TE determined in our sampled soils and sediments and levels reported for other Arctic ecosystems.

Table 25: Range of total elements concentration (µg/g) observed in our sampled soils and sediments, and means values from other arctic ecosystems.

Location	µg/g / Lake	Cr	Ni	Cu	Zn	Pb
This Work	SAS 1A	6.9 – 7.1	< LD	3.4 – 6.0	7.1 – 31	2.0 – 6.8
	SAS 2A	2.1 – 5.4	< LD	< LD	5.1 – 18	2.5 – 8.6
	KWK12	21 – 35	6.8 – 21	6.8 – 11	30 – 50	8.8 – 11
	BGR 1	51 – 95	21 – 58	21 – 27	74 – 94	16 – 19
Western Siberia[1]	Khasyrei	-	24	15	36	11
Greenland[2]	East	117	-	50	92	-
Svalbard[3]	Kongsfjorden	65	-	26	86	23

[1] Audry et al., 2011b; [2] Naidu et al., 1997; [3] Lu et al., 2012

With the exception of Zn in Greenland, in general the concentrations obtained for the studied TEs are in the same order of magnitude of the other presented ecosystems. However, and when comparing our sampled lakes, the concentrations founded in BGR1 are 2-10 times higher than in the others lakes, suggesting that it's "inorganic" origin may play an important role on the retention of TEs.

Figure 44 shows the negative significant Spearman correlations ($p<0.05$) between the trace elements content and the sedimentary organic matter.

The influence of soil organic matter on trace elements varies, but a reduced availability is usually related to complexation with humic acids and/or lignin (Cresser et al., 1993). These compounds contain a relatively large number of functional groups (OH, C=C, SH, CO_2H) that have a great affinity for interacting with metal ions that can form a soluble complex or chelate (Alina, 2010).

Thus the complexation of metal ions with humic substances contributes to a decrease of their availability, and in turn to an increase of mobility in water reservoirs (Weng et al., 2002), leading to less soil retention.

Contrary to what happened in water, where high association between dissolved organic carbon and trace elements was verified, in soils and sediments the retention of these elements appears to be related to other component present in the solid matrix rather than OM, possibly by adsorption in alumino-silicates or by precipitation as element-sulphides which was previously suggested in the section 4.1.3.

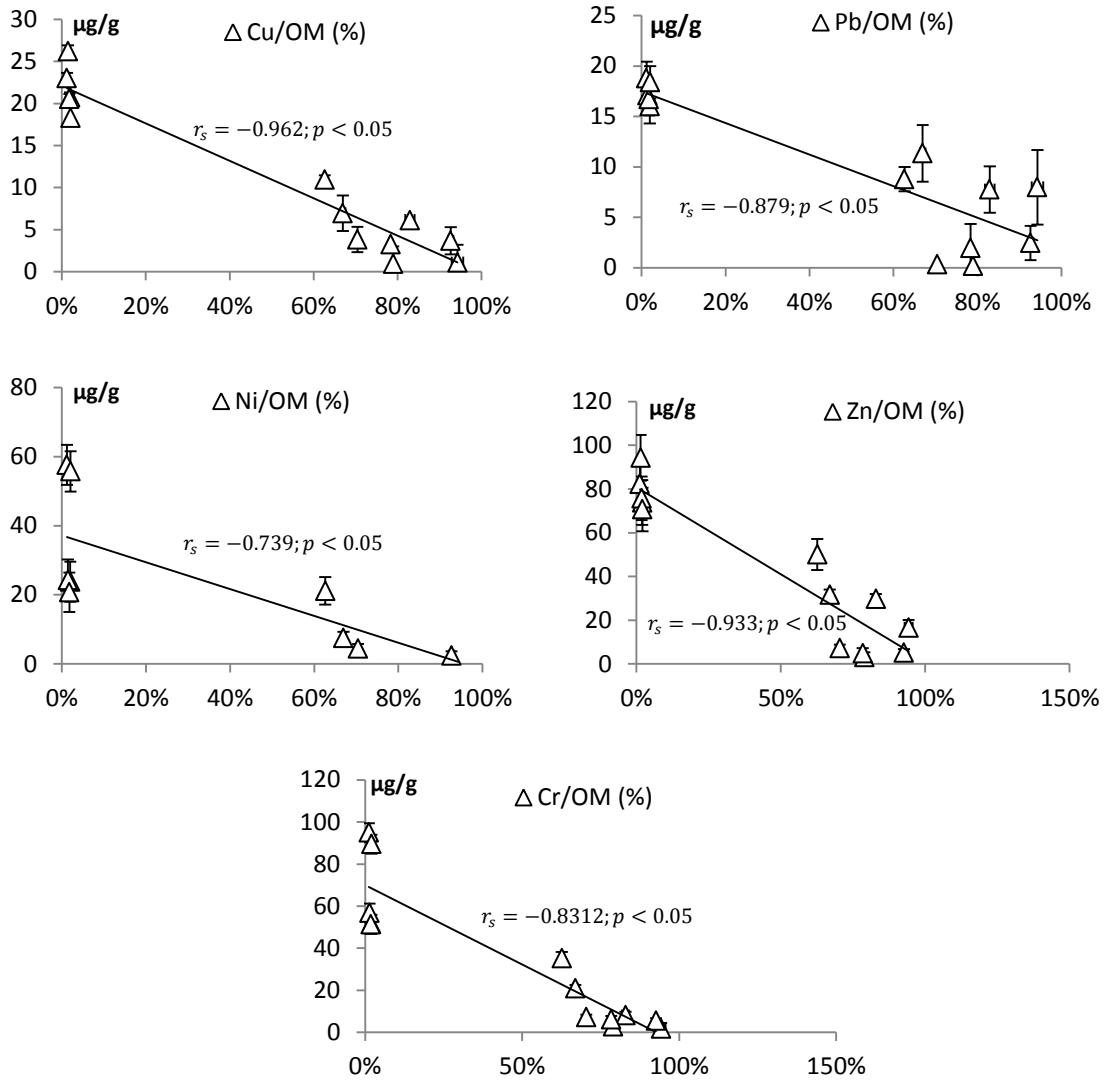

Figure 44: Trace elements significant correlation with sedimentary organic matter found in our sampled soils and sediments.

In order to better clarify both hypotheses Al content was also measured in the samples. The concentration of this element in soils and sediments is usually used as a proxy of the amount of inorganic matter content and also as an indicator of the granulometry of the inorganic particles that constitute the solids (Vale et al., 2008).

Table 26 presents the range of aluminium concentrations (%) determined in our sampled soils and sediments.

Table 26: Aluminium range concentrations (%) determined in the sampled soils and sediments.

	SAS 1A	SAS 2A	KWK12	BGR1
Al (%)	0.28 – 0.33	0.01 – 0.23	1.43 – 2.71	4.38 – 5.32

BGR1 samples presented a higher Al content (4.4 – 5.3%) while in the other lakes Al was lower than 2%. Again a clear tendency for the enrichment of inorganic material was observed in BGR lake, and, in less extent for KWK, suggesting that material which originated these lakes (lithalsa) influence their development in terms of organic and/or inorganic content (Calmels et al., 2008). The BGR Al levels are also inline with the results obtained by Calmels and Allard (2004) that identified silts and clays as the major components of this lake.

Table 27 represents the correlations (*p<0.05*) obtained between aluminium and the analyzed TEs (all data lakes).

Table 27: Spearmen correlations (p<0.05) obtained between Al content (%) and trace elements levels (µg/g) on sampled soils and sediments (all data lakes).

	Cr (µg/g)	Ni (µg/g)	Cu (µg/g)	Zn (µg/g)	Pb (µg/g)
Al (%)	0.962	0.850	0.951	0.948	0.924

The significant correlations clearly showed the influence of the inorganic fraction of the soils/sediments in the retention of the analyzed TEs. However does not clarify if this was an adsorption process or a precipitation mechanism.

4.2.5. Inorganic Sulphur: AVS, Pyrite and Elemental Sulphur (S^0)

Like the dissolved sulphur data, this work reported for the first time the inorganic-S data for thermokarst lakes soils and sediments.

The results of solid sulphur speciation in the samples collected in the lakes are present in table 28.

Table 28: Concentration of the inorganic sulphur compounds (AVS, pyrite, and elemental sulphur) and organic-S in the sediments of thermokarst lakes in our study; all data are expressed in µmoles per gram of dry weight.

µmol.g^{-1} / Lake	AVS	Pyrite	S^0	S_{org}	S_{inorg}	$S_{total} = S_{org} + S_{inorg}$
SAS 2A	2.4	1.6	0.2	4.8	4.2	9.0
SAS 1A	2.8	0.7	0.1	4.0	3.6	7.6
KWK12	2.0	0.4	0.2	3.0	2.6	5.6
BGR 1	0.8	0.3	0.2	0.6	1.2	1.8

Because chromium reduction is specified of inorganic-S determination (Canfiled, 1986), organic sulphur was determined by subtracting the total inorganic sulphur content (AVS+Pyrite+S^0) to the total sulphur obtained by elemental analysis.

In order to better visualize the different types of sulphur compounds in our samples, pie diagrams were made using the results of table 28.

In figure 45 the relative percentage of organic-S and inorganic-S compounds for each lake is presented.

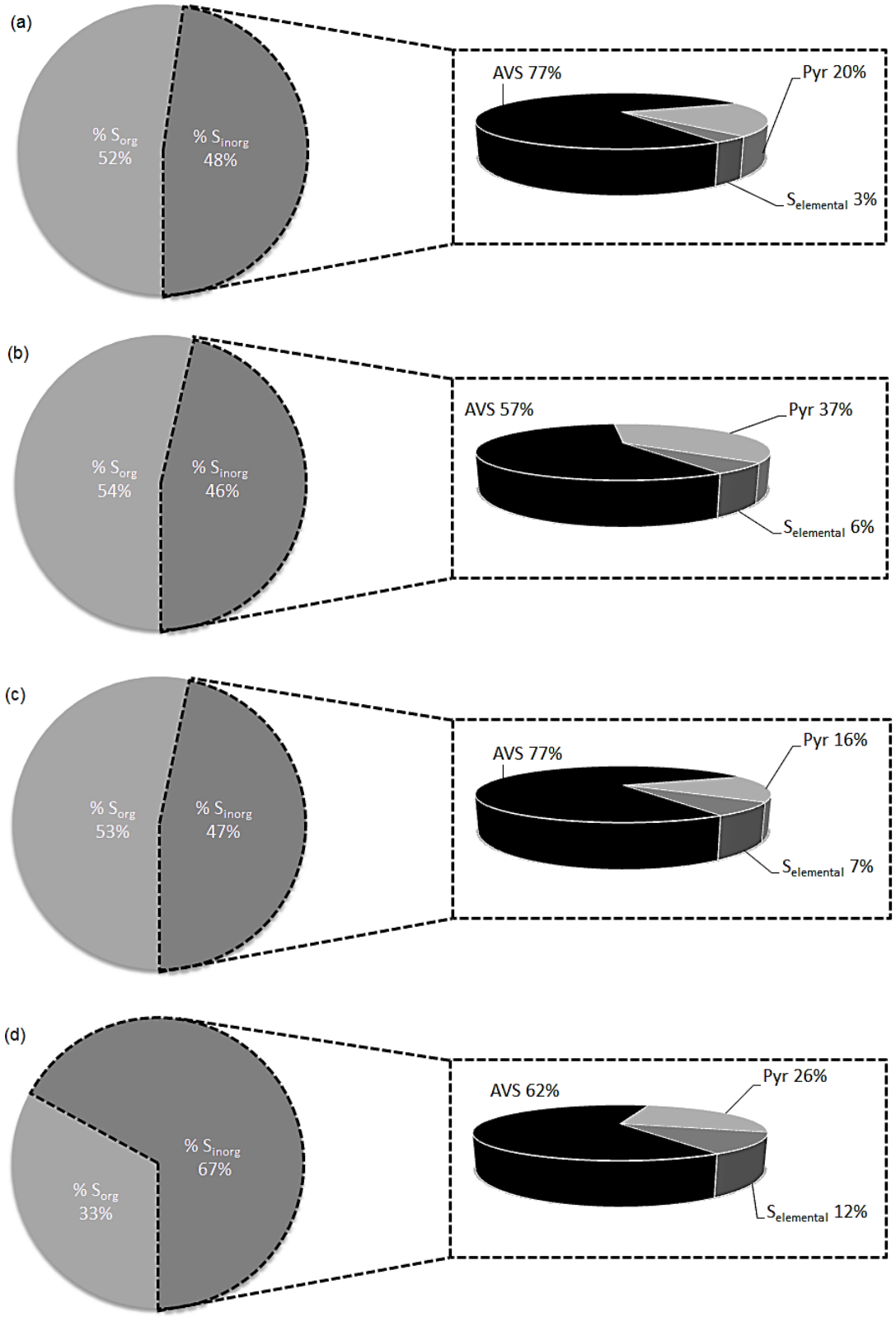

Figure 45: Graphic representation of total sulphur, its relative percentage of organic-S and inorganic-S (on the left) and also the relative amount of the inorganic-S species (on the right) in SAS 1A (a), SAS 2A (b), KWK12 (c) and BGR1 (d) samples.

The results clearly showed a difference in the content of organic and inorganic sulphur compounds between the lakes. While in the high carbon thermokarst lakes (SAS and KWK) the organic-S was the major constituent, in BGR lake the opposite was observed, suggesting that the major source of sulphur is natural organic matter.

In fact, a significant positive Spearman correlation ($r_s = 0.989$; *p<0.05*) was found between sedimentary organic matter (LOI) and organic-S, which leads to assume that this compound was most likely, associated with humic substances present in the soil (Vairavamurthy et al., 1997). Large organic polymers that have extensive sulfur cross-linking are protected from enzymatic decomposition and microbial attack contributing for organic matter preservation being, probably, the source of organic-S in the studied lakes (Russell et al., 2000; Lepot et al., 2009).

In the sampled lakes, AVS was the major constitute of inorganic-S.

Among the inorganic sulphur species, acid volatile sulphides (AVS) are constituted mainly by amorphous iron sulfide (FeS), and other trace elements that may co-precipitate during the precipitation process (Morse, 1994). These sulphides are redox sensitive and can be easily oxidize when environment became less anoxic (Rickard, 2012). In other way in high anoxic environments, pyrite is the most form of iron sulphide (Rickard and Morse, 2005; Zopfi et al., 2008). Additionally and according to Morse (1994) the formation of crystalline pyrite besides occurring in an extremely anoxic environment is a slowly geochemical process.

The results obtained in the sampled lakes appear to be contradictory to what is reported in literature: highly anoxic environment but AVS being the major inorganic sulphur compound. The only explanation for this observation is that the sulphides (AVS) in these lakes were recently formed by precipitation of FeS in the water column, which is in agreement with sulphide production on water, by OM degradation described in section 4.1.2. Thus, the sulphides present in the surface sediments of the studied thermokarst lakes result from the precipitation of dissolved sulphide in the water column formed in the oxidation of the dissolved organic matter by sulfate reduction (section 4.1.2.).

4.2.6. Sequential Extractions

Figure 46 presents the results obtained for lead and chromium in the sequential extractions.

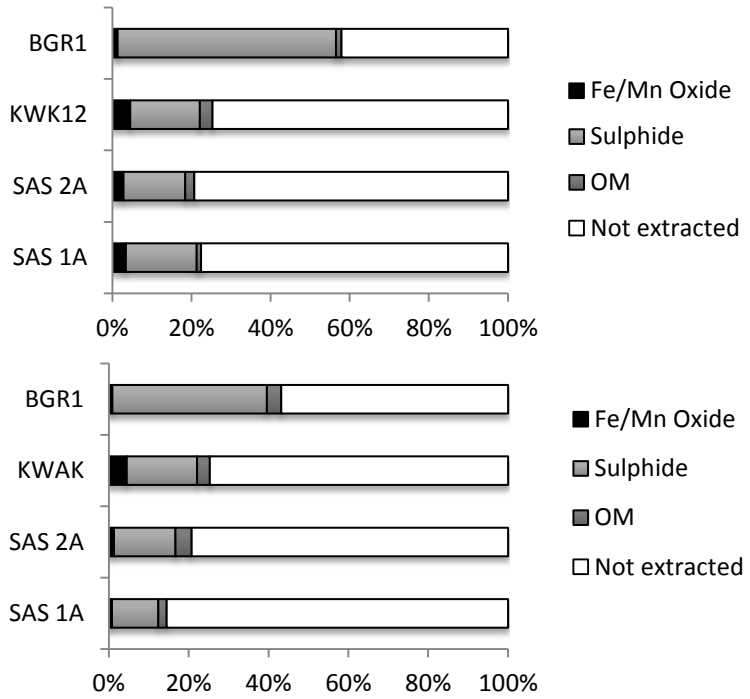

Figure 46: Sequential extraction fraction of Pb (up) and Cr (down) in (%).

It is generally accepted that the $NH_2OH.HCl$ solution solubilize the Fe and Mn oxy-hydroxides, HCl promotes the solubilization of sulphides and H_2O_2 are capable of oxidizing natural organic matter (Tessier et al., 1979), sulphide (Madureira, 1997), and OM (Tessier et al., 1979). During these extractions, the associated trace elements (TE) are also solubilized and their quantification indicate that the amount of TE present in the correspondent mineralogical fraction.

The results presented in figure 46 clearly show that a higher amount of Pb and Cr (similar results were obtained for the other TE) was associated with the sulphide fraction (HCl extraction) in the surface sediments. Thus, the retention of TEs in the topmost sediment layers in the study lakes was mainly in the form of TE-sulphides or TE that co-precipitated with Fe-sulphides (AVS or Pyrite). Since our solid sulphur speciation results showed that AVS is the most abundant solid sulphide form, it can be assumed that the retention of TE in the surface sediments of these lakes result from co-precipitation of those TE with AVS. Interestingly the most “inorganic lake” (BGR 1) was where a large amount of Cr and Pb was extracted with HCl suggesting that the permafrost soil composition plays also an important role in this TE accumulation process.

5. Conclusion

Thermokarst lakes are chemically dynamic, freshwater systems. Figure 47 represents a schematic model of the potential biogeochemical processes occurring in a thermokarst lake summarizing the conclusions obtained in the present study.

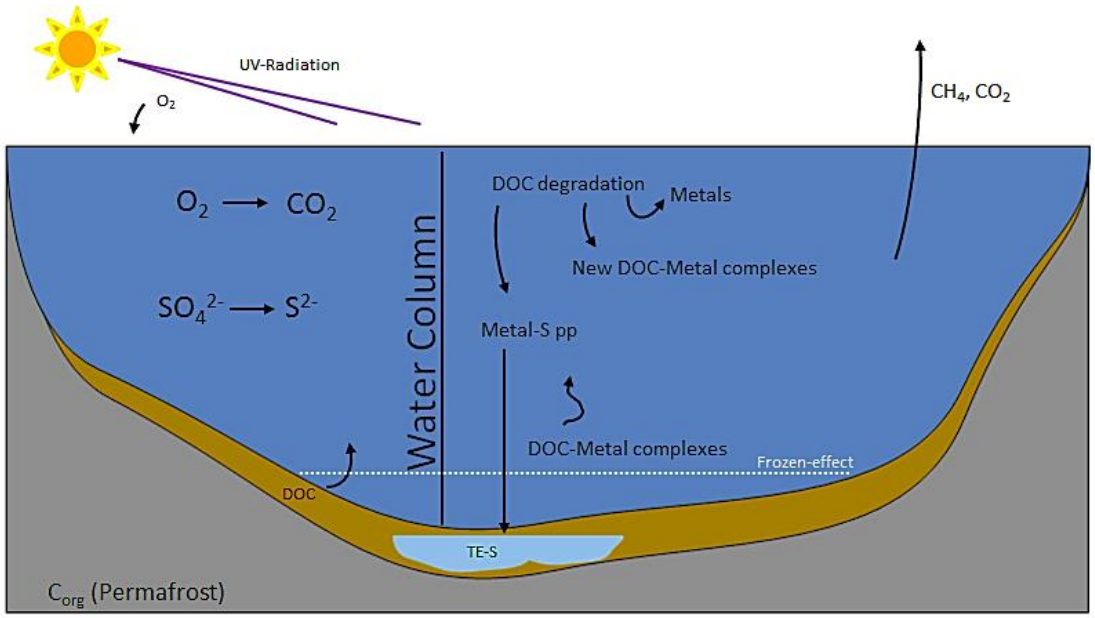

Figure 47: Schematic model of the potential biogeochemical processes occurring in a thermokarst lake.

The permafrost soils that the lakes are derived from play a major role in their chemistry. As an example the organic-sulphur in highly organic lakes (SAS and KWK) were the most dominant sulphur compounds and apparently had less content on other trace elements. However, the biogeochemical processes seemed to be identical in all the catchments.

In all the studied lakes dissolved oxygen decrease with depth suggesting its consumption by the mineralization of the natural organic matter. This mineralization was also indicated by a similar consumption of sulfate and the consequent production of dissolved sulphide. This process tends to reduce the concentration of DOC in the water column, which was more pronounced at the surface. This downward increase of DOC may also be related to photo-oxidation (of OM) at the surface and molecular diffusing (and possible the frozen effect) at the sediment/water interface.

The DOC in the studied lakes is from plant origin (δ^{13}C-DOC data) and is also the source of labile TEs to the water column. The experiments done in the UV-irradiation chamber indicated an increase of labile TEs in solution due to the mineralization of organic matter.

The vertical profiles for the studied TEs showed that besides their release during OM mineralization there were also other competing process in the water column: complexation with DOC (e.g. SAS 2A) and precipitation (or co-precipitation) as metal-sulphides (e.g. Cu and Pb in SAS 1A).

This precipitation was evident in all the studied lakes since they all had large amounts of amount of TE-sulphides in the surface sediments (sequential extractions) mainly in the form of AVS, the most reactive form of reduced inorganic sulphur compounds. In spite of the role of sulphur in the retention of TEs at the surface sediments, the association of these elements in aluminium-containing minerals (alumino-silicates) or other more refractory compounds should not be excluded since a considerable amount of those TEs would not have been extracted by the methods used in this study.

The ssNMR data clearly showed that NOM is mineralized in the sediments since the metabolites of cellulose degradation were identified by this technique. In water column, only indirect evidence of this mineralization process was obtained (UV experiments and DO and sulfate reduction).

6. Future Work

This work was a preliminary, exploratory study of the geochemistry of sub-arctic thermokarst lakes and providing some first information about trace element partitioning, speciation and fate. This opens up new topics for future research. In particular it will be interesting to:

1) Study the biogeochemistry of the lakes in winter, when a more anoxic system is probably found because of the snow and ice cover;
2) Fractionate the soils and sediments in different mesh sizes, and quantify the associated TE and OM to give a view of the molecular mass in each fraction, and thus to identify which TE have higher affinities;
3) Quantify iron concentrations, and determine if there is any relationship between AVS or Pyrite present, and any influence in the TE speciation or the limnological proprieties of the lake;
4) Establish a more efficient methodology to concentrate DOC in the water samples for quantification by ^{1}H NMR or HPLC-MS analysis.
5) Examine organic matter degradation in the water column by analyzing bacterial metabolites or by the use of incubation with stable isotopes.
6) Measure of diffusive and advective fluxes under summer and winter conditions (e.g. using benthic flux chambers) to better understand the role of sedimentary DOC in processes occurring in the water column and mixing effect.

7. References

Adriano, D. C. 2001. Trace Elements in Terrestrial Environments: Biogeochemistry, Bioavailability, and Risks of Metals; Springer Science & Business Media; 2th Edition; USA

Aiken G. R., McKnight D. M., Wershaw R. L., MacCartry P. 1985. An introduction to humic substances in soil, sediment and water. In: Aiken G. R., et al. (Eds.), Humic Substances in Soil, Sediment, and Water. John Wiley & Sons, New York, pp. 1–8

Alina Kabata-Pendias, Trace Elements in Soils and Plants, CRC Press, 4th edition 2010

Allard M. and Seguin M. K. 1987b. Le pergelisol au Quebec Nórdique: Bilan et perspectives. Géographie Physique et Quaternaire 41, pp 141-152

Allard M. and Séguin, M. K. 1987a. Permafrost in northern Quebec: state of knowledge and research needs. Le pergélisol au Québec nordique: bilan et perspectives 41 (1), pp 141–152

André V. and Duarte M. T. 2014. Pseudopolymorphism of levodopa: A novel ‘‘disappearing’’ dihydrate. Journal of Molecular Structure 1076, pp 238–243

Antoniades D., Douglas M. S. V. and Smol J. P. 2003. The physical and chemical limnology of 24 ponds and one lake from Isachsen, Ellef Ringnes Island, Canadian High Arctic. – International Review of Hydrobiology, 88: 519–538

Arlen-Pouliot Y. and Bhiry N. 2005. Paleoecology of a palsa and a filled thermokarst pond in a permafrost peatland, subarctic Quebec, Canada. The Holocene 15 (3), pp 408–419

Arp C. D. and Jones B. M. 2008. Geography of Alaska Lake Districts. U. S. Geological Survey Scientific Investigations Report, Nº 5215, pp 1-40

Audry S., Pokrovsky O. S, Shirokova L. S, Kirpotin S. N., Viers J., Dupré B. (2011a) Effect of permafrost thawing on the organic carbon and metal speciation in thermokarst lakes of western Siberia. Biogeosciences, 8, pp 565–583

Audry S., Pokrovsky O. S, Shirokova L. S, Kirpotin S. N., Dupré B. (2011b) Organic matter mineralization and trace element post-depositional redistribution in Western Siberia thermokarst lake sediments. Biogeosciences 8: pp 3341–3358

Baldock J. A., Oades J. M., Nelson P. N., Skene T. M., Golchin A., Clarke P. 1997. Assessing the extent of decomposition of natural organic materials using solid-state 13C NMR spectroscopy. Australian Journal of Soil Research 35(5), pp 1061–1083

Baldock J. A. and Preston C. M. 1995. Chemistry of carbon decomposition processes in forests as revealed by solid-state carbon-13 nuclear magnetic resonance. In: McFee, W.W., Kelly, J.M.

(Eds.), Carbon Forms and Functions in Forest Soils. Soil Science Society of America. Madison, Wisconsin, pp. 89–117

Barnett S. J., Adam C. D., Jackson A .R. W., Hywel-Evans P. D. 1999. Identification and characterisation of thaumasite by XRPD techniques, Cement and Concrete Composites 21, pp. 123-128

Barshick C. M.; Duckworth, D. C.; Smith D. H. 2000. Inorganic Mass Spectrometry Fundamentals and Applications; Marcel Dekker, Inc., New York, pp 67-144

Benedetti Marl F., Riemsdijk W. H. V., Koopal L. K., Kinniburgh D. G., Gooddy D. C. and Milne C. J. 1996. Metal ion binding by natural organic matter: From the model to the field. Geochimica et Cosmochimica Acta, Vol. 60, No. 14, pp 2503-2513

Benner R. and Storm M., 1993. A critical evaluation of the analytical blank associated with DOC measurements by high-temperature catalytic oxidation. Marine Chemistry 41, pp 153-160

Berner R. A. 1980. Early Diagenesis: A Theoretical Approach. Princeton University Press, New York

Beyer L., White, D.M., Bölter, M., 2001. Soil organic matter composition, transformation, and microbial colonization of gelicpodzols in the coastal region of east Antarctica. Australian Journal of Soil Research 39, pp 543–563

Bhiry N., Delwaide A., Allard M., Bégin Y., Filion L., Lavoie M., Nozais C., Payette S., Pienitz R., Saulnier-Talbot E., Vincent W. F. 2011. Environmental change in the Great Whale River region, Hudson Bay: Five decades of multidisciplinary research by Centre d'études nordiques (CEN). Ecoscience 18, pp 182–203

Blodau C., Hoffmann S., Peine A. & Peiffer S. 1998. Iron and sulfate reduction in the sediments of acidic mine lake 116 (Brandenburg, Germany): Rates and geochemical evaluation. Water, Air and Soil Pollution, 108, pp 249-270

Bockheim J. G., Hinkel K. M., Eisner W. R., Dai X. Y. 2004. Carbon pool sand accumulation rates in an age-series of soils in drained thaw-lake basins, Arctic Alaska. Soil Science Society of America Journal 68, pp 697–704

Boike J., Roth K. and Ippisch O. 2003. Seasonal snow cover on frozen ground: Energy balance calculations of a permafrost site near Ny-Ålesund, Spitsbergen. Journal of Geophysical Research 108, doi: 10.1029/2001JD000939

Bond A. M. 1980. Modern Polarographic Methods in Analytical Chemistry Marcel Dekker Inc., New York and Basel

Bouchard F., Francus P., Pienitz R., Laurion I., Feyte S. 2014. Subarctic thermokarst ponds: investigating recent landscape evolution and sediment dynamics in thawed permafrost of Northern Québec (Canada). Arctic, Antarctic, and Alpine Research, 46(1), pp 251-271

Brandes J. A. 2009. Rapid and precise δ13C measurement of dissolved inorganic carbon in natural waters using liquid chromatography coupled to an isotope-ratio mass spectrometer. Limnology and Oceanography: Methods, 7, pp 730–739

Breton J., Vallières C., Laurion I. 2009. Limnological properties of permafrost thaw ponds in northeastern Canada. Canadian Journal of Fisheries and Aquatic Sciences Vol. 66, pp 1635-1648

Brown R. J. E. 1970. Permafrost in Canada. University of Toronto Press, Toronto, pp 234

Burn C. R. 2002. Tundra lakes and permafrost, Richards Island, western Arctic coast, Canada. Canadian Journal of Earth Sciences 39, pp 1281–1298

Burn C. R. and Smith C. A. S. 1988. Observations of the 'thermal offset' in near-surface mean annual ground temperatures at several sites near Mayo, Yukon Territory, Canada. Arctic, 41(2), pp 99-104

Burn C. R. and Smith M. W. 1990. Development of thermokarst lakes during the Holocene at sites near Mayo, Yukon territory. Permafrost & Periglacial Processes 1, pp 161–175

Caglar B., Afsin B., Tabak A., Eren E. 2009. Characterization of the cation-exchanged bentonites by XRPD, ATR, DTA/TG analyses and BET measurement, Chemical Engineering Journal 149 pp. 242–248

Callaghan T., Johansson M., Anisimov O., Christiansen H., Instanes A., Romanovsky V., Smith S. 2011. Changing permafrost and its impacts. In: Snow, Water, Ice and Permafrost in the Arctic (SWIPA): Climate Change and the Cryosphere. Arctic Monitoring and Assessment Programme, Oslo, pp. 5.1-5.62

Calmels F., Allard M., and Delisle G. 2008. Development and decay of a lithalsa in Northern Québec: a geomorphological history. Geomorphology 97, pp 287–299

Calmels F. and Allard M. 2004. Ice segregation and gas distribution in permafrost using tomodensitometric analysis. Permafrost & Periglacial Processes 15(4), pp 367–378

Canário J., 2004. Mercúrio e monometilmercúrio na cala do norte do estuário do Tejo. Dissertação apresentada à Universidade Nova de Lisboa, Faculdade de Ciências e Tecnologia, para obtenção do grau de doutor em ciências do ambiente, pp 48

Canário J., Vale C., Caetano M., Madureira M. J. 2003. Mercury in contaminated sediments and pore waters enriched in sulfate (Tagus Estuary, Portugal). Environmental Pollution 126, pp 425–433

Canavan R. W., Van Cappellen P., Zwolsman J. J. G., van den Berg G. A. & Slomp C. P. 2007. Geochemistry of trace metals in a fresh water sediment: field results and diagenetic modelling. Science of Total Environment, 381, pp 263-279

Canfield D. E., Raiswell R., Westrich J. T., Reaves C. M., Berner R. A. 1986. The use of chromium reduction in the analysis of reduced inorganic sulfur in sediments and shales. Chemical Geology, 54, pp 149-155

Cao X., Olk D. C., Chappell M., Cambardella C. A., Miller L. F., Mao J. 2011. Solid-state NMR analysis of soil organic matter fractions from integrated physical–chemical extraction. Soil Science Society of America Journal, 75, pp 1374–1384

Carter M. R., and Gregorich E. G., Soil Sampling and Methods of Analysis, Canadian Society of Soil Sciente, 2th edition, CRC Press, 2008

Cauwet G. 1994. HTCO method for dissolved organic carbon analysis in seawater: influence of catalyst on blank estimation. Marine Chemistry 47, pp 55-64

Chester R. and Huges M. J. 1967. A chemical technique for the separation of ferromanganese minerals, carbonate minerals and adsorbed trace metals from pelagic sediments. Chemical Geology, 2, pp 249–262

ChemWiki site (09/07/2015): http://chemwiki.ucdavis.edu/Physical_Chemistry/Spectroscopy/Magnetic_Resonance_Spectroscopies/Nuclear_Magnetic_Resonance

Ciais P. and Sabine C. L. 2013. Carbon and other biogeochemical cycles. In: Stocker T. F., Qin D., Plattner G. K., Tignor, M. (Eds.). Climate Change 2013: The Physical Science Basis. Contribution of Working Group I to the Fifth Assessment Report of the Intergovernmental Panel on Climate Change. Cambridge University Press, Cambridge, pp 465-570

Combs, S.M., and Nathan, M.V. 1998. Soil organic matter. Pp. 57-58. In J.R. Brown (Ed.), Recommended Chemical Soil Test Procedure for the North Central Region. Columbia, MO.

Coplen T. B. 1996. Guidelines for reporting certain isotopic values relevant to ground-water studies. Ground Water. Vol. 34, pp 388

Corin N., Backlund P., and Kulovaara M. 1996. Degradation products formed during UV-irradiation of humic waters. Chemosphere. Vol. 33, No. 2, pp 245-255

Cory R. M., Ward C. P., Crump B. C. and Kling G. W. 2014. Sunlight controls water column processing of carbon in arctic fresh waters, Science, 345(6199), pp 925–928

Coté M. M. and Burn C. R. 2002. The oriented lakes of Tuktoyaktuk Peninsula, western Arctic coast, Canada: a GIS-based approach. Permafrost & Periglacial Processes 13, pp 61–70

Cresser M., Killham K., Edwards T., Soil chemistry and its applications, Cambridge Environmental Chemistry Series 5, 1993

Crevecoeur S., Vincent W. F., Comte J. and Lovejoy C. 2015. Bacterial community structure across environmental gradients in permafrost thaw ponds: Methanotroph-rich ecosystems. Front. Microbiol. 6:192. doi: 10.3389/fmicb.2015.001924

Czudek T. and Demek J. 1970. Thermokarst in Siberia and its influence on the development of low land relief. Quaternary Research 1, pp 103–120

Dahlén J., Bertilsson S., Petterson C. 1996. Effects of UV-A irradiation on dissolved organic matter in humic surface waters. Environment International, Vol. 22, No. 5, pp 501-506

Dai X.Y., Ping C.L., Michaelson G.J. 2002. Characterizing soil organic matter in Arctic tundra soils by different analytical approaches Organic Geochemistry 33, pp 407–419

Davison W. and Zhang H. 1994. In situ speciation measurements of trace components in natural waters using thin-film gels. Nature 367, pp 546–548

Davison W., Fones G. R., Harper M., Teasdale P., Zhang H. 2000. Dialysis, DET and DGT: in situ diffusional techniques for studying water, sediments and soil. In: Buffle J., Horvai G., editors. In-situ monitoring of aquatic systems: chemical analysis and speciation. IUPAC. England: John Wiley & Sons Ltd; pp 495–569

Davison W., Zhang H. and Grime G. W. 1994. Performance characteristics of gel probes used for measuring the chemistry of pore waters. Environnemental Science & Technology, 28, pp 1623-1632

Davison E. A. and Janssens I. A. 2006. Temperature sensitivity of soil carbon decomposition and feedbacks to climate change. Nature 440, pp 165-173

Dean J. R. 2005. Practical Inductively Coupled Plasma Spectroscopy, John Wiley & Sons Ltd, England, pp 23.

DeConto R. M., Galeotti S., Pagani M., Tracy D., Schaefer K., Zhang T., Pollard D., Beerling D. J. 2012. Past extreme warming events linked to massive carbon release from thawing permafrost. Nature 484, pp 87-93

Deshpande, B. N., MacIntyre, S., Matveev, A., Vincent, W.F. 2015. Oxygen dynamics in permafrost thaw lakes: Anaerobic bioreactors in the Canadian subarctic. Limnology and Oceanography, doi: 10.1002/lno.1*0126*

Di Toro D. M., Mahony J. D., Hansen D. J. & Berry W. J. 1996. A model of the oxidation of iron and cadmium sulfide in sediments. Environmental Toxicology and Chemistry, 15, pp 2168-2186

Elenkova N.G., Tsoneva R. A., Nedelcheva T. K. 1979. New turbidimetric method for determination of sulfate. Talanta Journal, Vol. 27. pp 67-68

Essington M. E. Soil and water chemistry: An Integrative Approach; CRC Press LLC; 2th edition; New York, 2005

Evans L. J. 1989. Chemistry of metal retention by soils. Environnemental Science & Technology, 23, pp 1048-1056

Fifield F. W., and Kealey D. Principles and Practice of Analytical Chemistry, 5th Edition, Blackwell Science Ltd, Germany, 2000

French, H. 2007. The periglacial environment, 3th Edition, Wiley, New York, 2007

Fritz M., Opel T., Tanski G., Herzschuh U., Meyer H., Eulunburg A., Lantuit H. 2015. Dissolved organic carbon (DOC) in Arctic ground ice. The Cryosphere, 9, pp 737-752

Froelich P. N., Klinkhammer G. P., Bender M. L., Luedtke N. A., Heath G. R., Cullen D., Dauphin P., Hammond D., Hartman B., Maynard V. 1979. Early oxidation of organic matter in pelagic sediments of the eastern equatorial Atlantic: suboxic diagenesis. Geochimica et Cosmochimica Acta 43, pp 1075–1090

Ginsquiani P. L., Giglioth G., and Businelli D. (1992). Heavy metals in the environment. Journal of Environmental Quality, 21, pp 303-335

Grosse G., Jones B., Arp C. 2013. Thermokarst lakes, drainage, and drained basins, in: Treatise on Geomorphology, edited by: Shroder, J., Giardino, R., and Harbor, J., Academic Press, San Diego, CA, vol. 8, Glacial and Periglacial Geomorphology, pp 325–353

Grosse, G., Romanovsky, V.E., Jorgenson, T., et al., 2011. Vulnerability and feedbacks of permafrost to climate change. Eos Transactions American Geophysical Union, Volume 92, pp 73–74

Gurney S. D. 2001. Aspects of the genesis, geomorphology and terminology of palsas: perennial cryogenic mounds. Progress Physical Geography, 25, pp 249–260

Hamilton P. B., Gajewski K., Atkinson D. E. and Lean D. R. S. 2001. Physical and chemical limnology of 204 lakes from the Canadian Arctic Archipelago. Hydrobiologia 457, pp 133–148

Harper M.P., Davison W., Zhang H., Tych W. 1998. Kinetics of metal exchange between solids and solutions in sediments and soils interpreted from DGT measured fluxes. Geochimica et Cosmochimica Acta 1998; 62(16), pp 2757–70

Harris, D. C. Quantitative Chemical Analysis, 8th, Freeman, New York 2010

Henneke, E., Luther III, G.W. and De Lange, G.J., 1991. Determination of inorganic sulphur speciation with polarographic techniques: Some preliminary results for recent hypersaline anoxic sediments.

In: M.B. Cita, G.J. de Lange and E. Olausson (Editors), Anoxic Basins and Sapropel Deposition in the Eastern Mediterranean: Past and Present. Marine Geology, 100, pp 115-123

Hillier S. 1999. Quantitative Analysis of Clay and other Minerals in Sandstones by X-Ray Powder Diffraction (XRPD), in Clay Mineral Cements in Sandstones (eds R. H. Worden and S. Morad), Blackwell Publishing Ltd., Oxford, UK. doi: 10.1002/9781444304336.ch11

Hinkel K. M., Frohn R. C., Nelson F. E., Eisner W. R., Beck R. A. 2005. Morphometric and spatial analysis of thaw lakes and drained thaw lake basins in the western Arctic Coastal Plain, Alaska. Permafrost & Periglacial Processes 16, pp 327–341

Hinkel K. M., Jones B. M., Eisner W. R., Cuomo C. J., Beck R. A., Frohn R. 2007. Methods to assess natural and anthropogenic thaw lake drainage on the western Arctic coastal plain of northern Alaska. Journal of Geophysical Research 112, F02S16

Hooda P. S. 2010. Introduction, in Trace Elements in Soils (ed P. S. Hooda), John Wiley & Sons, Ltd, Chichester, UK. doi: 10.1002/9781444319477.ch1

Hopkins D. M. 1949. Thaw lakes and thaw sinks in the Imuruk Lake area, Seward Peninsula Alaska. Journal of Geology 57, pp 119-131

Huerta-Diaz M. A., Tessier A. & Carignan R. 1998. Geochemistry of trace metals associated with reduced sulfur in freshwater sediments. Applied Geochemistry, 13, pp 213-233

INAP (International Network for Acid Prevention). 2002. Diffusive Gradients in Thin-films (DGT): A Technique for Determining Bioavailable Metal Concentrations. (http://www.inap.com.au/public_downloads/Research_Projects/Diffusive_Gradients_in_Thin-films.pdf)

Instanes A. 2005. Infrastructure: buildings, support systems, and industrial facilities. Arctic Climate Impact Assessment (ACIA) Scientific Report, C. Symon, Ed., Cambridge University Press, Cambridge, UK, pp 907–944

Iskrenova-Tchoukova E., Kalinichev A. G., Kirkpatrick R. J. 2010. Metal cation complexation with natural organic matter in aqueous solutions: molecular dynamics simulations and potentials of mean force. Langmuir, 2010, 26 (20), pp 15909–15919

Jansson J. K., and Tas N. 2014. The microbial ecology of permafrost. Nature Reviews Microbiology, 12, pp 414-425

Jeffries M. O., Zhang T., Frey K., Kozlenko N. 1999. Estimating late-winter heat flow to the atmosphere from the lake-dominated Alaskan North Slope. Journal of Glaciology 45(150), pp. 315–324

Jenkins, R. 1986. JCPDS - International Centre for Diffraction Data - Sample preparation Methods in X-Ray Powder Diffraction. Powder Diffraction, Vol.1, Nº 2, pp 51-63

Jones B., Grosse G., Arp C. D., Jones M. C., Walter A. K. M., Romanovsky V. E. 2011. Modern thermokarst lake dynamics in the continuous permafrost zone, northern Seward Peninsula, Alaska. Journal of Geophysical Research–Biogeosciences 116, G2

Jorgenson M. T. and Shur Y. 2007. Evolution of lakes and basins in northern Alaska and discussion of the thaw lake cycle. Journal of Geophysical Research 112, F02S17

Jorgenson M. T., Romanovsky V., Harden J. 2010. Residence and vulnerability of permafrost to climate change. Canadian Journal of Forest Research 40(7), pp 1219-1236

Kankaala P., Taupale S., Grey J., Sonninen E., Arvola L., and Jonse R. I. 2006. Experimental D13C evidence for contribution of methane to pelogic food webs in lakes. Limnology and Oceanography, 51, pp 2821-2827

Karlsson J., Christensen T. R., Crill P., Forster J., Hammarlund D., Jackowicz-Korczynski M., Kokfelt U., Roehm C., Rosén P. 2010. Quantifying the relative importance of lake emissions in the carbon budget of a subarctic catchment. Journal of Geophysical Research. Vol. 115. G03006.

Kenneth N. 2010. Reducing the Effects of Interferences in Quadrupole ICP-MS. Spectroscopy, Vol. 25 Issue 11, pp 30

Kling G. W., Kipphut G. W., Miller M. C. 1991. Arctic lakes and streams as gas conduits to the atmosphere: implications for tundra carbon budgets. Science 251, pp. 298–301

Kögel-Knabner, I., 1997. 13C and 15N NMR spectroscopy as a tool in soil organic matter studies. Geoderma 80, pp 243–270.

Kolmert A., Wikstrom P., Hallberg K. B. 2000. A fast and simple turbidimetric method for the determination of sulfate in sulfate-reducing bacterial cultures. Journal of Microbiological Methods 41, pp 179–184

Lamarre A., Garneau M., Asnong H. 2012. Holocene paleohydrological reconstruction and carbon accumulation of a permafrost peatland using testate amoeba and macrofossil analyses, Kuujjuarapik, subarctic Québec, Canada. Review of Palaeobotany and Palynology 186, pp 131–141

Larner B. L., Seen A. J., Snape I. 2006. Evaluation of diffusive gradients in thin film (DGT) samplers for measuring contaminants in the Antarctic marine environment. Chemosphere 65, pp 811–820

Laurion I., Vincent W. F., MacInture S., Retamal L., Dupont C., Francus P., Pienitz R. 2010. Variability in greenhouse gas emissions from permafrost thaw ponds. Limnology and Oceanography, 55, pp 115-133

Lawrence D. M. and Slater A. G. 2005. A projection of severe near-surface permafrost degradation during the 21st century. Geophysical Research Letters 32: L24401

Lepot K., Benzerara K., Rividi N., Cotte M., Brown G. E., Philippot P. 2009. Organic matter heterogeneities in 2.72 Ga stromatolites: alteration versus preservation by sulfur incorporation. Geochimica et Cosmochimica Acta 73, pp 6579–6599

Lewis A., van Hille R. 2006. An exploration into the sulphide precipitation method and its effect on metal sulphide removal. Hydrometallurgy. Volume 81, Issues 3–4, pp 197–204

Lim D. S. S., Douglas M. S. V., Smol J. P. and Lean D. R. S. 2001. Physical and chemical limnological characteristics of 38 lakes and ponds on Bathurst Island, Nunavut, Canadian High Arctic. International Review of Hydrobiology. 86, pp 1–22

Lin Z., Niu F., Xu Z., Xu J., Wang P. 2010. Thermal regime of a thermokarst lake and its influence on permafrost, Beiluhe Basin, Qinghai-Tibet Plateau. Permafrost and Periglacial Processes, pp. 692

Ling F. and Zhang T. J. 2004. Modeling study of talik freeze-up and permafrost response under drained thaw lakes on the Alaskan Arctic Coastal Plain. Journal of Geophysical Research 109, D01111

Ling F. and Zhang, T. 2003. Numerical simulation of permafrost thermal regime and talik development under shallow thaw lakes on the Alaskan Arctic Coastal Plain Journal of Geophysical Research-Atmospheres 108(D16), pp 4511

Lu Z., Minghong C., Juan W., Yin Z., Yang H. 2012. Levels and distribution of trace metals in surface sediments from Kongsfjorden, Svalbard, Norwegian Arctic. Environmental Geochemistry and Health, Doi. 10.1007/s10653-012-9481-z

Luther G. W. and Tsamakis E. J. 1989. Concentrations and form of dissolved sulfide in the oxic water column of the ocean. Marine Chemistry, 27, pp 165-177

Luther G. W., Ferdelman T. G., Kostka J. E., Tsamakis E. J., Church T. M. 1991. Temporal and spatial variability of reduced sulphur species (FeS, $S_2O_3^{2-}$) and porewater parameters in salt marsh sediment. Biogeochemistry, 14, pp 57–88

Luther III, G.W., Giblin, A.E. and Varsolona, R., 1985. Polarographic analysis of sulfur species in marine porewaters Limnology and Oceanography, 30, pp 727-736.

Mackay J. R. 1988. Catastrophic lake drainage, Tuktoyaktuk Peninsula area, District of Mackenzie. In: Current Research, Part D. Geological Survey of Canada, pp 83–90

Madureira M. J. 1997. Bioquímica do enxofre em sedimentos de sapais. Efeitos na Química do ferro e manganês. Dissertação apresentada à Universidade Técnica de Lisboa, Instituto Superior Técnico, para obtenção do grau de doutor em Química, pp. 219

Malcolm R. 1989. Applications of solid-state 13C NMR spectroscopy to geochemical studies of humic substances. John Wiley & Sons, New York, pp. 339–372

Mallory M. L., Fontaine A. J., Smith P. A., Robertson M. O. W. and G. Gilchrist. 2006. Water chemistry of ponds on Southampton Island, Nunavut, Canada: effect of habitat and ornithogenic inputs. – Archiv Hydrobiologie, 166, pp 411–432

Manasypov R. M., Pokrovsky O. S., Kirpotin S. N. and Shirokova L. S. 2014. Thermokarst waters across the permafrost zones of western Siberia, The Cryosphere, 8(4), pp 1177–1193

Manasypov R. M., Pokrovsky O. S., Kirpotin S. N., Shirokova L. S. 2013. Hydrochemical composition of thermokarst lake waters in the permafrost zone of western Siberia within the context of climate change. The Cryosphere Discuss., 7, pp 5333–5387

Mann E. A., Mallory M. L., Ziegler S. E., Tordond R., O'Driscoll N. J. 2015. Mercury in Arctic snow: Quantifying the kinetics of photochemical oxidation and reduction. Science of the Total Environment 509–510, pp 115–132

Mao J., Chen N., Cao X. 2011. Characterization of humic substances by advanced solid state NMR spectroscopy: demonstration of a systematic approach. Organic Geochemistry Journal, 42, pp 891–902

Marchenko S. and Etzelmuller B. 2013. Permafrost: formation and distribution, thermal and mechanical properties. In: Shroder J. (Editor in Chief), Giardino R., Harbor J. Eds.), Treatise on Geomorphology Academic Press, San Diego , CA, vol.8, Glacial and Periglacial Geomorphology, pp 202–222

Marsh P. and Neumann N. 2001. Processes controlling the rapid drainage of two ice-rich permafrost-dammed lakes in N. W. Canada. Hydrological Processes 15, pp 3433–3446

Martinez J. M. L., Chattah A. K., Monti G. A., Denis M. F. L., Buldain G. Y., Orto V. C. D. 2008. New copper(II) complexes of polyampholyte and polyelectrolyte polymers: Solid-state NMR, FTIR, XRPD and thermal analyses, Polymer 49, pp 5482–5489

Matthews J. 2012. The SAGE Handbook of Environmental Change. Volume 1: Approaches, Evidences and Causes. SAGE Publications Ltd, UK, pp 228

May T. W. and Wiedmeyer R. H. 1998. A Table of Polyatomic Interferences in ICP-MS, Atomic Spectroscopy. Vol. 19(5), September/October USA

Metzler D. E. Biochemistry Vol. 2. Chapt 18 Elsevier Edition. Academic Press. USA 2003

Michaelson G. J., Ping C. L., Kling G. W., and Hobbie J. E. 1998. The character and bioactivity of dissolved organic matter at thaw and in the Spring runoff waters of the arctic tundra north slope, Alaska, Journal of Geophysical Research, 103, pp 28939-28946

Michelutti N., Douglas M. S. V., Muir D. C. G. and Smol J. P. 2002. Limnological characteristics of 38 lakes and ponds on Axel Heiberg Island, High Arctic Canada. – International Review of Hydrobiology, 87, pp 385–399

Morgenstern A., Grosse G., Guenther F., Schirrmeister L. 2011. Spatial analyses of thermokarst lakes and basins in Yedoma landscapes of the Lena Delta. The Cryosphere 5, pp 849–867

Morse J. W. 1994. Interactions of trace metals with authigenic sulfide minerals: implications for their bioavailability. Marine Chemistry, Volume 46, Issues 1–2, pp 1–6

Naidu A. S., Blanchard A., Kelley J. J., Goering J. J., Hameedi M. J., Baskaran M. 1997. Heavy metals in Chukchi Sea sediments as compared to selected circumarctic shelves. Marine Pollution Bulletin, 35, pp 260–269

Negandhi K., Laurion I., Whiticar M. J., Galand P. E., Xu X., Lovejoy C. 2013. Small thaw ponds: an unaccounted source of methane in the Canadian High Arctic. PLoS ONE 8(11): e78204

Nelson P. N. and Baldock J. A. 2005. Estimating the molecular composition of a diverse range of natural organic materials from solid-state 13C NMR and elemental analyses. Biogeochemistry 72, pp 1–34

NIOSH. 2003. Manual of Analytical Methods, METHOD 7500, Issue 4, dated 15 March

Pandey A. K., Pandey S. D., Misra V. 2000. Stability Constants of Metal-Humic Acid Complexes and Its Role in Environmental Detoxification. Ecotoxicology and Environmental Safety 47, pp 195-200

Pansu M. and Gautheyrou J. 2003. Handbook of Soil Analysis: Mineralogical, Organic and Inorganic Methods, Springer, NY, 2003

Paul E. Soil Microbiology, Ecology and Biochemistry. Chap 9: The Metabolic Physiology of Soil Microorganisms, pp 259, 4th ed., Elsevier Inc., USA 2014

Paulerg B. G., Simpson A. J., McNally D. J., Lamoureux S. F., and Simpson M. J. 2010. Arctic permafrost active layer detachments stimulate microbial activity and degradation of soil organic matter. Environmental Science & Technology, 44, pp 4076–4082

Payette S. 2001. Les processus et les formes périglaciaires. In: Payette, S., Rochefort, L. (Eds.), Écologie des tourbières du Québec–Labrador. Les Presses de l'Université Laval, Québec, Canada, pp 199–239.

Piccolo A., Mejkalová D. S., Spaccini R. 2008. Multivariate analysis of CPMAS 13C-NMR spectra of soils and humic matter as a tool to evaluate organic carbon quality in natural systems, European Journal of Soil Science, 59, pp 496–504

Pienitz R., Smol J. P. and Lean D. R. S. 1997. Physical and chemical limnology of 24 lakes located between Yellowknife and Contwoyto Lake (Northwest Territories), arctic Canada. Canadian Journal of Fisheries and Aquatic Sciences, 54, pp 347–358

Pines, A., Gibby, M. G., & Waugh, J. S. 1973. Proton-enhanced NMR of dilute spins in solids. Journal of Physical Physics, 59(2), pp 569–590

Plug L. J., and West J. J. 2009. Thaw lake expansion in a two-dimensional coupled model of heat transfer, thaw subsidence, and mass movement. Journal of Geophysical Research 114, F01002

Pokrovsky O. S., Shirokova L. S., Pokrovsky B. G., Desmukh C., Kirpotin S. N., Viers J., Audry S. 2013. Biogeochemistry of organic carbon, CO_2, CH_4, and trace elements in thermokarst water bodies in discontinuous permafrost zones of Western Siberia. Biogeochemistry, 113, pp 573–593

Prowse T. D., Furgal C., Bonsai B. R. et al. 2009. Climate conditions in northern Canada: past and future. AMBIO A Journal of the Human Environment, 38(5), pp 257-265

Przytulska A., Bartosiewicz M., Rautio M., Dufresne F., and Vincent W. F. 2014. Climate effects on high latitude *Daphnia* via food quality and thresholds. PLoS ONE 10(5): e0126231

Rampton V. M. 1988. Quaternary Geology of the Tuktoyaktuk Coastlands, Northwest Territories. Geological Survey of Canada, 423, pp 98

Reuter J. H. and Perdue E. M. 1977. Importance of heavy metal-organic matter interactions in natural waters. Geochimica et Cosmochimica Acta. Vol 41 pp 325-334

Rickard D. 2012. Developments in Sedimentology. Chap. 14: Sedimentary Sulphides. Vol. 65, pp 544-593

Rickard D. and Morse J. 2005. Acid volatile sulfide (AVS). Marine Chemistry, 97, pp 141–197

Robertson S. 2011. Direct Estimation of Organic Matter by Loss on Ignition: Methods. SFU ScienceLab.

Romanovsky V., Smith S., Christiansen H. 2010. Permafrost thermal state in the polar Northern Hemisphere during the International Polar Year 2007-2009: a synthesis. Permafrost, Laptev Sea Region, Russia. Permafrost & Periglacial Processes 21, pp 106-116

Rossum J. R. and Villarruz P. 1961. Suggested methods for turbidimetric determination of sulfate in water. Journal American Water Works Association, 53, pp 873

Rumpel C, Eusterhues, Kogel-Knabner L. 2004. Location and chemical composition of stabilized organic carbon in topsoil and subsoil horizons of two acid forest soils. Soil Biology & Biochemistry Journal, 36, pp 177

Russell, M., Hartgers, W.A., Grimalt, J.O., 2000. Identification and geochemical significance of sulphurized fatty acids in sedimentary organic matter from the Lorca Basin, SE Spain. Geochimica et Cosmochimica Acta 64, pp 3711–3723

Schmidt M. W. L., Knicker H., Hatcher P. G., Kogel-Knabner L. 1997. Improvement of 13C and 15N CP/MAS NMR spectra of bulk soils, particle size fractions and organic material by treatment with 10% hydrofluoric acid, European Journal of Soil Science, 48, pp 319-328

Schmidt S., Moskal W., Mora S. J., Howard-Williams C., Vincent W. F. 1991. Limnological properties of Antarctic ponds during winter freezing. Antarctic Science Cambridge Journals, 3, pp 379–388

Schulte, E. E. and Hopkins, B. G. 1996. Estimation of soil organic matter by weight loss-on- ignition. pp 21-31. In F.R. Magdoff, M.A. Tabatabai, and E.A. Hanlon, Jr. (eds.), Soil Organic Matter Analysis and Interpretation. Soil Sci. Soc. Am Madison, WI.

Schuur E. A. G., McGuire A. D., Schädel C., Grosse G., Harden J. W, Hayes D. J., Hugelius G., Koven C. D., Kuhry P., Lawrence D. M., Natali S. M., Olefeldt D., Romanovsky V. E., Schaefer K., Turetsky M. R., Treat C. C., and Vonk J. E. 2015. Climate change and the permafrost carbon feedback. Nature 520, pp 171–179

Schuur E. A. G., Bockheim J., Canadell J. G., Euskirchen E., Field C. B., Goryachkin S. V., Hagemann S., Kuhry P., Lafleur P. M., Lee H., Mazhitova G., Nelson F. E., Rinke A., Romanovsky V., Shiklomanov N., Tarnocai C., Venesy S., Vogel J. G., Zimov S. A. 2008. Vulnerability of permafrost carbon to climate change: implications for the global carbon cycle. Bioscience 58, pp 701–714

Sepulveda-Jáuregui A., Walter Anthony K. M., Martinez-Cruz K., Greene S., and Thalasso F. 2015. Methane and carbon dioxide emissions from 40 lakes along a north–south latitudinal transect in Alaska. Biogeosciences, 12, pp 3197–3223

Settle F. A. 1997. Handbook of Instrumental Techniques for Analytical Chemistry. Prentice-Hall, Inc. pp 419-425

Shiller A. M., Duan S., van Erp P., Bianchi T. S. 2006. Photooxidation of dissolved organic matter in river water and its effect on trace element speciation. Limnology and Oceanography, 51, pp 1716–1728

Shirokova L. S., Pokrovsky O. S., Kirpotin S. N., Desmukh C., Pokrovsky B. G., Audry S., Viers J. 2013. Biogeochemistry of organic carbon, CO_2, CH_4, and trace elements in thermokarst water bodies in discontinuous permafrost zones of Western Siberia. Biogeochemistry, 113, pp 573–593

Silverstein R. M., Bassler G. C., Morrill T. C., 1991. Spectrometric Identification of Organic Compounds. Wiley, New York, Chap 5

Sinke A. J. C., Cornelese A. A., Cappenberg T. E., Zehnder A. J. B. 1992. Seasonal variation in sulfate reduction and methanogenesis in peaty sediments of eutrophic Lake Loosdrecht, The Netherlands. Biogeochemistry 16, pp 43-61

Smith L. C., Pavelsky T. M., MacDonald G. M., Shiklomanov A. I., Lammers R. B. 2007. Rising minimum daily flows in northern Eurasian rivers suggest a growing influence of groundwater in the high-latitude water cycle. Journal of Geophysical Research Biogeosciences 112: G04S47

Spyres G., Nimmo M., Worsfold P. J., Achterberg E. P., Miller A. E. J. 2000. Determination of dissolved organic carbon in seawater using high temperature catalytic oxidation techniques. Trends in Analytical Chemistry, Vol. 19, Nº. 8, pp 498-506

SSSA site (10/05/2015) – Soil Science Society of America https://www.soils.org/discover-soils/soil-basics/soil-types

Stolpe B., Guo L., Shiller A. M., Hassellov M. 2010. Size and composition of colloidal organic matter and trace elements in the Mississippi River, Pearl River and the northern Gulf of Mexico, as characterized by flow field-flow fractionation. Marine Chemistry, 118, pp 119–128

Streletskiy D., Anisimov O., Vasiliev A. 2015. Permafrost Degradation. In: Snow and Ice-Related Hazards, Risks and Disasters. Elsevier Inc. pp 303-344

Stumm W., and Morgan J. J. 1981. Aquatic Chemistry: An Introduction Emphasizing Chemical Equilibria in Natural Waters. New York: Wiley; 780 pp

Sugimura Y. and Suzuki Y. 1988. A high temperature catalytic oxidation method for the determination of non-volatile dissolved organic carbon in seawater by direct injection of liquid sample. Marine Chemistry, 24, pp 105-131

Tannera D. and Baranova V. I. 1999. A dynamic reaction cell for inductively coupled plasma mass spectrometry (ICP-DRC-MS). II. Reduction of interferences produced within the cell. Journal of The American Society for Mass Spectrometry, Vol. 10, pp 1083–1094

Tessier A., Campbell P. G. C., and Blosson M. 1979. Sequential extraction procedure for the speciation of particulate trace metals. Analytical Chemistry, vol. 51, no. 7, pp. 844–851

Torres M. E., Mix A. L., Rugh W. D. 2005. Precise δ13C analysis of dissolved inorganic carbon in natural waters using automated headspace sampling and continuous-flow mass spectrometry. Limnology and Oceanography: Methods 3, pp 349–360

Turner J. and Marshall G. 2011. Climate change in the Polar Regions. Cambridge University Press, UK

Turner K. W., Wolfe B. B., Edwards T. W. D. 2010. Characterizing the role of hydrological processes on lake water balances in the Old Crow Flats, Yukon Territory, Canada, using water isotope tracers. Journal of Hydrology 386(1–4), pp 103–117

Ulrich M., Morgenstern A., Gunther F. et al., 2010. Thermokarst in Siberian ice-rich permafrost: comparison to asymmetric scalloped depressions on Mars. Journal of Geophysical Research 115(E10), E10009

Urban N. R., Gorham E., Underwood J. K., Martin F. B., Ogden III J. G. 1990. Geochemical processes controlling concentrations of Al, Fe, and Mn in Nova Scotia lakes. Limnology and Oceanography, 35(7), pp 1516-1534

USDA site (10/05/2015) Natural Resources Conservation Service Soils: http://www.nrcs.usda.gov/wps/portal/nrcs/detail/soils/survey/partnership/ncss/?cid=nrcs142p2_054167

Vairavamurthy M. A., Maletic D., Wang S., Manowitz B., Eglinton T., Lyons T. 1997. Characterization of Sulfur-Containing Functional Groups in Sedimentary Humic Substances by X-Ray Absorption Near-Edge Structure Spectroscopy. Energy & Fuels 1997, 11, pp 546-553

Vale C., Canário J., Caetano M., Lavrado J., Brito P. 2008. Estimation of the antrophogenic fraction of elements in surface sediments of the Tagus estuary (Portugal). Marine Pollution Bulletin, 56(7), pp 1364-1367

van Everdigen R. O. 2005. (Ed.) Multi-Language Glossary of Permafrost and Related Ground-Ice terms, National Snow and Ice Data Center/World Data Center for Glaciology, Boulder, CO

Vincent W. F., Lemay M., Allard M., and Wolfe B. B. 2013a. Adapting to permafrost change: A science framework. Eos, Transactions of the American Geophysical Union 91: 373-375, doi: 10.1002/2013EO420002

Vincent W. F., Pienitz R., Laurion I., and Walter Anthony K. 2013b. Climate impacts on Arctic lakes. pp 27-42 in Goldman, C.R., Kumagai, M. and Robarts, R.D. (eds). Climatic Change and Global Warming of Inland Waters: Impacts and Mitigation for Ecosystems and Societies, John Wiley & Sons, Ltd, Chichester, U.K.

Viollier E., Jezequel D., Michard G., Pepe M., Sarazin G., Alberic P. 1995. Geochemical study of a crater lake (Pavin Lake, France): trace-element behaviour in the monimolimnion. Chemical Geology, 125, pp 61–72

Voellkopf U., Paul M., Denoyer E. R. 1992, Analysis of solid samples by ICP-mass spectrometry, Fresenius J., Analytical Chemistry, 342, pp 917-923

Vtyurina E. A. 1960. Temperature regime of the Lake Glubokoe. Trudy institute merzlotovedeniya im. V. A. Obrucheva. AN SSSR, Moscow, pp 132–140

Wallace H. J. 1978. Lake tapping in the Colville River Delta, Alaska. Proceedings of the 3th International Conference in a Permafrost Fairbanks, USA, pp 232-238

Walter K. M., Edwards M. E., Grosse G., Zimov S. A., Chapin III. F. S. 2007. Thermokarst lakes as a source of atmospheric CH4 during the last deglaciation. Science 318, pp 633–636

Wang Y., Li M., Zhao Z., Liu W. 2015. Effect of carbonic anhydrase on enzymatic conversion of CO2 to formic acid and optimization of reaction conditions. Journal of Molecular Catalysis B: Enzymatic 116, pp 89–94

Watanabe S., Laurion I., Chokmani K., Pienitz R., and Vincent W. F. 2011. Optical diversity of thaw ponds in discontinuous permafrost: a model system for water color analysis. Journal of Geophysical Research, 116:G02003

Weng L., Temmmingoff E. J. M., Lofts S., Tipping S., Riemsdijk W. H. V. 2002. Complexation with dissolved organic matter and solubility Control of heavy metals in a sandy soil. Environmental Science & Technology, 36, pp 4804-4810

Wharton R. A., Mckay C. P., Clow G. D. and Andersen D. T. (1993) Perennial Ice Covers and their Influence on Antarctic Lake Ecosystems, in Physical and Biogeochemical Processes in Antarctic Lakes (eds W. J. Green and E. I. Friedmann), American Geophysical Union, Washington, D. C. doi: 10.1029/AR059p0053

Williams P. J., and Smith M. W. 1989. The frozen earth. Fundamentals of geocryology. Publisher Cambridge University Press, Cambridge, (hardback). ISBN 0 521 36534 1. 306 pp. Permafrost & Periglacial Process, 4: 178–181

Winch S., Ridal J., Lean D. 2002. Increased metal bioavailability following alteration of freshwater dissolved organic carbon by ultraviolet B radiation exposure. Environmental Toxicology. Vol. 17, Issue 3, pp 267-274

Winefordner J. D. 2003. Sample Preparation Techniques in Analytical Chemistry, John Wiley & Sons Inc., 162, pp 229-235

Wu F. and Tanoue E. 2001. Isolation and partial characterization of dissolved copper-complexing ligands in streamwaters. Environmental Science & Technology, 35, pp 3646–3652

Xue H. B, and Sigg L. 1993. Free cupric ion concentration and Cu(II) speciation in a eutrophic lake. Limnology and Oceanography, 38, pp 1200–1213

Zhang T. 2005. Influence of the seasonal snow cover on the ground thermal regime: An overview. Reviews of Geophysics, Issue 43, RG4002

Zhang W., Miller P. A., Smith B., Wania R., Koenigik T., Doscher R. 2013. Tundra shrubification and tree-line advance amplify arctic climate warming: results from an individual-based dynamic vegetation model, Environmental Research Letters, 8, pp 10

Zhang H. and Davison W. 1995. Performance Characteristics of Diffusion Gradients in Thin Films for the in Situ Measurement of Trace Metals in Aqueous Solution. Anal Chem., 67, Nº 19, pp 3391–3400

Zhang T., Barry R. G., Knowles K., Heginbottom J. A., and Brown J. 1999. Statistics and characteristics of permafrost and ground-ice distribution in the Northern Hemisphere, Polar Geography, 23, pp 132–154

Zhou Z., Chena Na, Cao X., Chua T., Mao J., Mandel R. D., Bettis III E. A., Thompson M. L. 2014. Composition of clay-fraction organic matter in Holocene paleosols revealed by advanced solid-state NMR spectroscopy Geoderma Vol. 223–225, pp 54–61

Zimmerman A. J. and Weindorf D. C. 2010. Heavy Metal and Trace Metal Analysis in Soil by Sequential Extraction: A Review of Procedures. International Journal of Analytical Chemistry. ID 387803, Doi:10.1155/2010/387803

Zimov S. A., Voropaev Y. V., Semiletov I. P., et al. 1997. North Siberian lakes: a methane source fueled by pleistocene carbon. Science 277, pp 800–802

Zopfi J., Bottcher M. E., Jørgensen B. B. 2008. Biogeochemistry of sulfur and iron in *Thioploca*-colonized surface sediments in the upwelling area off central chile, Geochimica et Cosmochimica Acta 72, pp 827–843

Annex A: Physico-Chemical data for Nunavik thaw lakes

Table A 1: Limnological properties of the sampled thaw lakes: temperature (°C), conductivity (µS/cm), dissolved oxygen (mg/L), and pH.

Sample	Depth(m)	Temperature (°C)	DO ($mg.L^{-1}$)	pH	Cond ($\mu S.cm^{-1}$)
SAS 1A	Surf	15.40	10.59	5.54	42.6
	0.3	15.30	10.45	5.48	42.9
	0.6	14.53	7.70	5.43	42.2
	0.9	13.74	5.45	5.50	42.7
	1.1	12.66	1.84	5.15	43.4
SAS 2A	Surf	13.91	13.05	5.23	34.5
	0.2	12.70	6.35	5.34	34.1
	0.3	12.56	1.72	5.08	34.8
	0.4	11.15	0.00	4.93	34.9
	1.8	7.39	0.00	4.62	44.0
	2.3	3.74	0.00	5.21	185.4
KWK12	Surf	18.54	14.16	5.87	27.5
	0.5	15.19	8.98	5.64	27.0
	1	14.83	5.96	5.29	27.6
	1.5	11.71	0.00	4.85	39.1
	2.2	6.76	0.00	4.81	55.1
BGR 1	Surf	15.65	6.80	6.99	85.4
	1.8	14.98	5.58	6.88	84.9
	2.3	13.52	2.32	6.79	84.6
	2.8	10.60	0.00	6.62	84.5
	3.2	2.80	0.00	6.63	401.0

Annex B: Calibration Curves Parameters Uncertainty

The equation type of the calibration curves is $\mathbf{y = mx + b}$ where y is the signal (count.s^{-1}) of the analyte, and x is its concentration. The vertical deviation (d_i) for a point (x_i, y_i) is defined by the equation 1B where y is the ordinate of the straight line when $x = x_i$.

$$d_i = y_i - y = y_i - mx_i + b \qquad (1B)$$

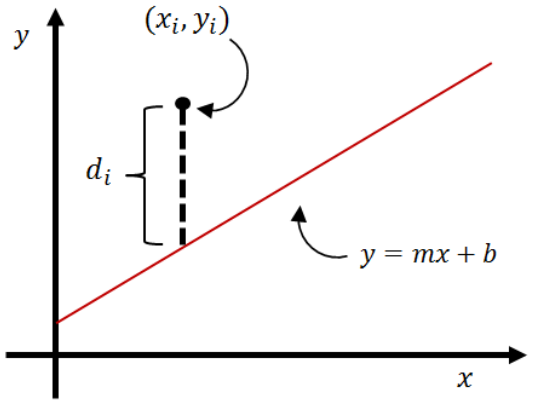

Figure B 1: Schematic representation of a straight line curve.

The uncertainties in the slope (m) and intercept (b) values are related to the uncertainty in measuring each value of y, and thus a first estimation of the standard of the y population is made by the following equation:

$$\boldsymbol{S_y = \sqrt{\frac{\sum(d_i^2)}{N-2}}} \qquad \boldsymbol{(2B)}$$

d_i is given by equation 1A, and N is the degrees of freedom, which in this case correspond to the number of standard solutions used for each element to construct the calibration curve.

Harris 2010 gives the follow expressions to calculate the standard deviation of m and b:

$$\begin{cases} \boldsymbol{s_m^2 = \frac{s_y^2 N}{D}} & \boldsymbol{(3B)} \\ \boldsymbol{s_b^2 = \frac{s_y^2 \sum(x_i^2)}{D}} & \boldsymbol{(4B)} \end{cases}$$, where $D = N\sum(x_i^2) - (\sum x_i)^2$.

Student's **t** is a statistical tool used most frequently to express confidence intervals and to compare results from different experiments. The confidence interval is computed from the equation $\pm \boldsymbol{t.s}$ where s is the standard deviations of a parameter.

Student's t will depend of N and the percentage of confidence level that we wish, so it must be applied as indicated from table B1 adapter from Harris 2010. In all cases a 95% confidence level was applied to determine that the confidence intervals.

Table B129: Values of Student's t adapted from Harris 2010 pp 73.

Degrees of freedom ($N-2$)	Confidence level (%)					
	90	**95**	**98**	**99**	**99.5**	**99.9**
3	2.353	3.182	4.541	5.841	7.453	12.924
4	2.132	2.776	3.747	4.604	5.598	8.610
5	2.015	2.571	3.365	4.032	4.773	6.869
6	1.943	2.447	3.143	3.707	4.317	5.959
7	1.895	2.365	2.998	3.500	4.029	5.408
8	1.860	2.306	2.896	3.355	3.832	5.041

The experimental data of ICP-MS for the standard solutions are show in the next tables

	y_i	x_i	y	${d_i}^2$	S_y	S_m	Δm	S_b	Δb
Cr ($N=7$)	11,242	198,741	11,3	2,6E-04	0,11	6,05E-4	**1,56E-3**	5,24E-2	**1,35E-1**
	5,621	99,953	5,7	4,8E-03					
	3,032	49,267	2,8	4,0E-02					
	1,233	19,885	1,2	3,1E-03					
	0,572	10,008	0,6	2,3E-03					
	0,271	4,860	0,3	3,5E-03					
	0,049	0,988	0,1	3,9E-03					
		$\sum = 383.70$		$\sum = 5.7E-2$					

	y_i	x_i	y	${d_i}^2$	S_y	S_m	Δm	S_b	Δb
Cu ($N=6$)	3,131	99,953	3,2	2,8E-03	0,06	7,60E-4	**2,11E-3**	3,53E-2	**9,79E-2**
	1,683	49,267	1,6	1,0E-02					
	0,693	19,885	0,7	1,4E-03					
	0,318	10,008	0,3	6,2E-04					
	0,151	4,860	0,2	8,6E-04					
	0,027	0,988	0,1	9,7E-04					
		$\sum = 184.96$		$\sum = 1.7E-2$					

	y_i	x_i	y	${d_i}^2$	S_y	S_m	Δm	S_b	Δb
Ni ($N=7$)	2,795	198,540	2,8	5,3E-05	0,03	1,47E-4	**3,78E-4**	1,27E-2	**3,26E-2**
	1,407	99,852	1,4	1,1E-04					
	0,756	49,217	0,7	2,4E-03					
	0,306	19,865	0,3	1,3E-04					
	0,147	9,998	0,2	8,6E-05					
	0,068	4,855	0,1	2,6E-04					
	0,012	0,987	0,0	3,2E-04					
		$\sum = 383.31$		$\sum = 3.4E-3$					

	y_i	x_i	y	d_i^2	S_y	S_m	Δm	S_b	Δb
Zn ($N = 5$)	1,708	203,166	1,7	6,4E-05	0,02	9,90E-5	**3,15E-4**	1,04E-2	**3,30E-2**
	0,839	102,179	0,9	5,0E-04					
	0,444	50,364	0,4	1,7E-04					
	0,182	20,328	0,2	1,1E-07					
	0,099	10,231	0,1	1,4E-06					
		$\sum = 386.27$		$\sum = 7.4E-4$					

	y_i	x_i	y	d_i^2	S_y	S_m	Δm	S_b	Δb
Pb ($N = 5$)	3,086	49,068	3,1	3,9E-03	0,12	3,04E-3	**9,66E-3**	7,31E-2	**2,33E-1**
	1,488	19,804	1,3	3,5E-02					
	0,618	9,968	0,7	3,9E-03					
	0,094	0,984	0,1	3,7E-04					
	0,014	0,096	0,1	1,9E-03					
		$\sum = 79.92$		$\sum = 4.5E-2$					

	y_i	x_i	y	d_i^2	S_y	S_m	Δm	S_b	Δb
Al ($N = 7$)	4,485	100,054	4,6	7,6E-03	0,10	1,14E-3	**2,93E-3**	4,91E-2	**1,26E-1**
	2,459	49,317	2,3	3,0E-02					
	0,980	19,905	1,0	3,8E-04					
	0,475	10,018	0,5	1,6E-03					
	0,348	4,865	0,3	4,2E-03					
	0,039	0,989	0,1	4,8E-03					
	0,025	0,493	0,1	3,7E-03					
		$\sum = 185.64$		$\sum = 5.2E-2$					

The calibration curves equation can be rewritten as:

$$(\boldsymbol{cps}) = (\boldsymbol{m} \pm \Delta\boldsymbol{m}).[\boldsymbol{metal}] + (\boldsymbol{b} \pm \Delta\boldsymbol{b})$$

With a 95% confidence.

Element	Slope		Intercept		R^2
Cr	(5.6 ± 0.2)	x10^{-2}	(1 ± 1)	x10^{-1}	0.9997
Ni	(1.40 ± 0.04)	x10^{-2}	(0.2 ± 0.3)	x10^{-1}	0.9997
Cu	(3.2 ± 0.2)	x10^{-2}	(0.3 ± 1.0)	x10^{-1}	0.9988
Zn	(8.3 ± 0.3)	x10^{-3}	(0.1 ± 0.3)	x10^{-1}	0.9998
Pb	(6.3 ± 1.0)	x10^{-2}	(1 ± 2)	x10^{-1}	0.9965
Al	(4.5 ± 0.3)	x10^{-2}	(1 ± 1)	x10^{-1}	0.9984

The standard deviation of x by fitting the equation $y = mx + b$ is given by (Harris 2010):

$$\boldsymbol{S_x = \frac{S_y}{|m|}\sqrt{\frac{1}{k} + \frac{1}{N} + \frac{(y - \bar{y})^2}{m^2 \sum (x_i - \bar{x})^2}}} \qquad (\boldsymbol{5B})$$

Where k is the number of replicate measurements of the unknown sample.

Annex C: TE concentration in aqua regia digestion

Table C 1: Trace elements concentration (µg/L) in acid digestion of soils/sed. for each element. The relatively standard deviation (RSD, %) for duplicates, detection limit (LD, µg/L) and limit of quantitation (LQ, µg/L) are also represented.

Sample		Cr	RSD	Ni	RSD	Cu	RSD	Zn	RSD	Pb	RSD	Al	RSD
SAS 1A	Soil#1	29 ± 7.5	26.5	<LD	-	25 ± 8.7	6.7	130 ± 10	1.7	29 ± 10	22.5	75 ± 3.7	1.0
	Soil#2	26 ± 7.5	14.2	<LD	-	14 ± 8.8	8.2	19 ± 10	8.6	8.3 ± 9.7	6.2	68 ± 3.7	3.9
	Sed	29 ± 5.3	-	18 ± 5.2	-	15 ± 6.2	-	29 ± 6.8	-	<LD	-	66 ± 2.6	
SAS 2A	Soil#1	5.9 ± 7.6	17.0	<LD	-	<LD	45.2	54 ± 9.4	40.7	26 ± 10	39.7	82 ± 2.7	
	Soil#2	9.5 ± 7.6	30.0	<LD	-	<LD	3.6	11 ± 10	16.8	<LD	73.1	78 ± 3.7	3.9
	Sed	22 ± 5.3	-	9.8 ± 5.3	-	15 ± 6.2	-	21 ± 6.9	-	10 ± 6.8	-	65 ± 2.6	
KWK12	Soil#1	86 ± 7.5	4.3	28 ± 3.4	12.4	28 ± 0.5	1.9	123 ± 10	5.8	44 ± 11	5.2	73 ± 3.7	3.4
	Soil#2	37 ± 3.2	-	22 ± 4.2	-	11.6 ± 12.9	-	53 ± 7.5	-	9.3 ± 12	-	114 ± 3	
BGR 1	Soil#1	68 ± 3.2	-	41 ± 4.2	-	16.6 ± 12.7	-	59 ± 7.4	-	13.5 ± 12.0	-	214 ± 3	
	Soil#2	37 ± 3.2	-	17 ± 4.2	-	15.0 ± 12.7	-	53 ± 7.4	-	11.6 ± 12.1	-	196 ± 3	
	Sed#1	40 ± 3.2	-	17 ± 4.2	-	18.5 ± 12.7	-	67 ± 7.4	-	12.1 ± 12.1	-	180 ± 3	
	Sed#2	38 ± 3.2	-	16 ± 4.2	-	15.3 ± 12.7	-	57 ± 7.5	-	12.5 ± 12.1	-	185 ± 3	
	LD	3.5		4.6		6.8		6.2		6.4		3.3	
	LQ	10.7		14.0		20.5		18.8		19.4		10.1	

Table C 2: Trace elements concentration in soils and sediments (µg/g). The uncertainly was calculated with a 95% intervals confidence. Because of high metals content some samples needed dilution. * 1:6 dilution; ** 1:4 dilution.

Sample		Mass (mg)	Cr	Ni	Cu	Zn	Pb	Al (%)
SAS 1A	Soil#1	211.8	6.9 ± 1.8	<LD	6.0 ± 2.1	31 ± 2	6.8 ± 2.3	0.331 ± 0.016
	Soil#2	205.8	6.4 ± 1.8	<LD	3.4 ± 2.1	4.6 ± 2.4	2.0 ± 2.4	0.276 ± 0.015
	Sed	200.9	7.1 ± 1.3	4.4 ± 1.3	3.8 ± 1.6	7.1 ± 1.7	<LD	0.285 ± 0.011
SAS 2A	Soil#1	209.6	2.1 ± 2.9	<LD	<LD	18 ± 4	8.6 ± 3.7	0.012 ± 0.001
	Soil#2	210.0	2.3 ± 1.8	<LD	<LD	2.7 ± 2.4	<LD	0.078 ± 0.004
	Sed	206.1	5.4 ± 1.3	2.4 ± 1.3	3.7 ±1.5	5.1 ± 1.7	2.5 ± 1.7	0.233 ± 0.009
KWK12	Soil#1	202.9	21 ± 1.8	6.8 ± 1.8	6.8 ± 2.1	30 ± 2.4	11 ± 3	1.43 ± 0.08
	**Soil#2	210.8	35 ± 3.1	21 ± 4	11 ± 0.5	50 ± 7.1	8.8 ± 1.2	2.71 ± 0.07
***BGR 1**	Soil#1	201.2	95 ± 4.5	58 ± 5.8	23 ± 0.6	82 ± 10	19 ± 1.7	5.32 ± 0.09
	Soil#2	206.0	51 ± 4.5	24 ± 5.8	21 ± 0.6	74 ± 10	16 ± 1.7	4.76 ± 0.08
	Sed#1	205.0	57 ± 4.5	24 ± 6.0	26 ± 0.7	94 ± 11	17 ± 1.7	4.38 ± 0.08
	Sed#2	201.6	51 ± 4.3	21 ± 5.7	21 ± 0.6	76 ± 10	17 ± 1.6	4.59 ± 0.08

Annex D: Concentrations (µg/L) of elements in water.

Table D 1: Total elements concentration (µg/L) in water column. The errors associated have 95% confidence.

Sample	Depth (m)	Cr	Ni	Cu	Zn	Pb	Al
SAS 1A	Surf	0.7 ± 0.1	(1.2 ± 0.1)x10	0.31 ± 0.03	1.4 ± 0.1	0.33 ± 0.03	(6.2 ± 0.6)x10
	0.3	1.1 ± 0.1	0.30 ± 0.03	0.37± 0.03	1.9 ± 0.2	0.21 ± 0.02	(6.7 ± 0.6)x10
	0.6	0.7 ± 0.1	< LD	0.28± 0.02	2.2 ± 0.2	0.5 ± 0.1	(6.1 ± 0.6)x10
	0.9	0.6 ± 0.1	< LD	0.44 ± 0.04	1.6 ± 0.1	0.37 ± 0.03	(6.0 ± 0.6)x10
	1.1	1.1 ± 0.1	< LD	0.40 ± 0.04	1.4 ± 0.1	0.22 ± 0.02	(6.9 ± 0.6)x10
SAS 2A	Surf	0.7 ± 0.1	< LD	0.8 ± 0.1	$(2.2 \pm 0.2)x10^2$	0.44 ± 0.04	(6.2 ± 0.6)x10
	0.2	0.6 ± 0.1	0.6 ± 0.1	0.6 ± 0.1	(3.5 ± 0.4)x10	(1.9±0.3)x10	(5.9 ± 0.6)x10
	0.3	0.6 ± 0.1	< LD	0.40 ± 0.04	(1.5 ± 0.1)x10	0.48 ± 0.05	(5.9 ± 0.6)x10
	0.4	0.4 ± 0.1	< LD	0.37 ± 0.03	(1.5 ± 0.2)x10	0.24 ± 0.02	(5.3 ± 0.7)x10
	1.8	1.2 ± 0.1	0.5 ± 0.1	1.3 ± 0.1	(3.2 ± 0.3)x10	0.7 ± 0.1	$(1.5 \pm 0.1)x10^2$
	2.3	1.4 ± 0.1	0.6 ± 0.1	1.8 ± 0.1	$(1.7 \pm 0.1)x10^2$	0.8 ± 0.1	$(1.8 \pm 0.1)x10^2$
KWK12	Surf	0.8 ± 0.1	5.3 ± 0.5	0.9 ± 0.1	2.7 ± 0.2	0.28 ± 0.02	(9.9 ± 0.7)x10
	0.5	0.7 ± 0.1	1.5 ± 0.1	0.6 ± 0.1	2.6 ± 0.3	0.27 ± 0.02	$(1.2 \pm 0.1)x10^2$
	1	0.8 ± 0.1	1.5 ± 0.1	0.6 ± 0.1	7.5 ± 0.6	0.27 ± 0.02	(9.4±0.7)x10
	1.5	-	-	-	-	-	-
	2.2	1.4 ± 0.1	0.44 ± 0.04	0.6 ± 0.1	10 ± 1.0	0.25 ± 0.02	$(1.0 \pm 0.1)x10^2$
BGR 1	Surf	0.50 ± 0.04	8.2 ± 0.5	0.8 ± 0.1	(2.3 ± 0.2)x10	0.6 ± 0.1	(3.5 ± 0.6)x10
	1.8	0.50 ± 0.04	2.4 ± 0.2	1.6 ± 0.2	(1.0 ± 0.1)x10	0.22 ± 0.02	(2.1 ± 0.6)x10
	2.3	0.9 ± 0.1	0.44 ± 0.04	0.8 ± 0.1	2.4 ± 0.2	4.6 ± 0.3	(3.6 ± 0.6)x10
	2.8	0.5 ± 0.1	0.37 ± 0.04	4.4 ± 0.4	< LD	0.24 ± 0.02	(3.0 ± 0.6)x10
	3.2	1.1 ± 0.1	3.4 ± 0.3	0.7 ± 0.1	4.0 ± 0.4	0.18 ± 0.02	< LD
	LD (µg/L)	0.3	0.4	0.2	1.1	0.2	7.0
	LQ (µg/L)	0.9	1.3	0.6	3.4	0.6	21.2

Table D 2: Concentrations of trace elements (µg/L) in water obtained by the calibration curves.

Sample	Depth (m)	Cr	Ni	Cu	Zn	Pb
SAS 1A	Surf	1.06	1.10	1.56	12	2.65
	0.3	2.32	3.75	3.09	13	6.95
	0.6	1.38	1.78	2.38	< LD	7.39
	0.9	1.59	1.95	1.99	2	5.40
	1.1	1.13	1.36	1.36	13	2.75
SAS 2A	Surf	1.06	0.76	1.87	36	3.93
	0.2	1.99	1.36	2.38	70	4.24
	0.3	0.94	0.67	1.60	47	3.88
	0.4	1.67	2.12	3.13	66	10.68
	1.8	1.25	2.21	2.46	82	7.91
	2.3	1.21	1.95	1.44	956	2.76
KWK12	Surf	1.02	0.59	1.13	14	1.48
	0.5	0.92	0.42	1.64	12	4.36
	1	0.98	2.81	1.83	7	4.95
	1.5	1.15	2.12	1.75	43	4.10
	2.2	1.29	2.55	1.56	23	1.48
BGR 1	Surf	1.00	0.42	1.32	5	2.68
	1.8	1.06	1.36	1.64	23	3.90
	2.3	1.21	0.85	1.09	4	1.34
	2.8	1.15	1.95	2.54	5	8.06
	3.2	1.00	0.42	1.32	5	2.68
	LD (µg/L)	0.02	0.07	0.11	2	0.46
	LQ (µg/L)	0.07	0.20	0.32	6	1.41

Table D 3: Labile concentrations (µg/L) of elements in water at different depths.

Sample	Depth(m)	Cr ($x10^{-2}$)	Ni ($x10^{-2}$)	Cu ($x10^{-2}$)	Zn ($x10^{-1}$)	Pb ($x10^{-1}$)
SAS 1A	Surf	6.1 ± 0.2	5.5 ± 0.4	7.2 ± 0.5	5.6 ± 0.5	1.0 ± 0.1
	0.3	13 ± 0.5	19 ± 0.4	14 ± 0.5	1.2 ± 0.1	2.5 ± 0.2
	0.6	8.1 ± 0.3	9.2 ± 0.4	11 ± 0.5	< LD	2.7 ± 0.2
	0.9	9.6 ± 0.4	10 ± 0.4	9.7 ± 0.6	7.2 ± 0.7	2.0 ± 0.2
	1.1	7.1 ± 0.3	7.5 ± 0.4	7.0 ± 0.6	6.7 ± 0.6	1.1 ± 0.1
SAS 2A	Surf	6.3 ± 0.3	4.0 ± 0.4	9.0 ± 0.5	24 ± 1.1	1.5 ± 0.1
	0.2	12 ± 0.4	7.3 ± 0.4	12 ± 0.6	43 ± 1.2	1.6 ± 0.2
	0.3	5.8 ± 0.2	3.7 ± 0.4	8.0 ± 0.6	31 ± 1.1	1.5 ± 0.1
	0.4	11 ± 0.4	12 ± 0.4	17 ± 0.6	42 ± 1.3	4.4 ± 0.2
	1.8	10 ± 0.4	16 ± 0.5	16 ± 0.7	64 ± 1.8	4.1 ± 0.2
	2.3	10 ± 0.4	14 ± 0.5	9.8 ± 0.8	672 ± 16.1	1.4 ± 0.1
KWK12	Surf	3.8 ± 0.2	1.9 ± 0.3	3.4 ± 0.5	4.4 ± 0.4	0.35 ± 0.03
	0.5	3.8 ± 0.2	1.5 ± 0.4	5.5 ± 0.5	4.3 ± 0.4	1.1 ± 0.1
	1	4.5 ± 0.3	1.1 ± 0.4	6.9 ± 0.6	7.7 ± 0.6	1.4 ± 0.1
	1.5	5.3 ± 0.3	8.6 ± 0.4	6.6 ± 0.6	22 ± 1.2	1.2 ± 0.1
	2.2	7.2 ± 0.4	12 ± 0.5	7.0 ± 0.7	17 ± 1.4	0.51 ± 0.05
BGR 1	Surf	6.4 ± 0.3	2.3 ± 0.4	6.8 ± 0.6	2.5 ± 0.2	1.1 ± 0.1
	1.8	6.9 ± 0.3	7.7 ± 0.4	8.6 ± 0.6	20 ± 1.2	1.6 ± 0.2
	2.3	8.2 ± 0.3	5.0 ± 0.4	6.0 ± 0.6	2.2 ± 0.2	0.6 ± 0.1
	2.8	8.6 ± 0.3	13 ± 0.5	15 ± 0.7	11 ± 1.0	3.8 ± 0.2
	3.2	9.8 ± 0.4	3.6 ± 0.6	11 ± 0.9	3.8 ± 0.3	1.6 ± 0.2

Annex E: Metal diffusion coefficients

Table E 1: Metal diffusion coefficients corrected for temperature using equation 3 at different lakes depths.

Lake	Depth (m)	Metal diffusion coefficient ($x10^{-6}$ $cm^{-2}.s^{-1}$)				
		Cr	Ni	Cu	Zn	Pb
SAS 1A	Surf	3.84	4.38	4.73	4.62	6.11
	0.3	3.83	4.37	4.71	4.60	6.09
	0.6	3.74	4.26	4.60	4.50	5.95
	0.9	3.65	4.16	4.49	4.39	5.80
	1.1	3.46	3.96	4.27	4.17	5.51
SAS 2A	Surf	3.66	4.18	4.52	4.41	5.83
	0.2	3.53	4.03	4.35	4.25	5.62
	0.3	3.51	4.01	4.33	4.23	5.59
	0.4	3.36	3.83	4.14	4.04	5.34
	1.8	2.66	3.04	3.28	3.20	4.24
	2.3	2.61	2.98	3.21	3.13	4.14
KWK12	Surf	4.21	4.81	5.19	5.07	6.71
	0.5	3.81	4.35	4.70	4.59	6.07
	1.0	3.43	3.92	4.23	4.13	5.46
	1.5	3.42	3.90	4.21	4.11	5.44
	2.2	2.86	3.27	3.53	3.45	4.56
BGR 1	Surf	3.86	4.41	4.76	4.65	6.15
	1.8	3.79	4.32	4.67	4.56	6.03
	2.3	3.62	4.13	4.46	4.36	5.76
	2.8	3.30	3.77	4.07	3.97	5.25
	3.2	2.52	2.88	3.11	3.03	4.01